MASTER

The influence of the fibre-matrix interface on the transverse mechanical behaviour and failure of carbon fibre reinforced composites

van Klinken, E.J.

Award date:
1992

The Influence of the Fibre-Matrix Interface on the Transverse Mechanical Behaviour and Failure of Carbon Fibre Reinforced Composites

by: E.J. v. Klinken

Graduate report
TUE WFW 92.051

Professor : Prof. dr. ir. H.E.H. Meijer
Coaches : Ir. J.M.M. de Kok
Ing. A.A.J.M. Peijs

Eindhoven University of Technology (TUE)
Department of Mechanical Engineering
Division of Fundamental Mechanics
Subdivision: Polymer Technology

June 1992

Samenvatting

Het doel van dit onderzoek is het bestuderen van de invloed van de vezel-matrix interface sterkte op het transversaal mechanisch gedrag en het bezwijken van uni-directionele vezelversterkte materialen onder transversale belasting. Daarvoor is gebruik gemaakt van een micromechanisch model van een transversaal belast uni-directioneel koolstofvezel versterkt epoxy composiet, waarin een interface is opgenomen. Dit micromechanisch model is geverifieerd met behulp van experimenten aan koolstofvezel versterkte epoxy, gebaseerd op vezels, die alleen in het niveau van de oppervlakte behandeling verschillen.

In de combinatie van experimenten en numerieke analyses is gebruik gemaakt van, respectievelijk, het zuurstof percentage op het vezeloppervlak en de interface modulus, die een vergelijkbare rol spelen in het bepalen van de interface eigenschappen. Uit zowel de numerieke analyses als de experimenten bleek dat er drie aparte gebieden in interface sterkte te onderscheiden zijn. Dit zijn a) geen of slechte hechting, respectievelijk resulterend in loslating en niet-catastrofale debonding van de vezel en de matrix, b) matige hechting, resulterend in catastrofale debonding van de vezel en de matrix en c) goede hechting, waar bezwijking van het composiet in de matrix wordt geïnitieerd. De transversale sterkte van het composiet blijkt in deze drie gebieden van verschillende factoren afhankelijk te zijn. In het geval van geen of slechte hechting in de interface wordt het bezwijken van het composiet in de interface geïnitieerd. Echter, nadat totale loslating of debonding heeft plaats gevonden heeft de matrix, met daarin de losse vezel, nog een reststerkte. De transversale sterkte van het composiet wordt door de matrix bepaald. Bij matige hechting in de interface, wordt de schade ook in de interface geïnitieerd, maar deze is catastrofaal voor het composiet, omdat dit bij een spanning boven de reststerkte van de matrix plaats vindt. De transversale sterkte van het composiet is dan ook alleen afhankelijk van de interface sterkte. Doordat de interface eigenschappen in dit gebied geen effect hebben op de spanningsverdeling in het composiet is dit een lineaire afhankelijkheid en is de transversale modulus onafhankelijk van de interface eigenschappen. In het geval van goede hechting bezwijkt de matrix voordat de interface zal kunnen bezwijken en wordt de transversale sterkte dus weer door de matrix bepaald.

De resultaten van het model blijken zowel kwalitatief als kwantitatief goed overeen te komen met de experimenten.

Contents

The Influence of the Fibre-Matrix Interface on the Transverse Mechanical Behaviour and Failure of Carbon Fibre Reinforced Composites

E.J. v. Klinken
Eindhoven University of Technology
Department of Mechanical Engineering

June 22, 1992

Abstract

A micromechanical study of continuous carbon fibre reinforced epoxy has been carried out using generalised plane strain finite element analysis. An interface element has been developed, to investigate the influence of the interface on the transverse composite properties. Three distinct regions of interfacial bonding have been studied, viz. a) no bonding at all or poor bonding, resulting in fibres releasing from the matrix or non-catastrophic debonding in the interface respectively, where the transverse composite strength is determined by the matrix material, b) intermediate bonding in the interface, resulting in catastrophic debonding, dominating the composite strength and c) good bonding, where failure is initiated in the matrix material between the fibres leading to composite failure. The numerical results have been validated by experiments on composites with different interface properties, based on fibres which have undergone different levels of a surface treatment. Translation from numerical to experimental results was performed by relating the interface modulus to the fibre surface oxygen concentration, which played similar roles in determining the interface properties in numerical and experimental analysis respectively. The interface properties were found not to affect the transverse composite modulus.

Introduction

High performance composites are a rapidly-growing class of materials with high strength and modulus and low density. For example, specific strength and modulus of uni-directional carbon fibre reinforced composites in the direction of the fibres are about five times higher than for high strength steel. Because of the low density compared to the mechanical properties, composites are applied in aircraft and aerospace parts, such as wings and bodies, in racing-cars, for frames and bodies, in flywheels and increasingly in automobile parts.

Two factors limit the applications of composites at a large scale. First of all, the product price is rather high as a result of the long fabrication cycles and the high price of the constituents. Secondly, uni-directional composites are extremely anisotropic, showing high performance in one direction only, viz. the fibre direction. The general name for composites, being fibre reinforced plastics, accounts for the fibre direction only. Perpendicular to this direction these materials in fact are fibre weakened plastics. Current studies performed in order to improve the transverse properties led to two- or even three-dimensional applications of fibres, such as laminated plates and two- or three-dimensional fabrics. These evolutions, however, did not solve the problem: the specific properties in the main direction are decreased severely and even in these structures, the low transverse properties of the uni-directional laminates initiate failure. Therefore it is necessary to improve the transverse properties, while maintaining the longitudinal properties. This can be done by, either, toughening the matrix (using ductile matrices), improving the transverse fibre strength or improving the bond strength of the interface between the fibre and the matrix.

The low transverse strain of uni-directional composites is a result of the high stress and strain concentrations, caused by the great difference in fibre and matrix properties. These stress and strain concentration factors cause initiation of damage at relative low loads. In the case of poor bonding between fibre and matrix, debonding, which is failure by separation of the two constituents, will occur. In the case of well bonded fibres, either one of the two constituents will fail. The most common failure mode is matrix cracking, but in highly anisotropic fibres, fibre splitting may also occur.

This report emphasizes the relation between the fibre-matrix bonding and the transverse properties of uni-directional composites, because interfacial bonding significantly affects these properties [1,2,3]. Improving the strength of one of the constituents does not affect the composite transverse strength if the failure is dominated by the fibre-matrix interface. The aim of this study is to obtain a better understanding of the influence of the interface properties on the transverse composite properties. Therefore a Finite Element Method (FEM) model based on regular fibre stacking is used. This FEM model has been developed previously by de Kok [4] and is refined by introducing the transfer of shear stresses across the interface. The results of the numerical analyses based on this model are verified by experiments on carbon fibre reinforced epoxies with various interface strengths. These interface strengths are based on the level of the oxidative surface treatment that has been applied to the fibres.

In chapter 1 the micromechanical modelling is described, chapter 2 contains the experimental data on the tested materials and in chapter 3 the confrontation of the numerical analyses and the test data is discussed. Conclusions and recommendations are presented in chapter 4.

1. Numerical analysis

Most recent studies on the transverse behaviour of composites are performed using FEM models [1,2,5,6,7]. Transverse behaviour of composites is too complicated to be analyzed analytically. Micromechanical models are able to predict quantitative mechanical properties fairly well [5,6].

The model geometry is based on the micromechanical model of a cross-section. Although photomicrographs show a completely random filament packing array, see figure 1.1, most models assume a regular filament packing. Using such a model, the following basic assumptions are made:

- fibre and matrix are homogeneous
- fibre and matrix are free of voids
- the fibres are regularly spaced and aligned
- mechanical processes like yielding and fracture take place along the whole length of the fibres

Commonly used arrays are the square, rectangular and hexagonal filament packing arrays, where analysis can be performed on one repeating unit, or basic cell. Because of symmetry, analysis can even be reduced to only one quadrant of this basic cell [1,6,7,9], see figure 1.1.

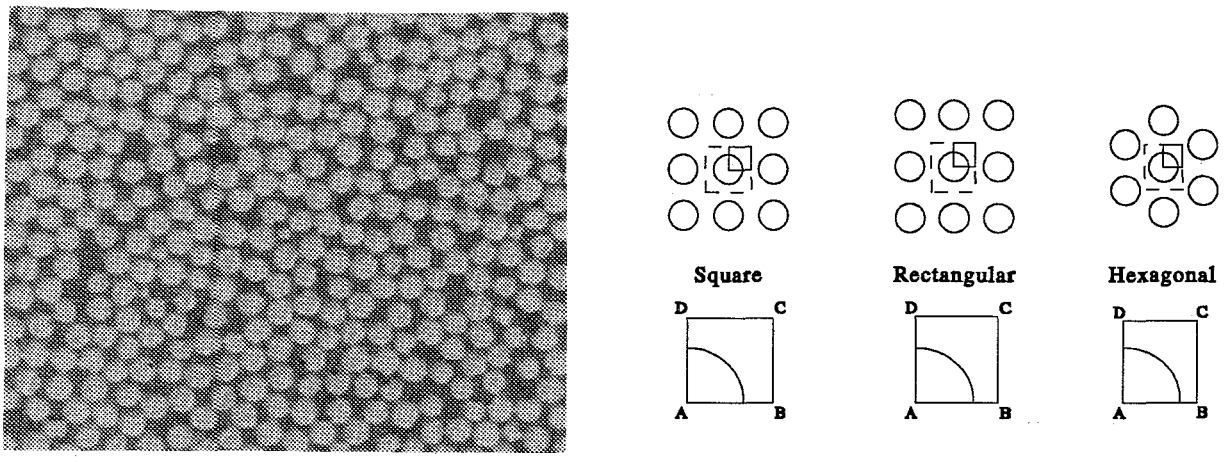

Figure 1.1: Real and model composites.

Real uni-directional composites behave transversely isotropic because of the random filament packing. However, due to the model geometry, both rectangular and square packing are highly anisotropic, whereas the hexagonal filament packing is only close to transversely isotropic. Although hexagonal packing seems, physically, the most realistic model, the best correlation with experimental data is obtained with the square filament packing array model [8]. If models accounting for random filament packing are used, the (nearly) hexagonal packing array shows an even better agreement [8], again indicating that this is, physically, the best model. However, these statistical models are too complex and are too much time consuming to be used in a manageable model. Since the square packing array model provides good results, this model geometry is used in this study.

Two extra assumptions are made in the framework of this investigation:

- the composite initially is in a free stress state (no residual stresses due to fabrication)
- epoxy and carbon show linear elastic stress-strain behaviour.

1.1 FEM modelling of composite with perfectly bonded fibres

A lot of work has been done on the modelling of composites with perfect bonded fibres. Well known is work performed by Adams and Doner [5], who used a square array model to determine the elastic properties of composites based on isotropic fibres. They determined the transverse modulus and maximum principle stress for various fibre/matrix stiffness ratios and filament spacings (fibre volume fractions). The calculated stiffnesses agree fairly well with the experimental values found for composites with isotropic fibres like glass and boron. However, predicted values for carbon/epoxy composites did not match the experimental results, since anisotropic fibres were not modelled.

The model presented in this section is not new in this context, but it is used as an introduction to the model with other interface conditions and to predict the ultimate transverse strength of a composite with perfectly bonded fibres. A two-dimensional mesh of the model composite with perfect compatible constituents (figure 1.2) is created using the pre- and postprocessor MENTAT [10]. Quadratic 8-node elements are used to achieve accurate results. Because of the high stress gradients at the interface the element size is reduced in the vicinity of the interface. Generalized plane strain formulation is used, allowing a constant strain in the fibre direction (third dimension), representing the situation in a cross-section through a continuous, infinitely long composite. This is a reasonable assumption away from the fibre end when the fibres are long compared to their diameter. By changing the radius of the fibre relative to the unit cell, different fibre volumes within the composite material can be simulated. In the experiments and numerical analyses the fibre volume fraction is kept at 50%, resulting in a fibre radius of 0.7979 times the width of the unit cell. Because of symmetry, the square model should remain rectangular under transverse tension. This results in the boundary conditions as they are shown in figure 1.2. The carbon fibres are assumed to be transversely isotropic, the matrix material is assumed to be isotropic and linear elastic. The mechanical properties of the constituents are listed in table 1.1 and 1.2 and refer to the materials used in the experiments (Courtaulds Grafil Apollo IM 43-750 intermediate modulus carbon fibre and Courtaulds Grafil XA-S high strength carbon fibre, further on denominated as Apollo and XA-S respectively, and Ciba Geigy Araldite epoxy matrix).

Table 1.1: Mechanical properties of the fibres used in the numerical analyses.

Carbon Fibre Type		Apollo	XA-S
Longitudinal modulus	E_L [GPa]	305[1)]	230[1)]
Transverse modulus	E_T [GPa]	12[2)]	18[2)]
Long. Poisson ratio	ν_{LT} [-]	0.009[2)]	0.013[2)]
Transv. Poisson ratio	ν_{TT} [-]	0.30[2)]	0.25[2)]
Shear Modulus	G_{LT} [GPa]	14[2)]	20[2)]

[1)] Courtaulds Grafil data sheet [11]
[2)] Estimated

Table 1.2: Mechanical properties of the matrix used in the numerical analyses.

Material	Ciba Geigy epoxy
Young's modulus [GPa]	3.2
Poisson ratio [-]	0.37
Strain to failure ε_{max} [%]	4.2

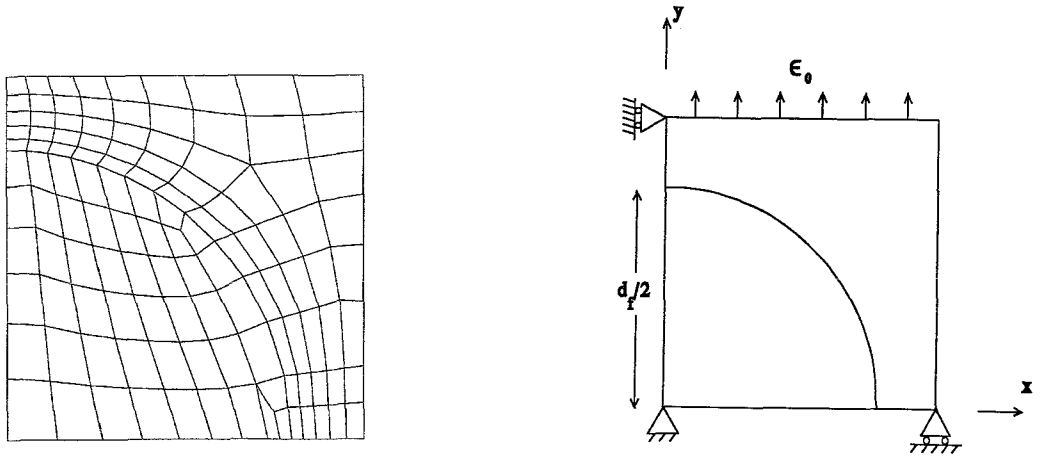

Figure 1.2: Finite element mesh for analyses on perfectly bonded fibres and corresponding boundary conditions.

Calculations were performed using the MARC [12] general purpose nonlinear finite element program for structural and thermal analysis. The post-processor used is MENTAT, which is able to produce a contour plot of any stress or strain. Transverse elastic properties and crack initiation (strength) can be predicted.

1.2 Analysis with perfectly bonded fibres

Calculations are performed for both composites with Apollo and XA-S fibres. Figure 1.3 shows contour plots for the calculated maximum principle stress and strain in the matrix for the Apollo carbon fibre epoxy composite. The contour plots for the XA-S/epoxy composite are not presented, because they displayed similar stress and strain states. The highest stress and strain concentrations occur between the fibres in the loading direction. In table 1.3 the main results of the calculations for both the Apollo and the XA-S fibre based composites are listed. All the results on the composite strengths presented in this and the following sections are calculated using the 4.2% maximum strain criterion.

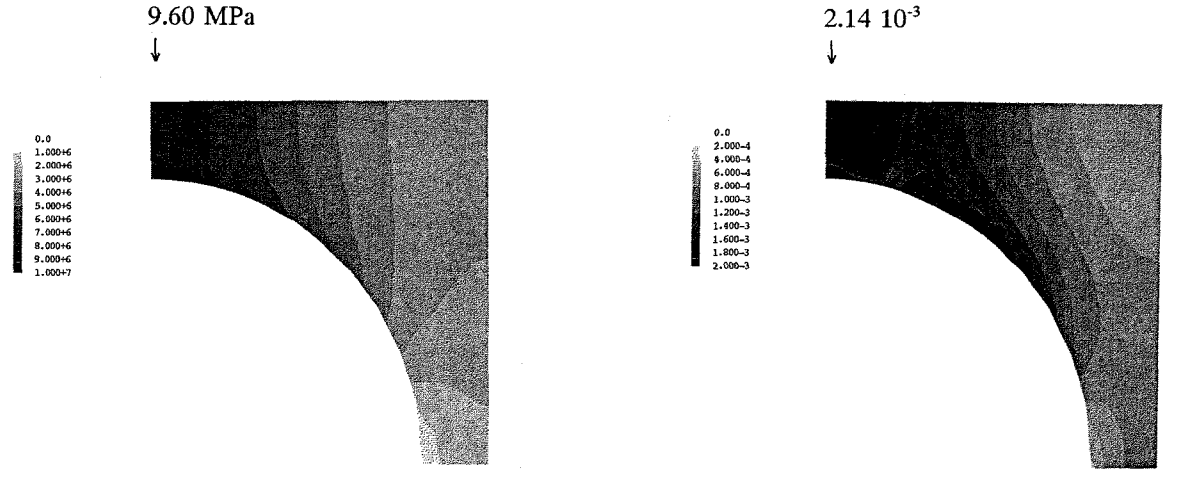

Figure 1.3: Contour plots of principle stress and strain of Apollo/epoxy composite, load 0.1% strain.

Table 1.3: Results for model with perfectly bonded fibres.

Material	Apollo/epoxy Composite	XA-S/epoxy Composite
Transverse Modulus [GPa]	6.65	7.83
Max. Princ. Stress Conc. Factor [-]	1.44	1.50
Max. Princ. Strain Conc. Factor [-]	2.14	2.59
Composite Strain to Failure [%]	1.96	1.62
Composite Strength [MPa]	130	127

This minor difference in transverse composite strength of the composites with Apollo and XA-S fibres can be explained by the twofold effect of the fibre modulus on the composites strength. First, the maximum strain concentration factor increases due to the higher transverse modulus of the XA-S fibre, resulting in a lower composite strain to failure. But, on the other hand, the transverse composite modulus also increases resulting in higher stresses at equal strains or, equal stresses at lower strains. Apparently, in this case, these two effects are approximately equal in magnitude, but influence the strength in the opposite direction, resulting in a minor difference in the transverse strength.

1.3 FEM modelling of composite with interface

The former analysis only accounts for composites with perfect bonding at the interface, where cracks initiate in and propagate through the matrix. Many composites, however, do not show good interfacial bonding and consequently show a different failure mode. Debonding of the two constituents occurs when the composite is loaded transversely. Usually the debonding will start between the fibres, where the tensile normal stress is the highest [1], see figure 1.3. After debonding is initiated it will propagate along the interface and eventually perhaps through the matrix. If an interface is incorporated in the micromechanical model, the effect of bond strength can be evaluated. This evaluation is checked by using composites with different interface properties, composites with carbon fibres which have undergone a different level of surface treatment.

The interface properties of carbon fibre reinforced epoxies can be changed by subjecting the carbon fibres to an oxidative surface treatment. As a result of this surface treatment the number of oxygen groups at the carbon fibre surface increases. In section 2.2 it is demonstrated that the amount of oxygen groups at the fibre surface mainly determines the interface properties. Other surface effects, such as fibre surface roughness, other chemical groups at the fibre surface, etc. can be neglected. The theory behind this phenomena is that chemical covalent bonds between the carbon fibre surface oxides and the epoxy resin are formed and that these chemical bonds are stronger than any other physical bond at the interface. Untreated fibres contain very few oxygen groups at the surface and consequently show little bonding at the interface, resulting in a low transverse strength. By increasing the surface treatment level, the number of covalent bonds at the interface increases, resulting in a higher interface strength and consequently a higher transverse composite strength.

The behaviour of a covalent C-C bond is approximated by a Morse potential. The first derivative, being the force between the atoms as a function of the distance, can be linearized in the region around the unloaded state. Consequently covalent C-C bonds are considered as linear springs, failing under tensile loading only. The type and number of bonds characterize the interface. Since the real number of covalent bonds is rather high, it is more convenient to use springs representing several bonds. In this case the modulus of the springs can be written as

$$E_S = NkL \tag{1.1}$$

where N, k and L represent the number of covalent bonds per unit of surface and the stiffness and length of

a covalent bond respectively. If the number of covalent bonds increases, the modulus of the interface also increases. However, the interface strain to failure, which is determined by the maximum extension of the covalent bond does not change with a changing number of bonds. According to this model the interface strength increases when the surface treatment level is increased, since the number of covalent bonds increases.

Probably, the bond at the interface is a polymer chain (in stead of a single C-C bond), because the epoxy will not start cross-linking right at the fibre surface. In this case it would be better to speak of an interphase instead of an interface. However, in order to prevent confusion, in this report the term interface will be used for the transition region between the fibre and matrix, no matter what the size of this region is. The stiffness of this polymer chain will be less than the stiffness of a single C-C bond. However, the interface properties can still be characterized with a modulus, which depends on the number of bonds between the fibre and matrix.

Crack propagation in the fibre-matrix interface in transversely loaded composites has been modelled previously by using spring elements at the interface [1,7]. Special springs, called gap elements, are used to connect the fibre and matrix and enable separation of the two constituents. Gap elements consist of two nodes, initially coinciding. Compressive stress is transferred directly, but tensile stress and shear stress lead to extension and shearing of the interface. When, due to interfacial failure, the constituent surfaces are not in contact, no stresses are transferred. The material properties depend on the stiffness of these interface springs. Using infinitely stiff springs results in a model of perfect bonding, reducing the stiffness to zero results in a model with not bonded fibres (compressive stresses are still transferred, because penetrating of the two constituents has to be prevented mathematically).

Crack propagation can also be simulated by reducing the stiffness of interface elements to zero. As long as the stiffness of the interface springs is not infinite (or zero), no singularities at the "crack-tip" will occur. Different criteria, like critical strain, critical stress or critical energy density, can be used to describe crack propagation and a stress strain curve of the model composite can be made. Figure 1.4 shows normalized stress-strain curves for composites with different stiffnesses of the interface elements.

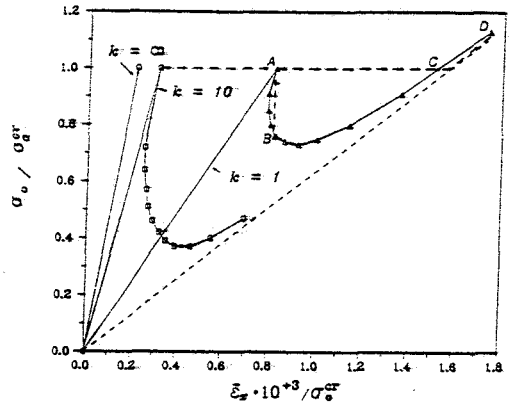

Figure 1.4: *Effective stress-strain relation for cracked and uncracked fibre-reinforced composite [7].*

Remark: Achenbach and Zhu [7] used gap elements as an interface, where infinite stiffness does not cause any singularities.

1.3.1 Introduction of interface transferring tensile stresses

The model presented in this section is based on the model for perfectly bonded fibres as it has been used in the previous sections and is developed by de Kok [4]. An interface is introduced by connecting the interfaces of the two constituents by 33 springs, called truss elements, which are placed equidistant and have the same cross-sectional area. Because of symmetry, the two outer elements, at ϕ = 0° and 90° (figure 1.5), are considered to be half elements and have a corresponding cross-sectional area. The total cross-sectional area of the truss elements equals the area of the fibre matrix interface. The interface modelled here is able to transfer radial loads only. The truss elements represent a certain number of covalent bonds. The modulus of these truss elements depends on this number of bonds, so when different levels of interfacial bond strength are modelled, the modulus of the interface elements is changed enabling the use of a single mesh for different interface properties. The length of a C-C bond is 1.5 Å, which is 3.10^{-5} times the mesh size. However, if the interface thickness is related to the cross-links of the epoxy matrix, the length of the interface elements must be approximately 30 Å, which is 6.10^{-4} times the mesh size. The choice of the interface thickness might be very relevant for a physically correct model, so two interface thicknesses have been used by de Kok [4] to investigate this influence, viz. 10^{-4} and 10^{-3} times the mesh size. Both matrix singularity ratio and composite transverse modulus have been calculated for a range of interface moduli for two interface elements sizes, viz. 10^{-3} and 10^{-4} times the mesh size. It was found that the size and stiffness of the interface elements cannot be varied unlimited. If the elements are too small or stiff a numerical solution cannot be obtained. This is because very small or stiff interface elements lead to an ill-conditioned stiffness matrix. He concluded that it would be better to use interface elements of 10^{-3} times the mesh size, which is the size of the interface elements used in the model presented in this report. In the model with interface, four node linear elements are used for the fibre and matrix. It would be better to use eight node quadratic elements, but this would lead to a more complex interface modelling. The mesh consequently is refined, which resulted in the mesh shown in figure 1.5.

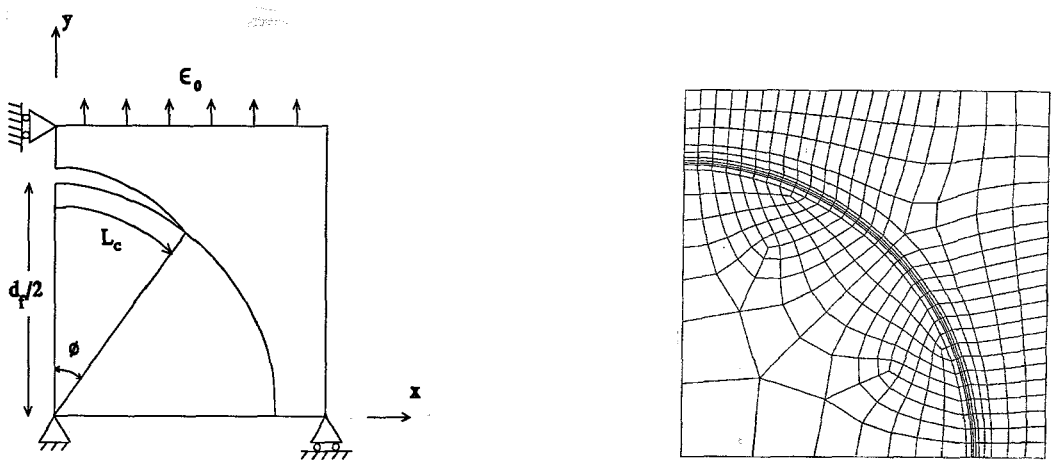

Figure 1.5: Micromechanical model and finite element mesh.

The analysis is performed for composites with the Apollo fibres, with mechanical properties as listed in table 1.2. The stress and strain in the composite with the interface transferring radial stresses only are calculated. The interface modulus used in this calculation was 5.0 GPa. The results of the analysis are shown in figure 1.6 and listed in table 1.4.

The results show that the stress and strain state in the model, as shown in figure 1.6, does not resemble the stress and strain state in the composite with perfect bonding (figure 1.3). Especially the part from ϕ = 45° to 90° is entirely different. The reason for this difference is the shear stress in the interface, which has been neglected in the model, resulting in odd stress states. The transverse modulus and strength are much lower compared to the model with perfect bonding in the interface. Further analysis on the behaviour during debonding is not performed with the use of this model. The model has to be extended by introducing a transfer of shear stresses in the interface.

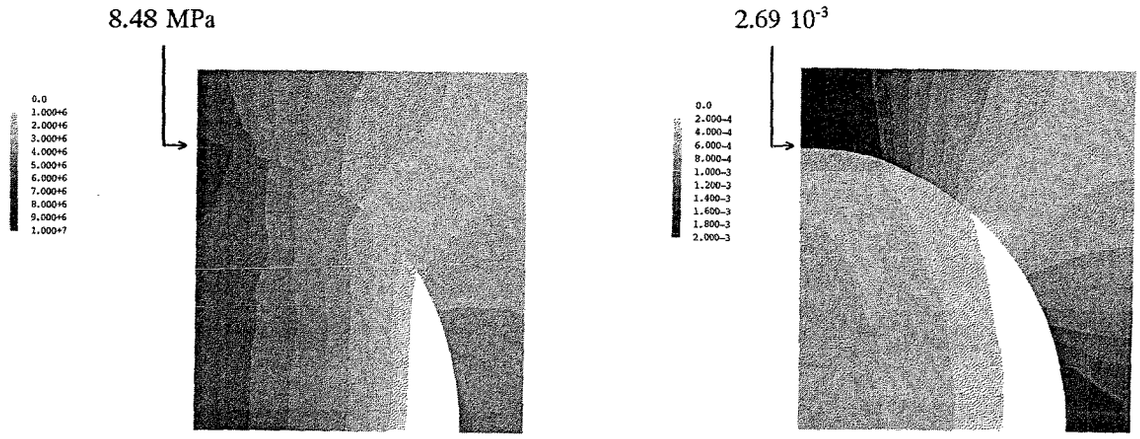

Figure 1.6: *Contour plots of principle stress and principle strain of Apollo/epoxy composite with interface elements transferring radial stresses only, load 0.1% strain.*

Table 1.4: *Results of analysis on model with interface transferring radial stresses only.*

Material	Apollo/epoxy Composite
Transverse Modulus [GPa]	4.46
Max. Princ. Stress Conc. Factor [-]	1.90
Max. Princ. Strain Conc. Factor [-]	2.69
Composite Strain to Failure [%]	1.56
Composite Strength [MPa]	69.6

1.3.2 Introduction of interface transferring both tensile and shear stresses

Introducing shear stresses in the interface is performed by adding another set of elements in the existing interface. These elements are (one-dimensional) truss elements, attached to two nodes, each at opposite sides of the interface, transferring traction proportional to the tangential difference in displacement (extension) of the two connected nodes. Thus a set of 33 artificial linear shear elements is introduced, accounting for the shear stresses in the interface. The length and cross-sectional area of these tangential springs is exactly the same as the corresponding radial truss elements. Analysis is performed for the Apollo/epoxy composite with an interface modulus, radial and tangential, of 5.0 GPa to obtain the stress and strain state in the material. The results of the analysis are shown in figure 1.7. The quantitative results for initiation of failure were similar with the results from the model for perfect bonding, which is shown in table 1.5.

From figure 1.3 and 1.7 and table 1.5 it can be concluded that the model with interface is physically correct. Both qualitative and quantitative agreement is shown. Before the study is extended to the analysis with a debonding interface, the influence of the interface properties has to be determined.

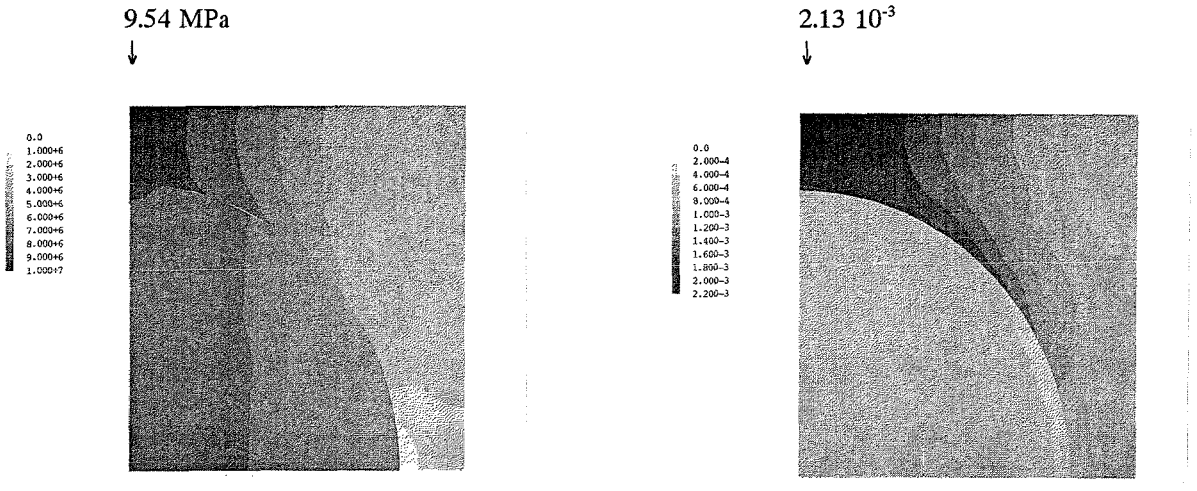

Figure 1.7: *Contour plots of principle stress and principle strain of Apollo/epoxy composite with interface elements transferring radial and shear stresses, load 0.1% strain.*

Table 1.5: *Comparison of results on Apollo/epoxy composite of model with perfect bonding and model with interface transferring both tensile and shear stresses.*

Interface Model Type	Perfect Bonding	Interface (E_r=E_r=5.0 GPa)
Transverse Modulus [GPa]	6.65	6.67
Max. Princ. Stress Conc. Factor [-]	1.44	1.43
Max. Princ. Strain Conc. Factor [-]	2.14	2.13
Composite Strain to Failure [%]	1.96	1.97
Composite Strength [MPa]	130	132

1.3.3 Influence of the interface properties on the transverse composite properties

The only influencing interface property is the interface modulus. Since the interface strain to failure is assumed not to depend on the number of covalent bonds, the strength, is also determined by the interface modulus. Calculations are performed for a range of interface moduli. Figure 1.8 shows the influence of the interface modulus on the composite modulus.

The interface modulus determines the transfer of stresses to the fibre. Low interface moduli result in low transverse composite moduli and high interface moduli result in high transverse moduli. Interface moduli close to the matrix Young's modulus (3.2 GPa) hardly affect the transverse composite modulus, indicating that variation of the interface modulus within this region has no effect on the stress state in the fibre and matrix. This has also been found in the contour plots for the different interface moduli. Figure 1.9 shows the influence of the interface modulus on the matrix singularity ratio, which is an indicator for the accuracy of the numerical solution.

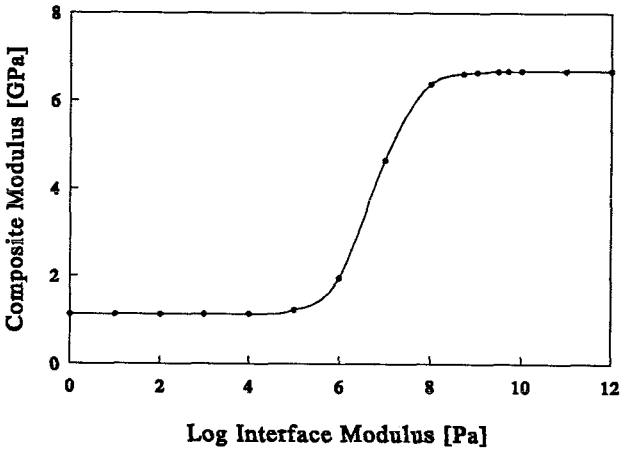

Figure 1.8: Influence of interface modulus on the composite transverse modulus.

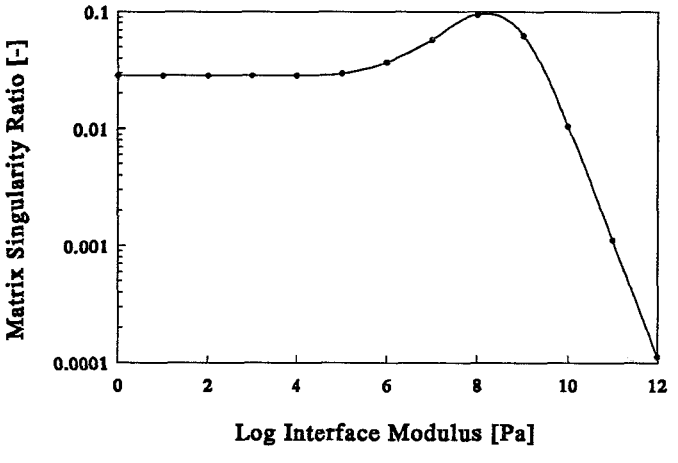

Figure 1.9: Influence of interface modulus on the matrix singularity ratio.

As mentioned before, very stiff interface elements lead to an ill-conditioned matrix so that numerical solution of the problem is not possible. In order to describe a range in interfacial bond strength, a range in interface moduli has to be chosen. The former figure shows that this range has to be within the range 10^8 Pa (lower interface moduli change modulus and the stress and strain state in the composite) and 10^{10} Pa (higher interface moduli cause problems in obtaining a numerical solution). Four different interface moduli are chosen to describe a range in interfacial bond strength, viz. 0.5, 1.0, 3.0 and 5.0 GPa. Further studies are concentrated on these four cases. Figures 1.10 and 1.11 show the results of the calculations, where the interface is considered. Stress and strain concentration factors for tension (radial) and shear (tangential) have been determined, and are shown in figures 1.10 and 1.11 respectively. Due to the fact that the stress-strain state does not change, the interface stresses are equal for the four different interface moduli. Consequently, the interface strains are different.

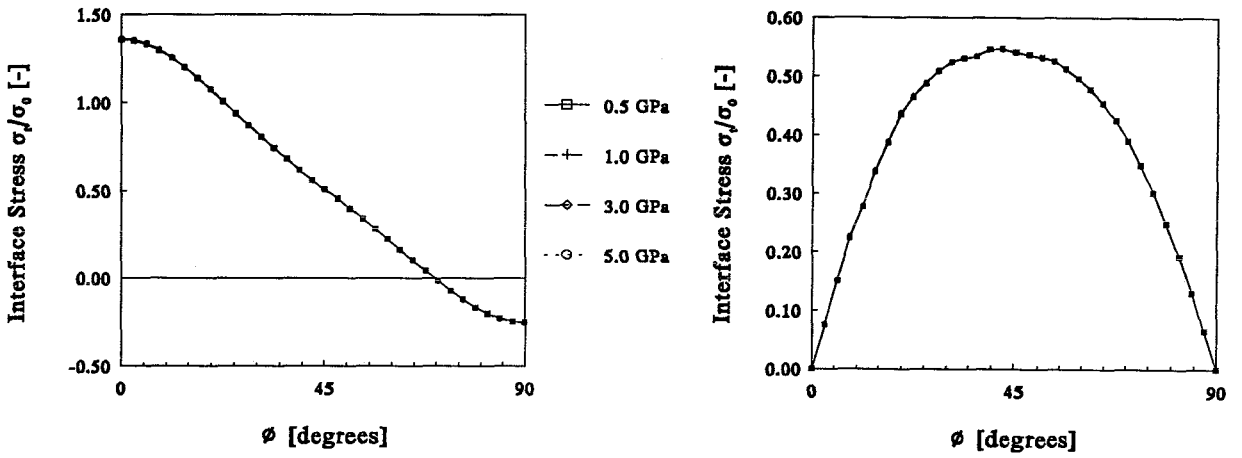

(a) Radial (b) Tangential

Figure 1.10: Normalized interface stresses along the fibre-matrix interface.

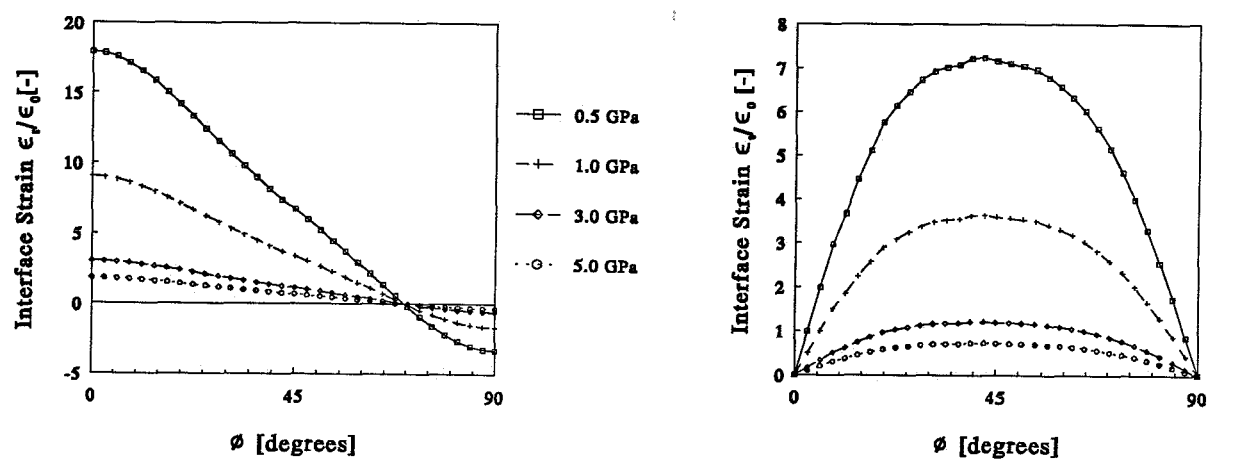

(a) Radial (b) Tangential

Figure 1.11: Normalized interface strains along the fibre-matrix interface.

The objective of the micromechanical modelling is to study debonding. However, before debonding can be studied, it is necessary to determine where and when debonding will initiate. Therefore a failure criterion has to be chosen. As mentioned before the maximum strain of the covalent bonds is thought to determine the strength of the interface. For the case where both tensile and shear strain are significant an interaction is required. A simple equation, based on energy, is the quadratic criterion

$$\left(\frac{\sigma}{\sigma_f}\right)^2 + \left(\frac{\tau}{\tau_f}\right)^2 = 1 \qquad (1.2)$$

where σ and τ are the normal and shear stress across the interface and σ_f and τ_f are the failure stresses for the interface in pure tension and shear. This criterion has been found to work well for predicting the interaction between transverse tension and shear stresses in composites at the macroscopic level [1,13].

Transposing equation 1.2 to a strain criterion with identical failure strains in pure tension and shear leads to

$$\varepsilon_r^2 + \varepsilon_t^2 = \varepsilon_{max}^2 \qquad (1.3)$$

where ε_r and ε_t are the radial (normal) and tangential (shear) strains in the interface. The maximum strain ε_{max} is assumed to be equal in tension and shear and is assumed to equal the maximum strain of the matrix. This failure criterion is used to describe failure in the interface. Figure 1.12 shows the failure criterion for the four different interface moduli, indicating where and when debonding initiates. According to this failure criterion, debonding will always initiate at $\phi = 0$.

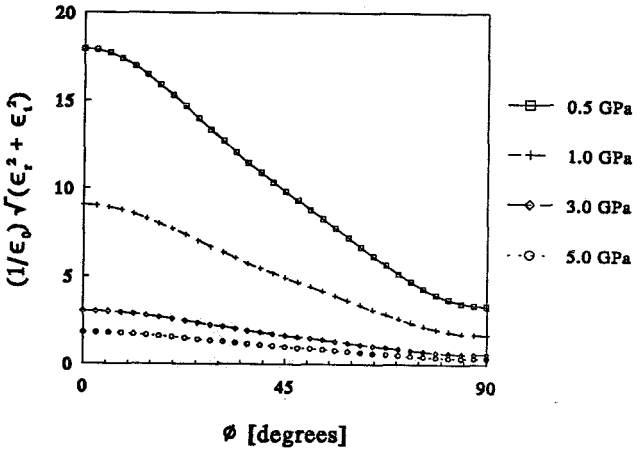

Figure 1.12: Failure criterion for initiation of debonding along the interface.

1.4 Analysis with debonding interface

To study debonding with the micromechanical model presented in the previous section, failure has to be incorporated in the interface. In transverse loading of the composite a crack in the interface initiates at ϕ=0, when the maximum strain is reached (provided that the interfacial bond strength is less than the matrix strength). The failure criterion, according to which failure is assumed to occur, was discussed in the previous section (formula 1.3). After the critical value of the criterion has been reached, both elements, transferring normal and shear stresses, fail simultaneously. There are two possible methods to describe debonding. First, incorporate the stress-strain curve of the interface in the model, failure included, and let debonding proceed automatically. Extensive software is needed for this method. Secondly, the elements where the critical value of the failure criterion has been reached are 'removed' by lowering the stiffness to zero. This method can be applied to any finite element program and has been reported before by Adams [14], who also used maximum strain as criterion for failure. Crack propagation is described by running a complete analysis for the presented model, reducing the modulus of the first interface element (at ϕ = 0), running a complete analysis for this situation and continue this procedure along the entire interface until all elements have been 'removed' and the composite has failed entirely. The propagation of the debonding will depend on the strain situation at the 'crack-tip' as a function of the normalized crack-length L_C. L_C = 0 and L_C = 1 correspond with an intact interface and total debonding along one side of the fibre respectively. Calculations have been performed and the results on the stress and strain as a function of the crack-length are shown in the figures 1.13 and 1.14 respectively.

After crack initiation occurred, both normal and shear stress and strain in the neighbouring element, being the present crack-tip, increase and lead to an unstable crack propagation. This is also shown in figure 1.15, where the failure criterion as a function of the crack-length is shown.

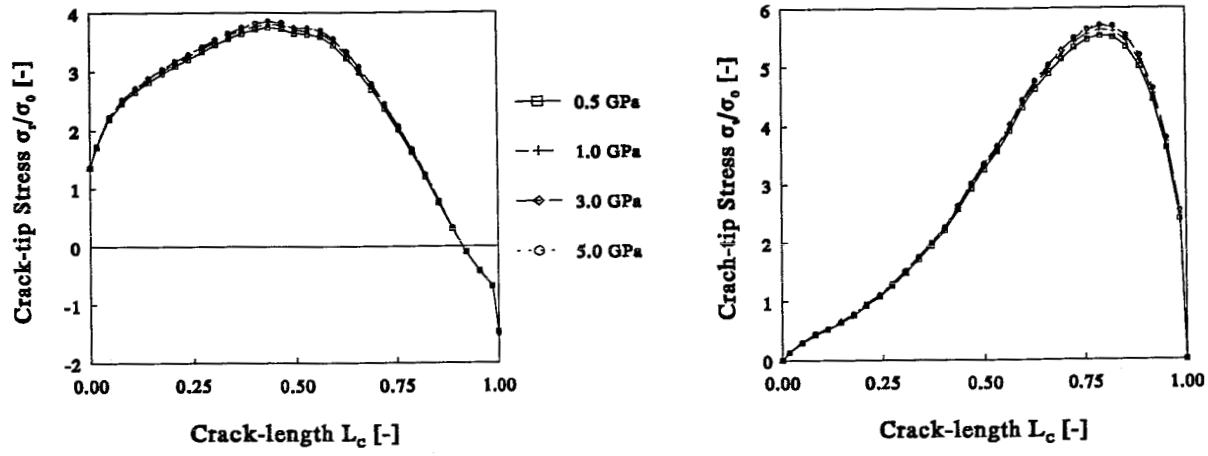

(a) Radial (b) Tangential

Figure 1.13: Normalized interface stresses at the crack-tip.

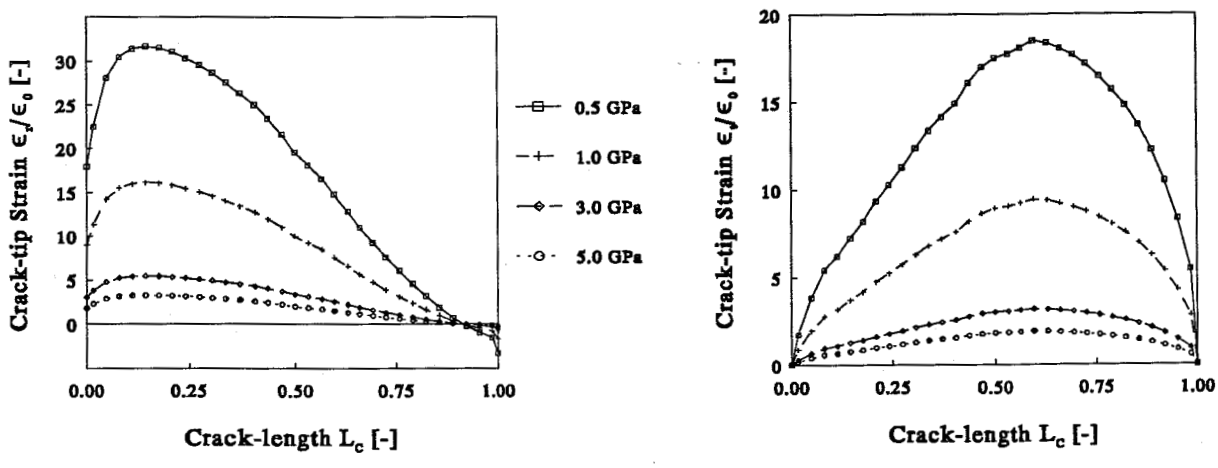

(a) Radial (b) Tangential

Figure 1.14: Normalized interface strains at the crack-tip.

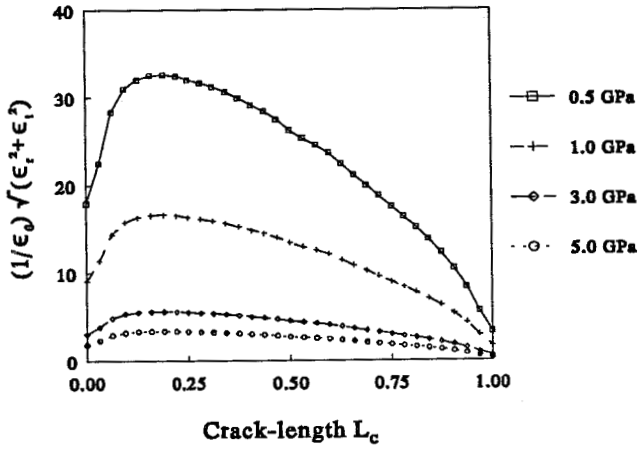

Figure 1.15: *Failure criterion for debonding as a function of crack-length L_C.*

Since stresses and strains at each increment (number of elements 'removed') are known, a stress-strain curve of the micromechanical model can be made for the four different interface moduli. These stress-strain curves are shown in figure 1.16. The values of the corresponding failure stress, are listed in table 1.6.

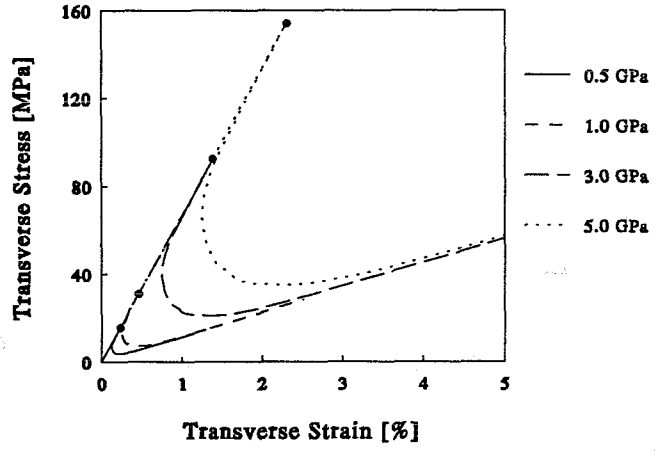

Figure 1.16: Transverse stress-strain curves of the basic cell.

All calculated stress-strain curves show linear elastic behaviour up to initiation of debonding. The initial transverse modulus of all the composites is the same, so that the stress and/or strain required to initiate debonding increases linear with the interface modulus and/or strength. After debonding is initiated, an unstable crack-growth starts since the debonding is able to propagate at a stress lower than the stress applied.

Table 1.6: Quantitative results of analysis with the four different interface properties.

Interface Modulus [GPa]	0.5	1.0	3.0	5.0
Interface Strength [MPa]	21	42	126	210
Composite Strength [MPa]	15.5	30.9	92.5	154
Composite Modulus [GPa]	6.61	6.65	6.67	6.67
Composite Strain to Failure [%]	0.234	0.465	1.39	2.31

In the case of high interfacial bond strengths, the composite will fail instantaneously after total debonding, because the matrix is not able to sustain the applied load. However, for weak interfacial strengths, the matrix might be able to sustain the applied load after complete debonding. Thus after unstable debonding, the crack will not propagate directly through the matrix material, but will leads to another linear stress-strain behaviour, with a much lower modulus, until matrix failure will occur. Hence, the transverse behaviour of the composites does not depend solely on the interface properties, but also on the composite stress to failure after debonding. This residual stress will be calculated in the next section.

1.5 Analysis with not bonded fibres

If there is no bonding at all at the interface, or if total debonding has occurred, which has not initiated matrix failure directly, the transverse strength of the composite is determined by the residual strength of the matrix. The model that should be used to describe this behaviour is a model with an interface transferring compressive stresses only. The micromechanical model described in the previous section can be used for this analysis, when the appropriate interface behaviour is incorporated (compressive stresses only).

The calculation is performed for an Apollo/epoxy composite, with an interface modulus of 0.5 GPa, because this phenomena occurs for weak interfaces only. Analysis resulted in the stress and strain states shown in figure 1.17 and the quantitative data listed in table 1.7.

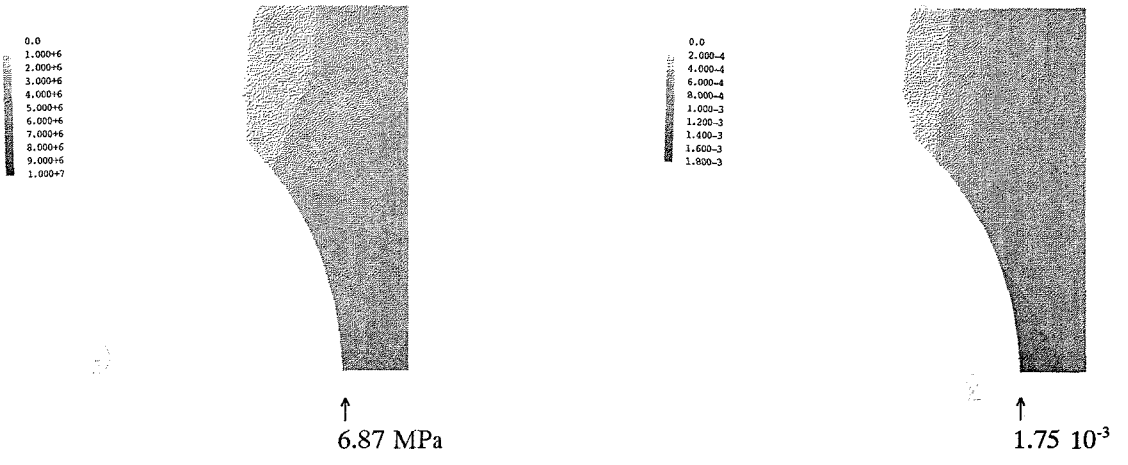

Figure 1.17: *Contour plots of principle stress and strain of Apollo/epoxy composite, no bonding at the interface, load 0.1% strain.*

Table 1.7: *Results of analysis on model with no bonding at the interface (transferring radial compressive stresses only).*

Material	Apollo/epoxy Composite
Transverse Modulus [GPa]	1.12
Max. Princ. Stress Conc. Factor [-]	6.12
Max. Princ. Strain Conc. Factor [-]	1.75
Composite Strain to Failure [%]	2.40
Composite Strength [MPa]	27.0

The lower limit for the predicted transverse strength is 27 MPa, whereas the corresponding critical interfacial bond strength is 37 MPa, meaning that if the interface strength is higher than 37 MPa, debonding will be catastrophic and lead to brittle failure. However, if the interface strength is below 37 MPa, the residual strength of the matrix is high enough to postpone complete failure, resulting in a tougher behaviour. The resulting stress-strain curves of the model composites are shown in figure 1.18. Interface strengths higher than 37 MPa lead to linear elastic behaviour up to failure and interface strengths lower than this critical value lead to a nonlinear stress-strain behaviour.

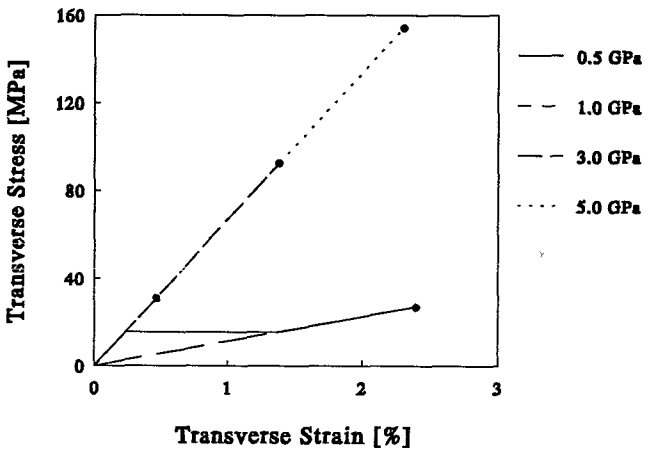

Figure 1.18: Stress-strain curves of the model composites.

1.6 Combination of the results derived from the micromechanical model

Figure 1.19 shows a combination of the results of this chapter. When the interface modulus (and interface strength) is varied, three different failure modes occur.

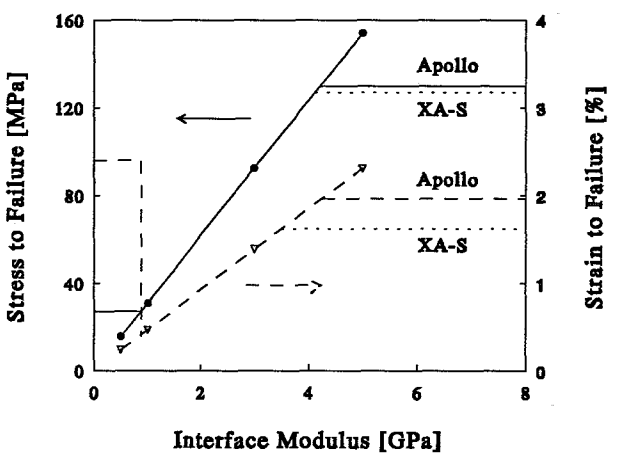

Figure 1.19: Predicted transverse strength and strain to failure.

When the interfacial bond strength equals zero, the transverse composite strength is matrix dominated, because releasing of the constituents will occur. Increasing the interfacial bond strength up to values lower than 37 MPa results in non-catastrophic debonding. After debonding has occurred, the matrix is able to sustain loads up to 27 MPa and consequently the transverse composite strength is still matrix dominated. When the interfacial bond strength is increased up to values between 37 and 177 MPa, catastrophic debonding will occur. In this region the transverse composite strength and strain to failure depend linearly on the interface modulus, because of the fact that the stress and strain state in the interface is not affected by the interface modulus. Further increase of the bonding at the interface results in matrix failure. The ultimate transverse composite strength is determined by the matrix. No improvement of the transverse strength can be achieved by improving the interfacial bond strength. In this case the matrix must be improved.

For validation of this predicted relation between interface strength and transverse composite strength and failure mode, experiments on carbon fibre reinforced epoxy composites are performed, which will be discussed in the next chapter.

2 Experiments

For verification of the numerical analysis, described in the previous chapter, it is necessary to determine the influence of the interface on the transverse properties experimentally. The experimental work presented consists of the mechanical characterization of uni-directional carbon fibre reinforced epoxy composites. In order to obtain a range in interface properties, composites with four intermediate modulus carbon fibres, different in the applied surface treatment level only, were tested. Since the predicted limits in bond strength have not been achieved within this range of experiments, additional experiments are performed on composites with silicon oil treated fibres (poor or no bonding) and high strength carbon fibres (good bonding), to verify the ultimate strengths predicted in the previous chapter. A fibre-matrix interface characterization is performed in order to relate the experimental results with the numerical analysis.

2.1 Materials

Two types of fibre are used, viz. Courtaulds Grafil type Apollo IM 43-750 intermediate modulus carbon fibres and Courtaulds Grafil type XA-S high strength fibres. Both types of fibre were supplied in 12k filament strands. The fibre diameters are 5.1 μm for the Apollo and 6.8 μm for the XA-S fibrtes.

Carbon fibres are prepared by carbonizing polyacrylonitrile fibres at approximately 1500°C. Sometimes the fibres are, after they have been carbonized, graphitized at temperatures up to 3000°C, to attain highly oriented structures (high modulus). After the carbon fibre is formed, the surface of the fibre is usually oxidized to increase the adhesion of the resin matrix to the fibre. The Apollo fibres have undergone a wet oxidative surface treatment, at four different levels, 0%, 10%, 50% and 100% of the standard surface treatment level, where 0% refers to the untreated fibres and 100% to the fibres subjected to the commercial treatment time. The XA-S fibre has also been surface treated. In addition to oxidative surface treatments, there may be additional treatments with finishes or sizings to enhance compatibility with the polymer matrix. The Apollo fibres were not finished or sized, the XA-S fibres contain an epoxy sizing.

The matrix material used, was a Ciba Geigy Araldite epoxy system (LY556/HY917/DY070).

2.2 Fibre-matrix interface characterization

In order to correlate the transverse properties of the composites to the interface properties, an interface characterization is necessary. Since the matrix material has not been changed in this investigation, characterization of the fibre surface will be sufficient to characterize the interface.

Oxidation treatments may change the surface of carbon fibres in several ways, including: increase in surface area, increase in surface ruggedness, reduction in longitudinal tensile strength, change in chemical functionality and/or reactivity, removal of surface layers and change in surface energy. Herrick [3] showed that the increase in chemical reactivity during an oxidative treatment is more important than a change in surface area for improving the shear strength of carbon fibre composites. Because the composite shear strength is related to the interfacial shear strength the same can be concluded concerning the interfacial shear strength. This conclusion has been confirmed by investigations of Scola and Brooks [3] and Drzal et al. [3]. Horie et al. [3] studied the interaction between oxidized carbon fibres and an epoxy resin and concluded that both hydrogen bonding and covalent bonding between the carbon fibre surface and the epoxy resin were important factors in the fibre-matrix adhesion. It is clear, that the fibre surface treatment influences the bonding mainly through the chemical reactivity of the fibre and in a lesser extend through other changes of the fibre surface. Fitzer et al. [3] reported that a good correlation was found between the amount of surface oxides and the improvement of composite mechanical properties. They postulated that "the bonding is mainly controlled by the chemical reaction between the carboxyl groups (COOH) on the fibre surface and the free hydroxyl groups of the phenolic resin". Naturally the reaction between carboxyl groups and epoxy resin is of a similar significance. This reaction is shown in figure 2.1.

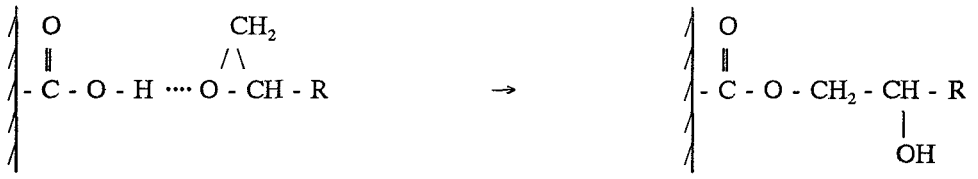

Figure 2.1: Reaction of carboxyl groups on fibre surface with epoxy resin.

The chemical composition of solid surfaces can be determined by a technique called X-ray Photoelectron Spectroscopy (XPS), also known as Electron Spectroscopy for Chemical Analysis (ESCA). Analysis on oxygen and carbon groups have been performed. Because the reactive groups all contain oxygen, the number of reactive sites is proportional to the surface oxygen concentration (O/C) determined by XPS. Appendix A contents background information on XPS and data on the experimental procedures and hardware settings.

The XPS measurements have been performed on a PHI (Physical Electronics) Model 550, ESCA/SAM system with a PHI Model 04-153 MgK_{α} X-ray source of 400 W (V = 10 kV, I = 40 mA). The data were acquired and analyzed with a PHI Multiple-technique Analytical Computer System (MACS). The base pressure in the sample chamber was about 3.10^{-8} Torr (4.10^{-6} Pa). The spectrometer has not been calibrated because the C1s peak occurred at 284.5 eV, which indicates that the apparatus was calibrated properly [15,16]. The surface oxygen concentrations of the four different Apollo fibres and the XA-S fibre (after removal of the epoxy sizing) have been determined. Two samples of each material have been analyzed, resulting in two survey scans and two sets of detail scans (multiplex) of each material. One set of each material is shown in § A.4 of appendix A. Quantitative results on oxygen concentrations have been determined three times for each multiplex set, using the peak area sensitivity technique. The results are listed in table 2.1.

Table 2.1: Fibre surface oxygen concentration.

Fibre Type	Surface Treatment Level (STL)	Oxygen Conc. (O/C) [%]	O/C curve-fit* [%]
Apollo	0%	4.55	4.30
	10%	5.98	6.37
	50%	10.48	10.46
	100%	11.80	11.80
XA-S	-	29.32	-

* Values according to formula (2.1)

Plotting the data for the oxygen concentration versus the surface treatment level shows an exponential relationship, see figure 2.2. Curve-fitting an exponential function on the data results in

$$O = 12.2 - 7.9e^{-\frac{STL}{33.4}} \qquad (2.1)$$

which is an accurate fit, indicated by the correlation value R = 0.9995. The maximum deviation of 7% occurs at the 10% surface treatment level. The good agreement with the exponential function indicates that the oxidative fibre surface treatment is a first order reaction.

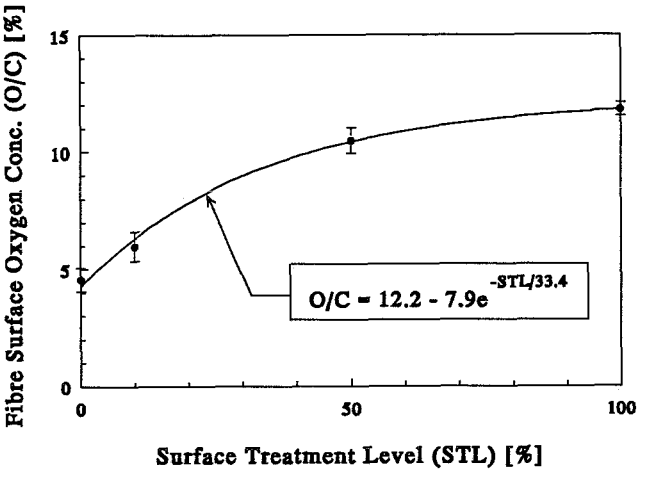

Figure 2.2: Measured fibre surface oxygen concentration and corresponding fit.

The survey scans, see § A.4, show three peaks, viz. the O1s peak (532 eV), the N1s peak (400 eV) and the C1s peak (284.5 eV). The O1s peak area clearly increases with increasing surface treatment level. The nitrogen peak area also increases. As mentioned before in § 2.2, the influence of nitrogen on the bonding at the interface can be neglected, since the chemical reaction producing the bond strength is based on carbon fibre surface oxides. The shape of the oxygen peak does not depend on the surface treatment level (see detail scans), indicating that the chemical composition of the fibre surface does not alter qualitatively.

The oxygen concentration at the XA-S fibre surface seems to be rather high. However values about 30% have been reported earlier by Hopfgarten [3] and Brewis et al. [3]. Due to the higher oriented structure in the Apollo intermediate modulus fibres, less reactive sites at the fibre surface are available and subsequently less oxygen is added. This explains the large difference in oxygen concentration between the two types of fibres. The peaks in the survey scan of the XA-S fibre at 103 and 153 eV represent the presence of silicium groups at the XA-S fibre surface. This has not been found on the Apollo fibre surfaces, and since no details on the fibre surface treatments are available, the reason for this difference in fibre surface can not be explained.

Shifts of elemental peaks occurring in detail scans generally are subscribed to changes in the chemical composition The minor shifts occurring in the measured detail scans, however, are too small to be subscribed to such a change and can therefore be neglected.

2.3 Sample preparation

Samples of uni-directional composites, that can be loaded transversely, are required, in order to obtain information on the influence of the interface properties on the transverse properties of the different composites. These samples have been manufactured using filament winding, shown in figure 2.3.

The fibre strands are impregnated in a preheated epoxy bath (at 40°C) and subsequently guided on a framework (figure 2.4 a), rotated by the driving unit at a selected speed. To reduce breakage of the fibres teflon guiders have been used. The guider-winding speed ratio controls the pitch of the strands at the frame. The strands are wound right next to each other up to a width of 80 or 160 mm, being the widths of the moulds used (figure 2.4 b,c).

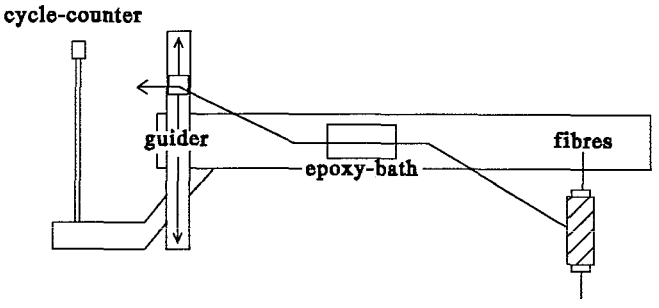

Figure 2.3: Filament winding equipment.

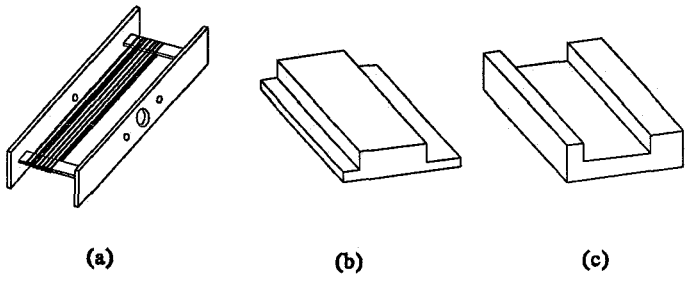

Figure 2.4: Framework and moulds.

A cycle-counter counts the number of strands wound on the framework. When a predetermined amount of fibres has been wound on the framework, the whole set-up is placed in a vacuum-oven at 0.5 bar and 60°C for 30 minutes, for degassing the epoxy resin. Subsequently, the framework with impregnated fibres is placed in the moulds with release coated mylar sheets at both sides of the framework, to ensure demoulding of the composite after curing. Small strips of certain thicknesses are placed at the sides of the moulds to control the thickness and consequently the fibre volume fraction of the manufactured composites. Precuring takes place in a press at 80°C during one hour at a pressure of 4 bar. Post-curing continues in an oven at 80°C for 4 hours and 140°C for 8 hours. The manufactured uni-directional composites are approximately 1.5 mm thick. 25 mm wide samples are cut from these plates using a diamond saw. Since polished specimens show higher strengths and less deviation in mechanical testing, all specimens are polished.

2.4 Silicon oil sizing of fibres

To extend the range of interface strengths, the untreated and the 100% treated fibres are sized with silicon oil, the latter to check the result of the applied silicon oil sizing. The same filament winding device (see figure 2.3) is used for the sizing procedure. The strands are now guided through a bath containing Rhodorsil 47V1000 silicon oil solved in n-hexane, through a tube with a hot air blower and wound on a glass framework. The framework with the silicon oil sized fibres is placed in an air-circulation oven at 80°C for 20 minutes to remove the n-hexane thoroughly. These sized fibres are used to make uni-directional composites as described in the previous section. The used weight percentages silicon oil on n-hexane are 0.1, 1 and 2.5% for the untreated fibres. The 100% treated fibres received a 1 weight% silicon oil sizing.

2.5 Mechanical testing of the composites

The samples are tested using transverse uni-axial tension and transverse three-point bending. It has been found, that three-point bending is the most sensitive test in determining the bonding in the interface and that premature failure, due to defects, is avoided. This has also been reported by Madhukar and Drzal [17]. Strength data are obtained using three-point bending. Uni-axial tension is used to characterize the matrix material and to study the influence of the silicon oil sizing of the fibres on the stress-strain behaviour of the composites. This twofold testing results from the sensitivity of carbon fibre reinforced epoxies to small defects inside the material, such as high local fibre volume fractions and inclusions of voids. Compared to uni-axial tension, the region of ultimate stress in three-point bending is very small, resulting in a much smaller probability of the presence of a strength affecting defect. On the other hand, the strongly localised stress in three-point bending results in a global stress-strain behaviour which is not sensitive to strain dependent stress strain behaviour. Three-point bending can only be used for linear behaviour. When non-linear behaviour occurs, uni-axial tension should be used.

During testing, damage evolution is monitored using acoustic emission. The system used is a PAC (Physical Acoustic Corporation) LOCAN AT 140 recorder, a PAC 1220 A pre-amplifier and a PAC R15 sensor. The gain and threshold have been set to 40 and 25 dB respectively. Appendix B contains background information on acoustic emission and data on experimental procedures and hardware settings.

Characteristic AE data for failure of both the composites and the pure epoxy are a single 95-98 dB hit, followed by about 30 hits with lower amplitudes. The following graphs have been studied:

- hits versus time (rate/cumulative)
- energy versus time (rate/cumulative)
- amplitude distribution: hits versus amplitude
- energy distribution: energy versus amplitude

2.5.1 Transverse uni-axial tension

2.5.1.1 Experiments

Tension tests are performed on a FRANK type 81565 tensile machine. The specimens are provided with tabs at both sides, in order to prevent failure at the specimen-grips. The dimensions of the composite specimens are approximately 80x24x1.5 mm, the tensile speed is set to 0.5 mm/min. The dimensions of the dog-bone shaped epoxy specimens are approximately 170x17x2.5, while the cross-section in the middle is approximately 11x2.5 mm. Tests on epoxy are performed using an extensometer and a transverse strain measuring device, to ensure the obtaining of accurate input data for the micromechanical FEM model.

2.5.1.2 Mechanical properties

Figure 2.5 shows a stress-strain curve of the epoxy. The stress-strain behaviour of the epoxy is not as linear as it should be (assumption in § 1.1). The quantitative uni-axial tension results of epoxy are listed, together with the three-point bending results, in table 2.4. Appendix C contains a Scanning Electron Micrograph of a fracture surface of pure epoxy. From this picture it can be seen that it fails in a brittle manner.

Figure 2.6 shows representative stress-strain curves of the tested composites. The quantitative results are listed in table 2.2. The results of the 2.5% silicon oil treatment only are listed here, since the other two levels (0.1% and 1%) did not show any significant changes in transverse behaviour with respect to the untreated fibres.

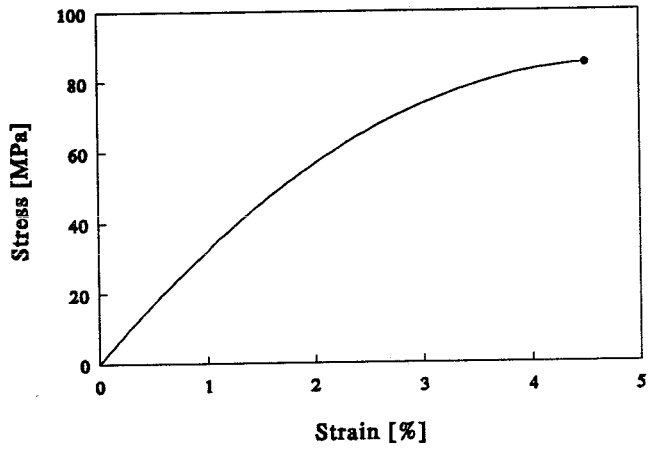

Figure 2.5: Uni-axial stress-strain curve of the Ciba Geigy epoxy.

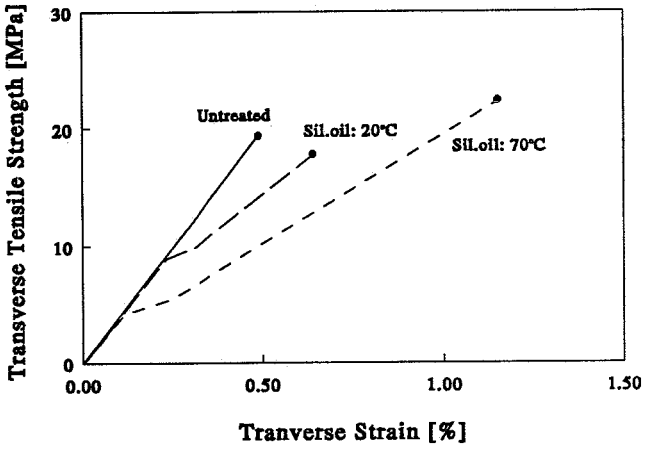

Figure 2.6: *Stress-strain curves of untreated Apollo fibre composites, with silicon oil sizing (at 25°C and 70°C) and without silicon oil sizing.*

Table 2.2: Uni-axial tension mechanical properties.

Material	Surface Treatment Level	Silicon Oil Sizing	σ_{max} [MPa]	E [GPa]	ε_{max} [%]
Apollo/ epoxy comp.	0%	-	19.4	4.56	0.49
	0%	2.5%	17.8	3.97	0.64

Since tensile experiments on the composites are performed without the use of an extensometer, results for displacement depending properties, like modulus and strain, are not accurate. The results are discussed together with the results of three-point bending in section 2.5.2.3.

2.5.1.3 Acoustic emission results

Acoustic emission results are difficult to interpret. Measurements on identical specimens, with identical stress-strain curves always show rather large deviation in acoustic emission. Representative AE measurements for all materials have been chosen. These are shown in § B.6 of appendix B. Quantitative results are listed in table B.4, where the influence of the silicon oil is shown. It appeared that 0.1% and 1% silicon oil treatment does not change the acoustic emission qualitatively and that it hardly affects the acoustic emission quantitatively. Unfortunately results of the 2.5% silicon oil treatment were not available. This is one of the reasons for discussing the AE results of tension and bending together in § 2.5.2.4. The other reason is the fact that trends in acoustic emission from tensile and flexural tests are similar. Quantitative AE results however differ significantly between the two test methods. Due to the larger volume being loaded in uniaxial testing, the amount of hits and the correlated cumulative energy are higher.

2.5.2 Transverse three-point bending

As mentioned before three-point bending has been used to determine the material properties. Due to the large displacement compared to tension, the transverse strain and modulus are determined more accurately. Also an automatic selection of specimens takes place. Poor specimens usually break in the vicinity of the loading nose instead of directly underneath the loading nose.

2.5.2.1 Three-point bending theory

The three-point bending tests have been performed according to ASTM D 790 standards. Figure 2.7 shows a three-point bending test set-up.

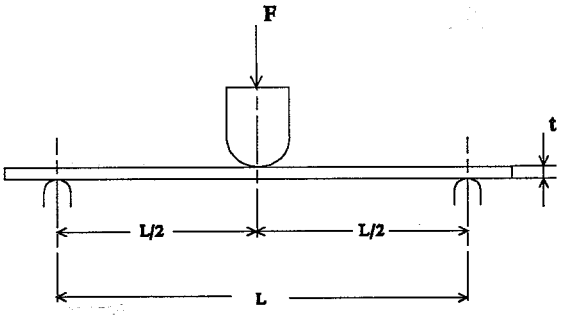

Figure 2.7: Three-point bending test set-up.

The tested specimen will fail directly under the loading nose as a result of the local maximum stress. The stress at this location consists of two components, viz. tensile and shear stress. Under the restriction of small displacements the tensile stress can be expressed as

$$\sigma = \frac{3L}{2wt^2}F \tag{2.2}$$

According to the ASTM standard, it is not allowed to perform a three-point bending test with a length-thickness ratio less than 16, which means that the shear stress always is less than 3% of the tensile stress and can therefore be neglected. The transverse Young's modulus can be calculated from

$$E = \frac{L^3}{4wt^3}\frac{\Delta F}{\Delta s} \tag{2.3}$$

where s is the displacement of the loading nose.

2.5.2.2 Experiments

The bending tests are performed on a FRANK type 81565 tensile machine. The dimensions of the specimens are approximately 80x24x1.5 mm, the loading nose speed is set to 5 mm/min. The length-thickness ratio used is 40 and the span L is 60 mm. The radius of the supports and loading nose is 1 mm and 3.5 mm respectively. The supports and loading nose are covered with a thin teflon foil in order to prevent acoustic emission to originate from friction at the support-sample contacts.

2.5.2.3 Mechanical properties

The stress-strain curves of the tested materials obtained in bending do not show any non-linearities and are therefore not presented here. The quantitative results obtained in bending are listed in table 2.3. Quantitative data for the mechanical properties of the used matrix material are listed in table 2.4. The strains to failure are determined by dividing the strengths by the corresponding Young's moduli.

Table 2.3: Three-point bending mechanical properties.

Material	Surface Treatment Level	Silicon Oil Sizing	σ_{max} [MPa]	E [GPa]	ε_{max} [%]
Apollo/ epoxy comp.	0%	-	38.9	5.83	0.67
	10%	-	73.1	6.17	1.18
	50%	-	82.7	6.50	1.27
	100%	-	92.8	6.10	1.52
	0%	2.5%	37.5	5.82	0.64
	100%	1%	64.4	5.64	1.14
XA-S/ep.	-	-	111	6.88	1.61
Epoxy	-	-	137	3.28	4.18

Table 2.4: Material parameters epoxy.

Test method	E [GPa]	σ_{max} [MPa]	ε_{max} [%]	ν [-]
Uni-axial tension	3.2	85	4.5	0.37
Three-point bending	3.3	137	4.2	-

Influence of fibre surface treatment

The transverse composite modulus appears to be independent of the fibre surface treatment level. However, the surface treatment does increase the composite strength, see figure 2.8, and this increase appears to be in a two stage mechanism. One possible explanation, reported before by Drzal et al. [3] is the following. During the fibre surface treatment first, an outer, weak, defect-laden fibre surface layer is removed. This results in a surface which is capable of supporting higher loads. Secondly, surface oxygen groups are added which can interact with the polar epoxy matrix contributing to higher fibre-matrix interfacial strength.

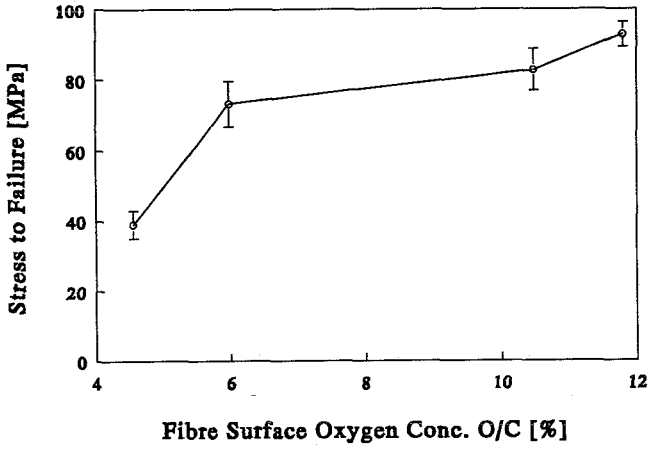

Figure 2.8: Influence fibre surface treatment on stress to failure.

Due to the surface treatment, the transverse strength of the composites increases. However, the strength of the 100% treated fibre composites has not reached a maximum yet. Scanning Electron Micrographs of fracture surfaces of the four different Apollo fibre composites show that although the bonding at the interface must have been increased as a result of the fibre surface treatment, the failure mode remained debonding in the interface. SEM micrographs of a fracture surface of XA-S fibre composite show matrix dominated failure (see appendix C). Consequently, a further improvement of the bond strength will not lead to a higher transverse composite strength, since the ultimate strength has been achieved.

Influence of silicon oil sizing of the fibres

Comparison of the properties of composites based on 100% treated fibres with and without silicon oil sizing shows a decrease in the composite strength from 92.8 to 64.4 MPa as a result of the sizing. Apparently, the silicon oil partly restrains the fibre and matrix to bond, probably by shielding a part of the reactive sites present at the fibre surface. This results in a lower interface strength and consequently a lower transverse composite strength.

The silicon oil sizing of the 0% treated fibres does not affect the mechanical properties significantly. However, the tensile stress-strain curves of the 2.5% silicon oil treated fibres show a significant change, viz. a knee at about 9 MPa. This knee occurs at a lower stress, about 4 MPa, when the testing temperature is increased from room temperature to 70°C (see figure 2.6), indicating that the change in modulus originates from the presence of thermally induced residual stresses due to fabrication. This knee has been reported before for composites with not bonded fibres [6]. Due to the matrix shrinkage by cooling from cure temperature to room temperature the interface is in normal compression initially. Superimposing of a tensile stress on the interface, depending linearly on the applied strain, results in a stress-strain behaviour of a composite with perfectly bonded fibres and a composite without bonding divided by a transition region, being the knee in the stress-strain curve. This knee, together with the fact that no extra acoustic emission was recorded at the knee, indicates that the fibres are not bonded to the matrix at all. SEM micrographs of the fracture surface of the 2.5% silicon oil treated fibre (appendix C), also shows that the fibres are not well bonded to the matrix.

2.5.2.4 Acoustic emission results

Quantitative AE results in three-point bending are listed in table 2.5 and shown in figure 2.9.

Table 2.5: Acoustic emission results of three-point bending.

Material	Surface Treatment Level	Silicon Oil Sizing	# Hits Before Failure	Total # Hits	AE Energy Before Failure	Total AE Energy
Apollo/ epoxy comp.	0%	-	8.5	33	163	12813
	10%	-	69	105	1414	14520
	50%	-	118	147	3218	18190
	100%	-	128	162	2872	14460
	0%	2.5%	28	55	840	9750
XA-S/ep. comp.	-	-	38	74	733	8617

Potential sources for acoustic emission in transversely loaded uni-directional composites generally are fibre splitting, matrix cracking and debonding. Scanning Electron Micrographs showed that no fibre splitting occurred in the tested composites. Uni-axial tensile tests on epoxy showed that matrix cracking results in a single 97 dB hit (figure B.6, appendix B). This hit has been observed in every test on any material as the hit at failure. From the fact that epoxy fails in a brittle manner, and that a micro-crack initiates global failure immediately, the conclusion can be drawn that the series hits before failure in figure B.6 (a) and (b) are due to noise (specimen grips, etc.). This means that noise in this context consists of peaks with a maximum of 5 hits. These hits are low energetic compared to the matrix cracking energy and have low amplitudes, in the range of 25 to 40 dB. The regular contour of the cumulative hits versus time plot (figure B.6 (b)) confirms this conclusion.

Influence of fibre surface treatment on acoustic emission

Both uni-axial tension and three-point bending tests on the different composites show equal contours of hits versus time plots. These plots are given in § B.6. Acoustic emission data of the tested composites show a similar contour as the data of the tested epoxy. Before failure a series of low energetic hits occurs with amplitudes in the range 25-40 dB and failure is denoted by a single hit with an amplitude of 97 db, followed by a series of approximately 30 low energetic hits.

Two trends in the acoustic emission results as a function of fibre surface treatment level are evident. First, the number of recorded hits before failure increases with increasing fibre surface treatment level (see figure 2.9), and second, a shift to higher amplitudes takes place (see § B.6, figure B.7 to B.10). The increasing number of hits is caused by the increase in data-acquisition time as a result of an increase in strength. Both noise, which is presumed to be more or less constant in time, and debonding, initiated at local defects, generate more hits. The fact that a shift to higher amplitudes takes place can also be explained by the increase in strength of the composites. The local stress relaxations due to micro-failure, like debonding, occur at higher stresses, resulting in higher stress wave amplitudes and higher energy (see figure 2.10). In the amplitude distributions of the composites based on the 50% and 100% treated fibres, where this shift has taken place, these two sources can even be distinguished. Noise: amplitudes in the range 25 to 40 dB, debonding: amplitudes in the range 40 to 55 dB (see figures B.13 (e),(f) and B.14 (e),(f)).

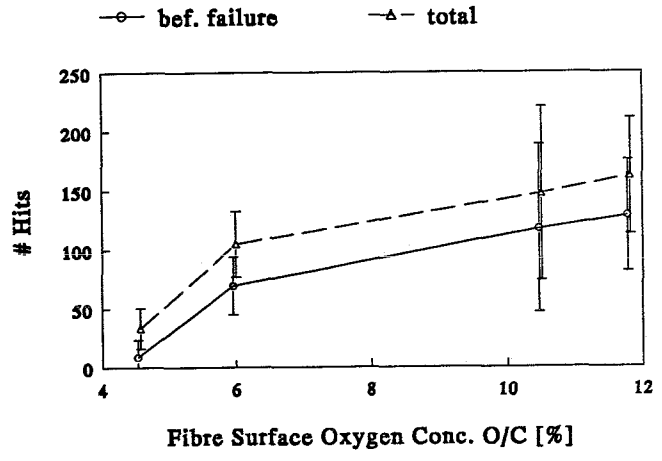

Figure 2.9: Influence of fibre surface treatment on number of acoustic emission hits in bending.

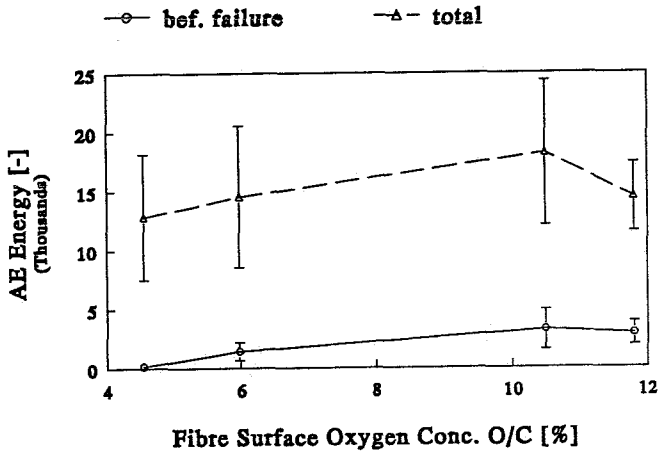

Figure 2.10: Influence of fibre surface treatment on acoustic emission energy in bending.

The change in failure mode from debonding to matrix failure for the composites with Apollo fibres and the composites with XA-S fibres respectively, has also been noticed in the acoustic emission results. Compared to the composites with 100% treated Apollo fibres few hits before failure have been recorded in the tests on composites with XA-S fibres. If there would not have been a change in failure mode, more hits should have been recorded.

3 Confrontation of numerical and experimental results

The previous chapters both described the influence of the interface on the transverse properties of carbon fibre reinforced epoxy composites. To validate the micromechanical modelling presented in chapter 1, the numerical analysis is confronted with the experimental results of chapter 2. The numerical analysis predicted the transverse behaviour of composites, for every possible interface strength. The interface properties were found to affect the composite properties in a great extent and the relation between interface properties and transverse composite properties has been determined. The experiments, actually performed to verify this relation, also show large varieties in transverse properties when the interface is altered physically.

The number of reactive sites at the carbon fibre surface determines the interface properties. This is the basis for both the numerical analysis and the experiments and the reason why these two separate studies can be compared. Both the numerical analysis and the experiments account for the real number of covalent bonds in the interface, viz. by the interface modulus and the oxygen concentration at the carbon fibre surface respectively. Consequently, the transverse composite properties must depend on the interface modulus and the oxygen concentration in a similar way.

The influence of the interface properties on the three main transverse properties, modulus, strength and strain to failure, are discussed below.

3.1 The influence of the interface properties on the transverse composite modulus

Both the numerical and experimental analysis displayed a transverse composite modulus which does not depend on the interface properties. The quantitative agreement is reasonable and is shown in table 3.1.

Table 3.1: Comparison of numerical and experimental results of transverse composite modulus.

Analysis Type	Numerical Analysis	Experimental Analysis
Apollo/epoxy Transv. Modulus [GPa]	6.65	6.15
XA-S/epoxy Transv. Modulus [GPa]	7.83	6.88

The modulus of the composite with not bonded fibres has not been measured, but from figure 2.6 it can be seen that this modulus is not much lower than the initial modulus, which is the modulus for composites with well bonded fibres. The reason for this quantitative disagreement is probably due to the presence of thermally induced residual stresses, restraining the fibres to release along the entire interface. Due to these stresses the transverse modulus of the real composite will be higher, because less releasing of the fibres from the matrix occurs than is predicted with the micromechanical model.

3.2 The influence of the interface properties on the transverse composite strength and strain to failure

The numerical analysis shows a clear relation between the interface strength on the transverse composite strength and strain to failure. Three distinct regions were found, viz. a) no or poor bonding, resulting in fibres releasing from the matrix in the case of no bonding and non-catastrophic debonding in the interface in the case of poor bonding, b) intermediate bonding, resulting in failure in the interface showing a linear relation between composite strength and strain to failure and interface strength, and c) good bonding, where failure initiates and propagates in the matrix material. These three distinct regions in interface properties have been found in the experimental results derived from three-point bending too. Composites with untreated

Apollo fibres sized with 2.5% silicon oil showed no bonding in the interface, determining the lower limit in transverse composite strength. The composites with surface treated Apollo fibres showed an evident increase in transverse composite strength with increasing surface treatment level. Although the increase in transverse properties due to the surface treatment was more than a factor 2, the ultimate strength was not reached, since even the standard (100%) treated Apollo fibres did not display a bonding high enough to sustain the applied load until matrix failure was initiated. In order to achieve this 'perfect' bonding, the range of experiments was extended to the application of high strength fibres as reinforcement for the epoxy. This composite showed good bonding, resulting in failure of the matrix before debonding was initiated. Figure 3.1 and 3.2 show a fit of the numerical results on the experimental data.

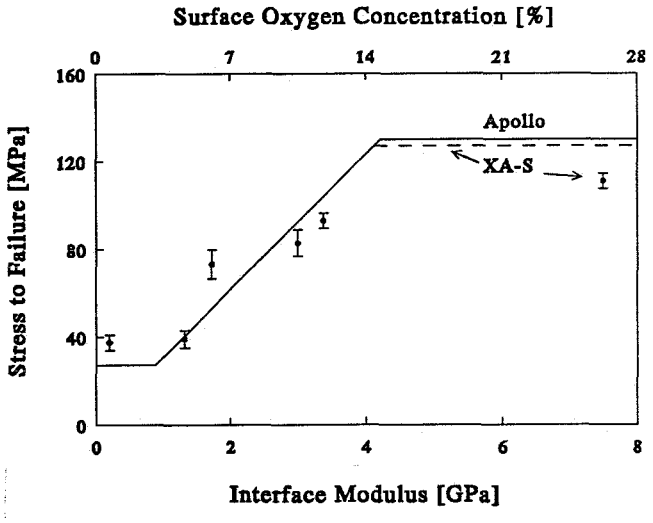

Figure 3.1: Numerical and experimental results of the influence of the interface on the transverse composite strength.

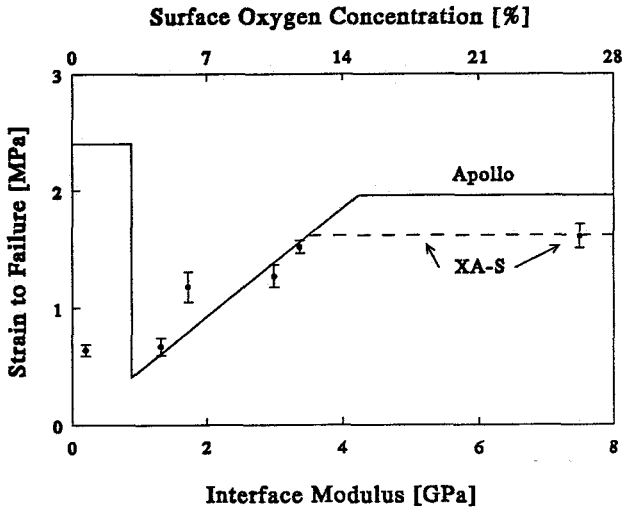

Figure 3.2: Numerical and experimental results of the influence of the interface on the transverse composite strain to failure.

The influence of the oxygen concentration and the influence of the interface modulus are similar. A good qualitative and a reasonable quantitative agreement is obtained between the numerical relation and the experimental results, showing that the model is quite accurate. The limits to the transverse strength are not predicted very well. The predicted value for the composite with not bonded fibres is too low. A possible

reason is that thermally induced residual stresses due to matrix shrinkage after curing has not been incorporated in the model. These residual stresses are beneficial to the transverse strength [1], resulting in higher measured values for strength. This theory, however, does not explain the difference in predicted and experimental data for the perfect bonded fibres, where a deviation in the opposite direction occurs. Apart from this unexplained difference between predicted and experimental results, it still may be concluded that the numerical analysis predicts the transverse composite strength reasonably well.

For the results on the strain to failure a similar conclusion can be drawn: Except for the composite with not bonded fibres, reasonable accurate results are achieved. The reason for this rather large deviation is probably the presence of thermally induced stresses, These stresses restrain the fibres to release entirely from the matrix, resulting in a lower strain to failure for the real composites.

4 Conclusions

Micromechanical models can be used to investigate the transverse behaviour of uni-directional composites. An interface can be introduced to investigate the influence of the interface properties on the transverse properties of the composite. Combination of experimental and numerical results show fairly good agreement.

Micromechanical modelling of the fibre-matrix interface should include the transfer of both tensile and shear stresses across the interface to obtain a physically correct model.

Both in the numerical and the experimental analysis, three distinct regions in the interface properties were found, viz.:

a) No bonding at all or poor bonding, resulting in fibres releasing from the matrix in the case of no bonding and non-catastrophic debonding in the interface in the case of poor bonding. The strength and strain to failure are determined by the matrix.

b) Intermediate bonding, resulting in catastrophic debonding, showing a linear relation between interface modulus (or strength) and composite strength and strain to failure. This is due to the fact that the stress and strain state in the composite is not affected by the interface properties in this region.

c) Good bonding, where failure initiates and propagates in the matrix material. The transverse strength and strain to failure are, again, determined by the matrix.

The transverse composite modulus is not affected by the interface properties. This has been found both in the experiments and in the numerical analysis. The latter, for reasonable interface moduli, i.e. interface moduli close to the matrix Young's modulus only. Thus it can be concluded that the modulus of the real interface is close to that of the matrix.

In carbon/epoxy composites the interface strength is determined by the level of surface treatment, which can be characterized by the oxygen concentration at the fibre surface. In the translation of numerical results to experimental results the oxygen concentration at the fibre surface and the interface modulus, used in the numerical analysis, play a key role.

Recommendations

In order to obtain better agreement between experiments and numerical analyses, thermally induced residual stresses due to matrix shrinkage after curing should be included in the micromechanical model.

Use a linear epoxy. Linear elastic behaviour of materials is standard in any FEM program. Moreover, a linear epoxy is easier to incorporate in a study on the influence of the interface properties, since any other difficulty, like influence of nonlinear matrix behaviour, should be avoided. For instance when different interface properties lead to different stress-strain states in the matrix material, the influence of the local nonlinear behaviour and the influence of the interface properties could not be distinguished from the global stress-strain behaviour.

For correct predictions of the transverse strength, a proper failure criterion should be available. Therefore the used failure criterion should be verified by performing different tests on the epoxy, and maybe adapted or even replaced.

If debonding initiates at stresses below the lower limit of the transverse composite strength, all fibres are expected to debond entirely. Consequently the energy absorbed in the material will be relatively high. The potentials of these composites with poor bonding for energy absorption in tension should therefore be investigated.

References

[1] M.R. Wisnom, "Factors Affecting the Transverse Tensile Strength of Unidirectional Continuous Silicon Carbide Fibre Reinforced 6061 Aluminum", J. of Comp. Mater., **24**, p. 707-726 (1990).

[2] J.D. Achenbach and H. Zhu, "Effect of Interfacial Zone on Mechanical Behavior and Failure of Fibre-Reinforced Composites", J. of Mech. Phys. Solids, **37**, 3, p. 381-393 (1989).

[3] T.F. Cooke, "High Performance Fibre Composites with Special Emphasis on the Interface", J. of Pol. Eng., **7**, 3, p. 197-254 (1987).

[4] J.M.M. de Kok, "The Influence of the Interface on the Transverse Properties of Carbon Fibre Reinforced Composites", CIP-DATA Kon. Bibliotheek, Den Haag, ISBN 90-5282-182-8 (1992)

[5] D.F. Adams and D.R. Doner, "Transverse Normal Loading of a Unidirectional Composite", J. of Comp. Mater., **2**, 1, p. 152-164 (1967).

[6] R.P. Nimmer, R.J. Blankert, E.S. Russell, G.A. Smith and P.K. Wright, "Micromechanical Modeling of Fibre/Matrix Interface Effects in Transversely Loaded SiC/Ti-6-4 Metal Matrix Composites", J. of Comp. Techn. & Research, **13**, 1, p. 3-13 (1991).

[7] J.D. Achenbach and H. Zhu, "Effect of Interphases on Micro and Macromechanical Behavior of Hexagonal-Array Fibre Composites", J. of Appl. Mech., **57**, p. 956-963 (1990).

[8] D.F. Adams and S.W. Tsai, "The Influence of Random Filament Packing on the Transverse Stiffness of a Uni-directional Composites", J. of Comp. Mater., **3**, 3, p.368-381 (1969).

[9] D.F. Adams, "Micromechanical Predictions/Experimental Correlations of the Influence of the Interface on the Mechanical Properties of a uni-directional composite", ICCI-1, may 27-30 1986, p. 351-365.

[10] H.H. Fong, MENTAT manual, Marc Analysis Research Corporation, Palo Alto, CA 94306, USA, 1989.

[11] Technical Data Sheet for Grafil Continuous Carbon Fibres, Courtaulds Grafil data Ltd, Coventry, Great Britain.

[12] H.H. Fong, MARC manual, Marc Analysis Research Corporation, Palo Alto, CA 94306, USA, 1989.

[13] Z. Hashin, "Failure Criteria for Unidirectional Fibre Composites", J. of Applied Mechanics, **47**, p. 329-334 (1980).

[14] D.F. Adams, "A Micromechanical Analysis of Crack Propagation in an Elastoplastic Composite Material", Fibre Science and Technology, **7**, p. 237-256 (1974).

[15] A. Proctor and P.M.A. Sherwood, "X-ray Photoelectron Spectroscopic Studies of Carbon Fibres-III", Surface and Interface Analysis, **4**, 5, p. 212-219 (1982).

[16] D. Briggs, "Chapter 9; Applications of XPS in Polymer Technology", Practical Surface Analysis, p. 359-395 (1983).

[17] M.S. Madhukar and L.T. Drzal, "Fibre-matrix Adhesion and Its Affect on Composite Properties: II. Longitudinal (0°) and Transverse (90°) Tensile and Flexure Behaviour of Graphite/Epoxy Composites", J. of Comp. Mater., **25**, p.958-991, (1991).

[18] K. Siegbahn, "Alpha, beta and gamma-ray Spectroscopy", North Holland, Amsterdam (1965).

[19] C. Nordling, E. Sokolowski and K. Siegbahn, Ark. Fys, **13**, 483 (1958).

[20] W.P. Mason, H.J. McSkimin, W. Sockley, "Ultrasonic Observations of Twinning in Tin", Physical Review, **73**, 10, p. 1213-1214 (1948).

[21] J. Kaiser, "Information and Conclusion from Measurements and Noise in Tensile Stressing of Metallic Materials", Archir für die Eisenhuettenwesen, **24**, 12, p. 43-45 (1953).

[22] A.D. Rustidge, "A Study on the Fracture Behaviour of Carbon and Polyethylene Hybrid Composites with the Aid of Acoustic Emission Technique" (in dutch), Internal Report TUE Holland, Department of Chemistry, Division Polymer Technolgy (march 1990).

[23] 8900 Locan AT User's Manual, Rev. 1, Physical Acoustics Corporation, P.O. Box 3135, Princeton, New Jersey, 1987.

Appendix A. X-ray Photoelectron Spectroscopy (XPS)

X-ray Photoelectron Spectroscopy (XPS), also known as Electron Spectroscopy for Chemical Analysis (ESCA), is a widely-used analytical technique for investigating the chemical composition of solid surfaces. The solid to be investigated is irradiated with monoenergetic x-rays in high vacuum, resulting in emission of electrons. The emitted electrons are sorted by their kinetic energy and so a spectrum is obtained, which is a plot of the number of emitted electrons per energy interval versus their kinetic energy. Each element has a unique spectrum, and the spectrum of a mixture approximately is the sum of the individual elemental spectra. So identifications of the chemical composition of the solid can be derived from the exact position of the peaks. Quantitative data can be obtained from the peak heights or areas. The detected electrons originate from the top few atomic layers only, while the investigated area approximately measures 10 mm^2.

A.1 Evolution of XPS

Although the first photoemission studies began in the early part of this century, application of this technique to study the chemical composition of solid surfaces did not begin until the 1950's when a research group directed by Siegbahn [18] made precise energy measurements under x-ray irradiation. In a series of publications this research group showed that XPS could be used to identify and distinguish elemental species, [19]. These discoveries led to the advent of commercial XPS systems in the late 1960's and early 70's.

A.2 Theory

Photons, emerged by the x-ray source, have limiting penetrating power in a solid, in the order 1 to 10 microns. They interact with the atoms in this surface region by the photoelectric effect, causing electrons to be emitted. Probabilities of interaction of the electrons with matter far exceed those of the photons, so while the path length of the photons is of the order of micrometers, that of the electrons is of the order of tens of Ångstroms. Thus, while ionization occurs to a depth of a few micrometers, only those electrons that originate within nanometres below the solid surface can leave the surface without energy loss. It is these electrons which produce the peaks in the spectra. The emitted electrons have kinetic energies given by

$$KE = h\nu - BE - \phi_S \qquad (A.1)$$

where hν represents the photon energy, BE the binding energy of the atomic orbital from which the electron originates, and ϕ_S the spectrometer work function, accounting for the potential the electron has to overcome to leave the material and to enter the electron multiplier. The binding energy may be regarded as an ionization energy of the atom for the particular shell involved. Since there is a variety in possible ions from each type of atom, there is a corresponding variety of kinetic energies of the emitted electrons. The electrons leaving the sample are detected by an electron spectrometer according to their kinetic energy. The analyzer normally is operated as an energy window, accepting only those electrons having a kinetic energy within the range of this fixed window, referred to as pass energy. If the photon energy, which depends on the x-ray source, is known, and the spectrometer work function has been determined, a plot of the number of emitted (detected) electrons versus the corresponding binding energy can be made. An example of a survey scan, measured for a relatively large range in binding energy, is shown in figure A.1. Usually interest in the specific elements exists, leading to a detail scan, also called multiplex, which is measured for a small range in binding energy and at a higher resolution. Examples are shown in figure A.2.

For many XPS investigations, it is important to determine the relative concentrations of the various constituents. Methods for quantifying XPS measurements have been developed, utilizing peak height and peak area sensitivity factors, the latter being the more accurate one.

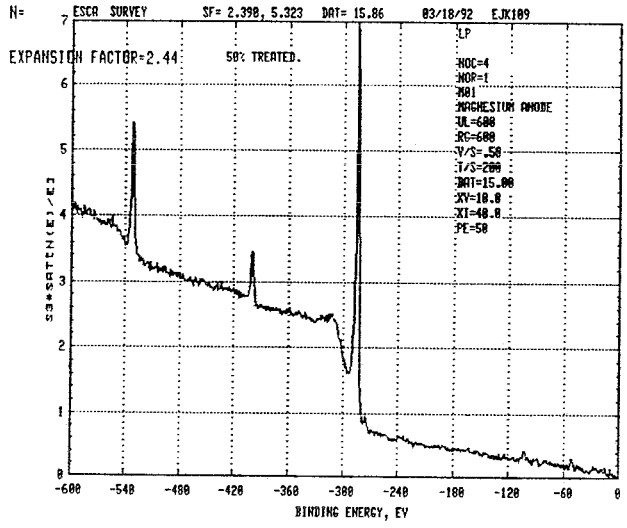

Figure A.1: Survey scan of 50% treated Apollo carbon fibre.

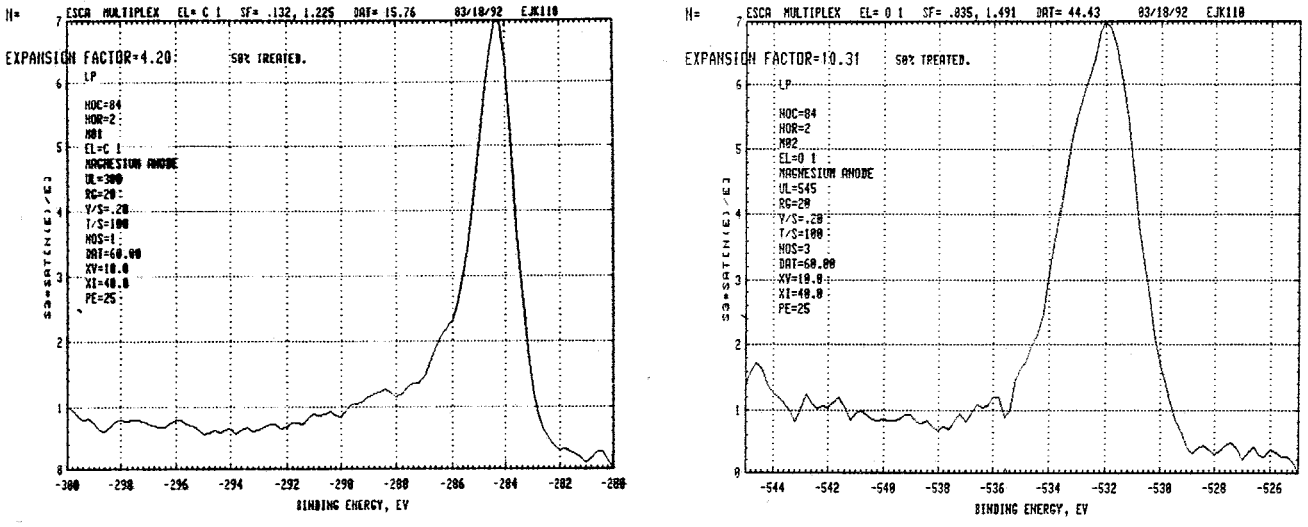

a) Carbon C1s b) Oxygen O1s

Figure A.2: Multiplex of carbon and oxygen of 50% treated Apollo carbon fibre.

A.3 Experiments

The chemical composition of the surface of five carbon fibres are characterized using XPS technique. Four Apollo fibres, different only in the level of surface treatment, and one XA-S fibre are investigated. Analysis on oxygen and carbon groups has been performed. Because the reactive groups all contain oxygen, the number of reactive sites is proportional to the surface oxygen concentration (O/C) determined by XPS.

A.3.1 Preparing and mounting samples

Since the information from XPS measurements originates from the top few atomic layers, contaminants and sizings have to be removed. The epoxy sizing of the XA-S fibres is removed by solving the epoxy in acetone. Clean strands are wound on a small aluminum plate, which can be mounted on the sample probe directly. Attention has to be paid to close packing of the fibres to prevent any signal to originate from the aluminum. Whenever this is doubted, a survey scan of the aluminum plate should be made before analyzing the samples to be able to point out any (unwanted) contribution of the aluminum. It was found that no contribution of the aluminum occurred when the strands had been wound three times on the aluminum plate.

A.3.2 XPS equipment and settings

The XPS measurements have been performed on a PHI (Physical Electronics) Model 550 ESCA/SAM system with a PHI Model 04-153 MgK_{α} X-ray source of 400 W (V = 10 kV, I = 40 mA). The data were acquired and analyzed with a PHI Multiple-technique Analytical Computer System (MACS). Figure A.3 shows the used XPS equipment schematically.

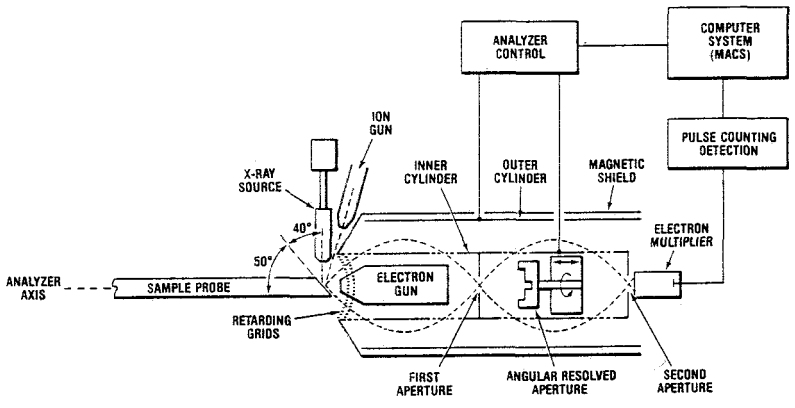

Figure A.3: Schematic representation of the PHI Model 550 ESCA/SAM system.

Because XPS is a surface analyzing technique, measurements must be performed in an inert environment. This environment is provided in ultra high vacuum (UHV) systems. The base pressure in the sample chamber was about 3.10^{-8} Torr (4.10^{-6} Pa). The spectrometer has not been calibrated because the C1s peak occurred at 284.5 eV, which indicates that the apparatus was calibrated properly [15,16].

The most important hardware settings are listed in table A.1. Other settings are listed on the survey and multiplex scans in figure A.1 and A.2.

Table A.1: Hardware settings.

	survey	multiplex
Data-aquisition time [min]	16	60
Pass energy [eV]	50	25
Resolution [eV/step]	0.5	0.2

A.4 Results

The materials are scanned twice. One set of survey and multiplex scans per material is included in this section. The figures A.4, A.5 and A.6 show survey scans, and detail scans of carbon and oxygen respectively. Quantitative analysis is performed three times per set of scans, resulting in the oxygen concentrations (O/C) which are listed in table 2.1 of section 2.2.

Figure A.4: *Survey scans of:* *- Apollo IM 43-750: 0, 10, 50 en 100% treated carbon fibres*
- XA-S high strength carbon fibre.

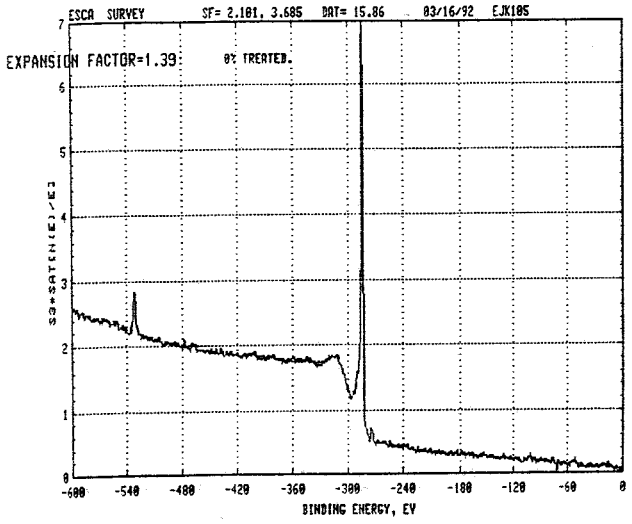

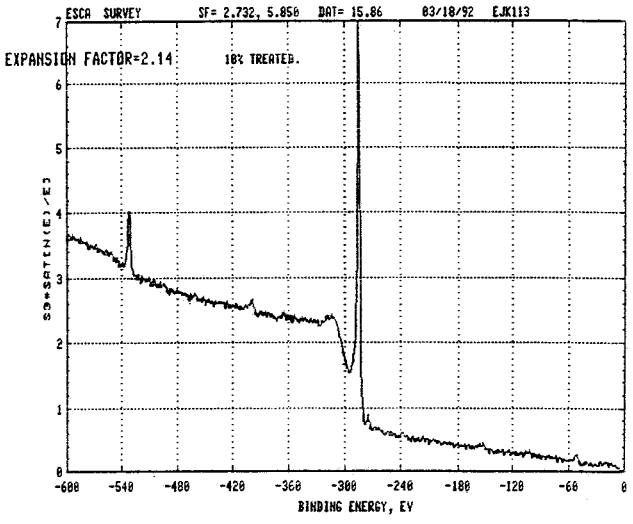

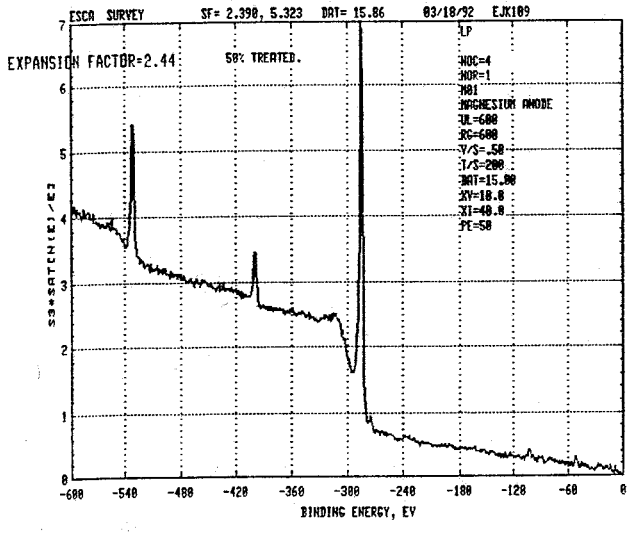

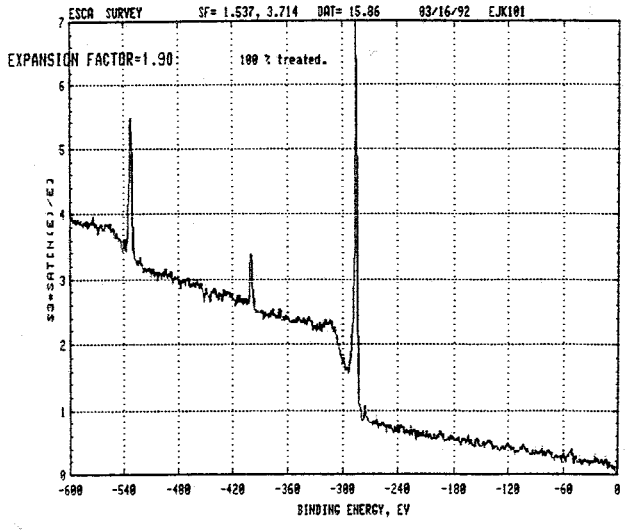

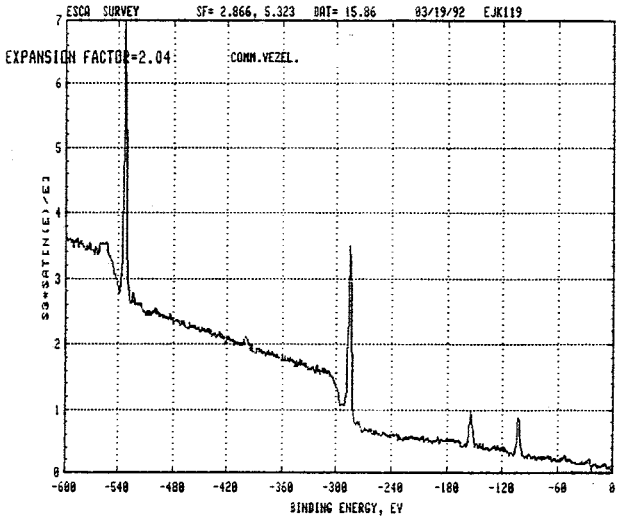

Figure A.5: *Detail scans of carbon C1s peak of:*
- *Apollo IM 43-750: 0, 10, 50 en 100% treated carbon fibres*
- *XA-S high strength carbon fibre.*

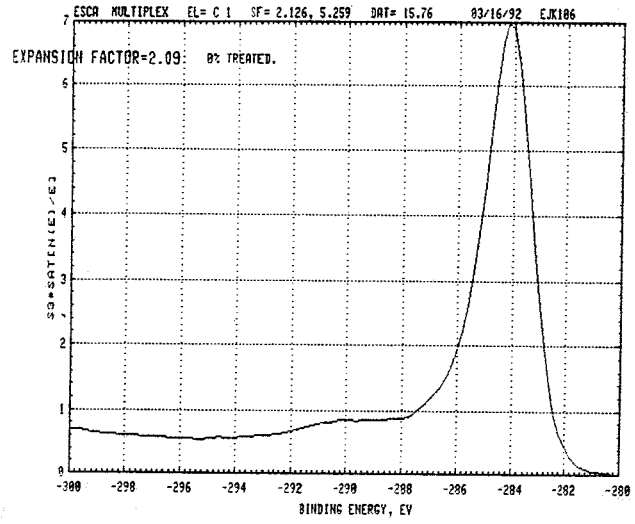

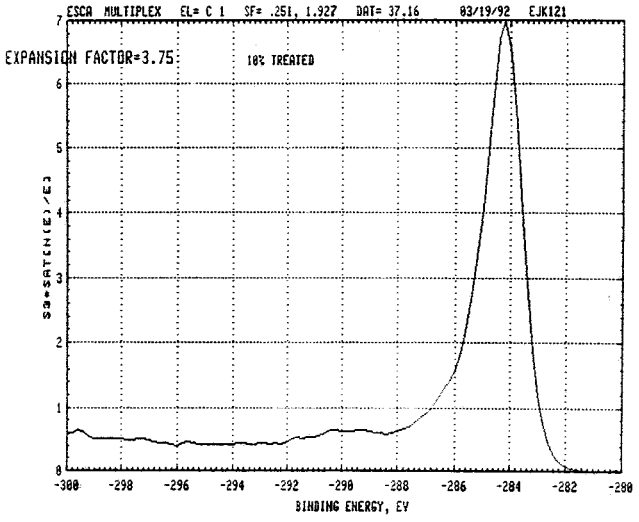

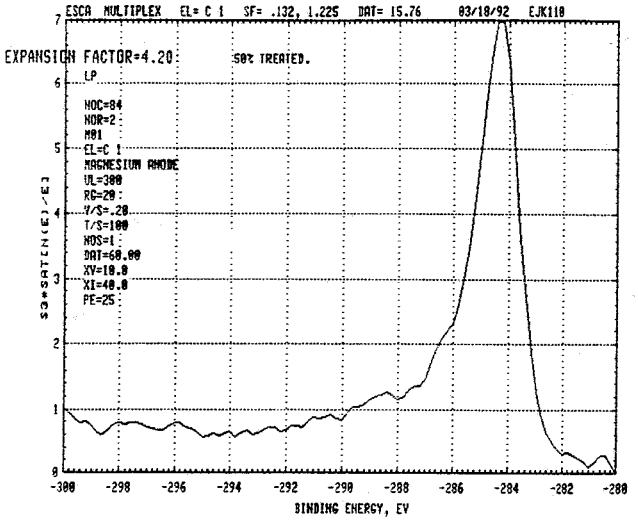

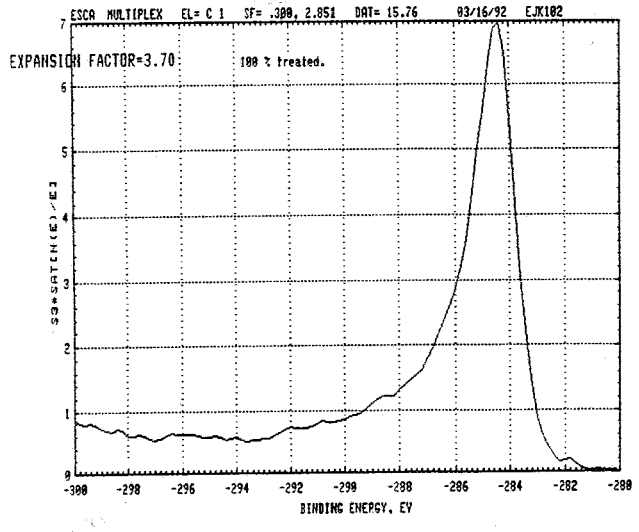

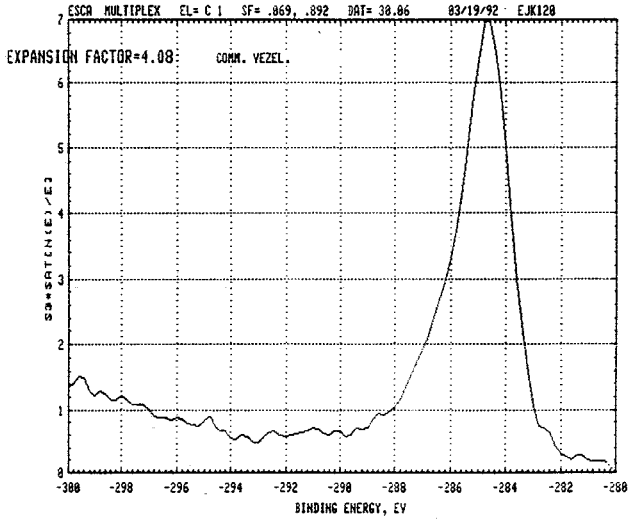

Figure A.6: *Detail scans of oxygen O1s peak of:*
- *Apollo IM 43-750: 0, 10, 50 en 100% treated carbon fibres*
- *XA-S high strength carbon fibre.*

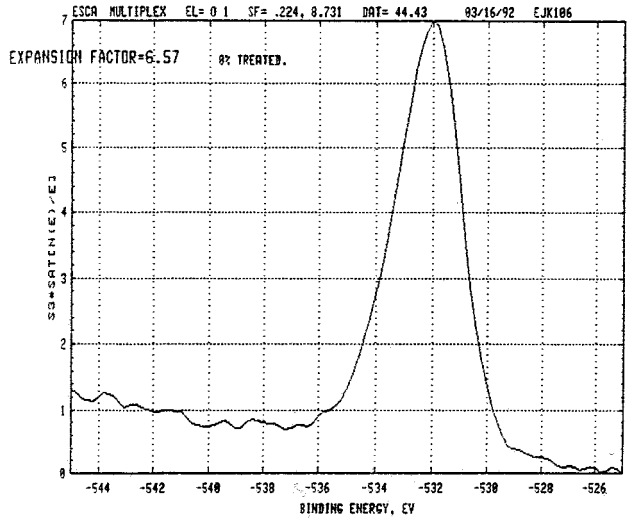

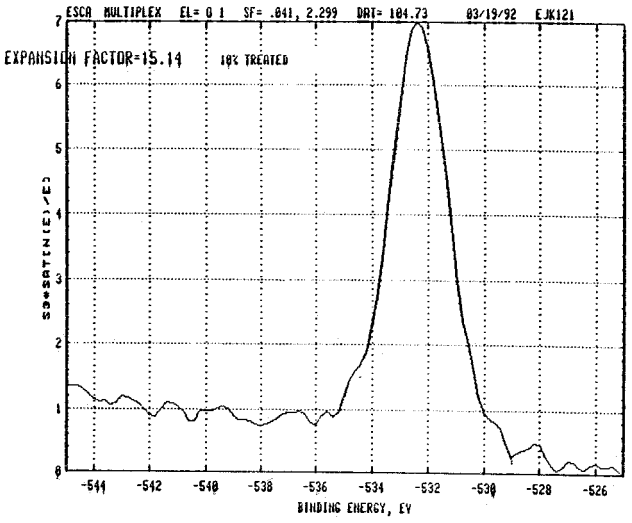

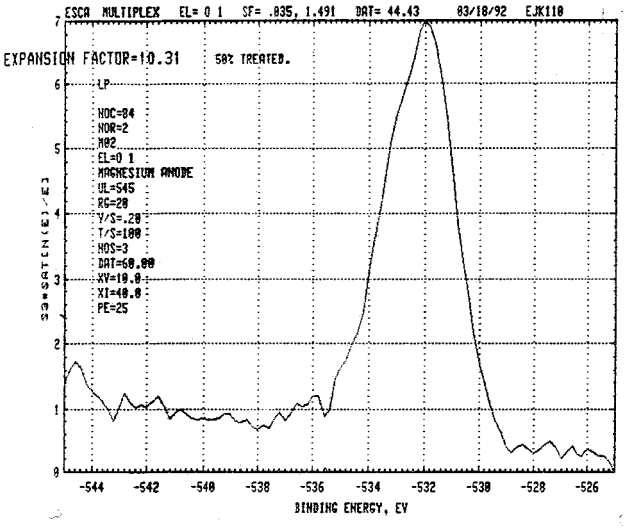

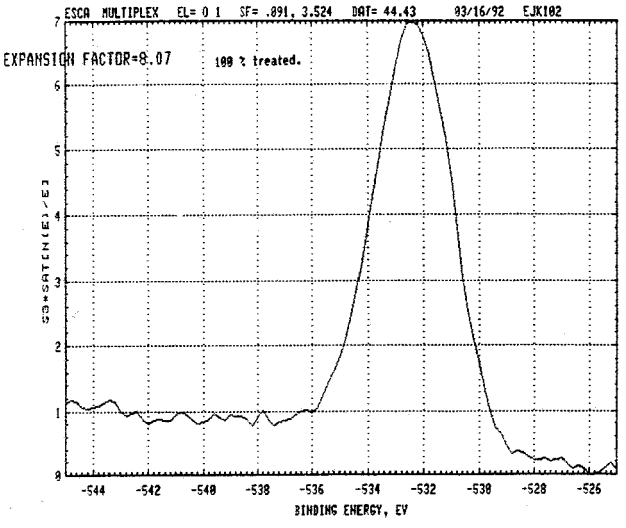

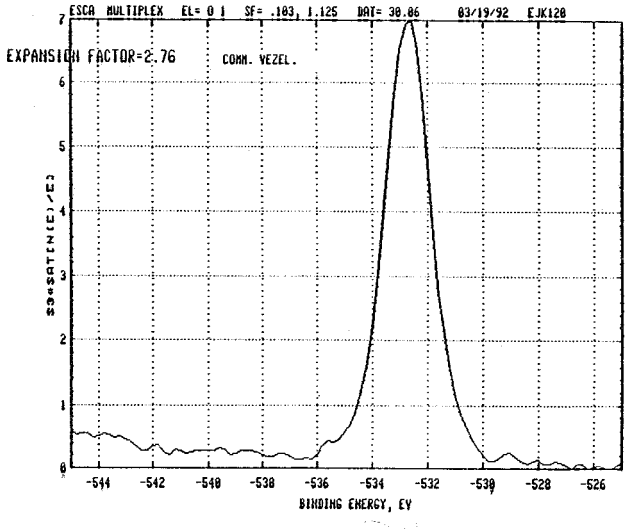

Appendix B: Acoustic emission

When a solid is subjected to stress at a sufficient high level, sound is generated in the material and is emitted in discrete pulses. This phenomena is called acoustic emission (AE) and can be used as an indication for the amount of damage present in a certain solid structure. Acoustic emission is a non destructive test method, which can be used in three ways:

1) Use several detectors and timing circuits, together with a three-dimensional geometry, to locate the source of AE.
2) Monitor the acoustic emission rate during stressing, to discover any sudden changes in rate which might be indicative of the formation of new defects, such as cracks.
3) Monitor the emission rate and attempt to relate this to the size of a defect in order to determine the remaining safe life of a structure.

Advantages of acoustic emission methods are:

- the high sensitivity of the system
- the real-time detection
- the continuous monitoring
- the possibility to locate defects
- the fact that the entire structure is evaluated.

The main problem of acoustic emission, however, is that only global information is provided. It is difficult to relate a certain amount of acoustic emission to an amount of real damage. Apart from sufficient experience, understanding of material behaviour is essential. Another problem is sorting out acoustic emission from noise, which presence is inherent to the sensitivity of the system.

B.1 Evolution of acoustic emission technique

At the end of the 1940's Mason et al. [20] first used acoustic emission methods at the Bell laboratory in the USA. The first break-through in the field of AE, however, came from Germany, where Kaiser [21] applied acoustic emission to metals in 1953. He found and stated that if a crystal of a material is stressed while the emission was monitored, and when the stress is relaxed and then reapplied, no new emissions will occur until the previous maximum stress has been exceeded. This effect is called the Kaiser effect. It is not universal, but has been observed in both metals and composites. In the 1960's the first industrial applications followed. In the 1980's acoustic emission technique became a standard procedure in the non-destructive testing of spot-weldings, composites and pressure vessels. An other, developing, area of AE application is investigation of fracture mechanisms in materials. This is where acoustic emission technique is used for in this investigation.

B.2 Theory

Within the framework of this investigation acoustic emission is thought to originate from crack initiation and propagation in the material. When a solid is subjected to stress at a sufficient high level, micro-cracks are created. A part of the energy released due to the sudden stress relaxation is transmitted into elastic waves, propagating in the material. This explains the other name for acoustic emission, which is Stress Wave Emission (SWE). These elastic waves can be detected at the surface of the solid using a highly sensitive piezo-electric sensor, which produces an electric signal as a function of it's acceleration. This electric signal is recorded after it has been filtered. Figure B.1 shows a schematic diagram of basic acoustic emission equipment.

A signal originating from one event (crack initiation or propagation) is called hit. A hit can be characterized by parameters like amplitude, duration, rise time, energy, counts and counts to peak. All of these parameters, except for the amplitude, depend on the threshold. The threshold can be set, to distinguish real hits from

noise and has to be set above the noise level. Signals with an amplitude less than the threshold are not recorded. Figure B.2 shows a hit with the parameters characterizing the hit, where 'time' represents the duration of the hit.

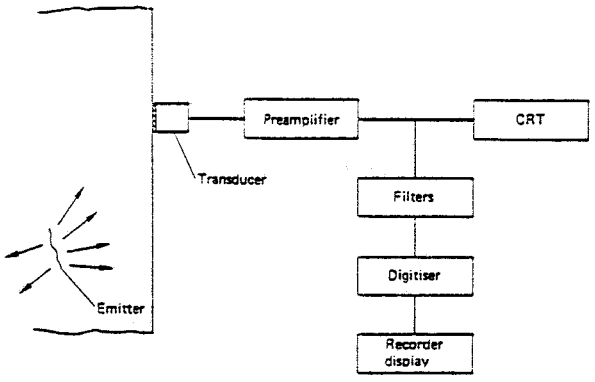

Figure B.1: Schematic diagram of basic AE equipment.

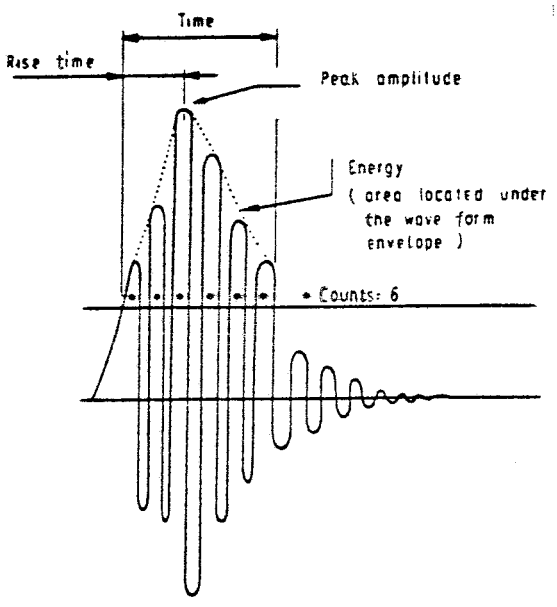

Figure B.2: AE hit with characterizing parameters [22].

By recording acoustic emission during a mechanical test on a material, trends in damage propagation and different fracture mechanisms can be obtained. In this investigation acoustic emission technique is used to detect trends in emission when the interface strengths of the tested composites are altered. In transversely loaded uni-directional composites three main sources for AE are possible, viz. matrix cracking, fibre splitting and debonding of the fibre-matrix interface. Actually AE results are hard to interpret, but in combination with the normal mechanical tests, application of AE does contribute to a better understanding of the behaviour of the composites during testing.

B.3 Experiments

B.3.1 Mounting of sensor to the sample

The AE sensor was glued on to the sample surface using "3M Scotch Electroplating Tape 470", with "Apiezon L Vacuum Grease" between the sensor and the sample, to ensure sound transmission over the contact surface.

B.3.2 AE-Equipment and settings

For the acoustic emission measurements Physical Acoustics Corporation (PAC) equipment is used, as listed in table B.1 is used.

Table B.1: AE-equipment.

AE Recorder	PAC LOCAN AT 140
Preamplifier	PAC 1220 A
Sensor	PAC R15

The preamplifier has been set to 40 dB. The R15 in the sensor type stands for a 150 kHz resonance frequency, meaning that frequencies in the AE signals up to 120-130 kHz are measured accurately. Above this frequency resonance of the sensor itself restrains the measurements to be accurate.

The settings of the equipment affect the recorded signal, and therefore have to be chosen carefully. The setting parameters are threshold, gain, peak definition time (PDT), hit definition time (HDT) and hit lockout time (HLT). These parameters are defined in section B.5. PAC advised the settings listed in table B.2 for measurements on composites. The used settings are taken from Rustidge [22], who performed AE measurements on carbon/polyethylene fibre hybrid composites and are listed in table B.3.

Table B.2: Settings for measurements on composites advised by PAC [23].

PDT	20 - 50 μs
HDT	100 -200 μs
HLT	300 μs

Table B.3: Used AE equipment settings.

Threshold	25 dB
Gain	40 dB
PDT	50 μs
HDT	200 μs
HLT	300 μs

B.3.3 AE signal recording

It is possible to filter noise, originating from the sample-grips or supports, out of AE measurements. This is done by applying two sensors at the sample, one close to either grip. The sensors have to be located at either side of the region where real acoustic emission occurs. Thus signals initiated at the supports or specimen-grips and propagating to the inside (noise) can be distinguished signals propagating in the opposite direction

(real acoustic emission). Unfortunately this method could not be applied because one of the two channels of the recorder was not working well. Noise originating from the supports in three-point bending was more or less prevented by covering the supports with a thin teflon foil.

B.4 Results

A representative measurement of each combination of material and test method has been sorted out and is shown in § B.6, using the following plots:

- hits versus time (rate/cumulative)
- energy versus time (rate/cumulative)
- amplitude distribution (hits versus amplitude)
- energy distribution (hits versus energy).

The quantitative results obtained in uni-axial tension and three-point bending are listed in table B.4 and B.5 respectively.

Table B.4: Acoustic emission results of uni-axial tension.

Material	Surface Treatment Level	Silicon Oil Sizing	# Hits Before Failure	# Total Hits	AE Energy Before Failure	Total AE Energy
Epoxy	-	-	138	167	1438	8562
Apollo/ epoxy comp.	0%	-	110	141	1675	16075
	0%	0.1%	84	133	2690	16460
	0%	1%	76	122	2280	19557
	100%	1%	95	151	1333	19800

Table B.5: Acoustic emission results of three-point bending.

Material	Surface Treatment Level	Silicon Oil Sizing	# Hits Before Failure	Total # Hits	AE Energy Before Failure	Total AE Energy
Apollo/ epoxy comp.	0%	-	9	33	163	12813
	10%	-	69	105	1414	14520
	50%	-	118	147	3218	18190
	100%	-	128	162	2872	14460
	0%	0.1%	16	46	725	18725
	0%	1%	26	51	700	14350
	0%	2.5%	28	55	840	9750
	100%	1%	9	51	188	13450
XA-S/ep.	-	-	38	74	733	8617

Potential sources for acoustic emission in transversely loaded uni-directional composites in general are fibre splitting, matrix cracking, debonding and noise. Scanning Electron Microscopy graphs showed that no fibre splitting occurred in the tested composites. Uni-axial tensile tests on epoxy showed that matrix cracking results in a single 97 dB hit. This hit has been observed in both tensile and flexural experiments on all material as the hit at failure. From the fact that epoxy fails in a brittle manner, and that a micro-crack initiates global failure immediately, the conclusion can be drawn that the series hits before failure in figure B.6 (a) and (b) are due to noise (specimen grips, etc.). This means that noise in this context consists of peaks with a maximum of 5 hits. These hits are low energetic compared to the matrix cracking energy and have low amplitudes, in the range of 25 to 40 dB. The regular contour of the cumulative hits versus time plot (figure B.6 (b)) confirms this conclusion. The transverse tests on the different materials generally show similar contours of acoustic emission data: Before failure a series of low energetic hits occurs with amplitudes in the range 25-40 dB and failure is denoted by a single hit with an amplitude of 97 dB, followed by a series of about 30 low energetic hits.

Influence of fibre surface treatment

Two trends in the acoustic emission results as a function of fibre surface treatment level are evident. First, the number of recorded hits before failure increases (see figure B.3 (a)), and second, a shift to higher amplitudes takes place.

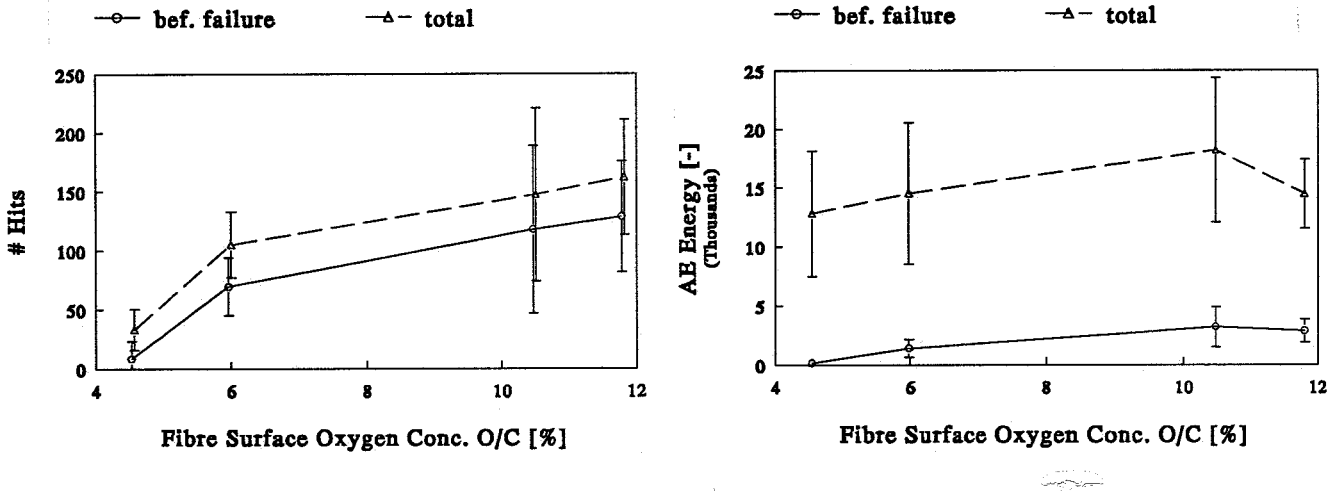

(a) Influence on # AE hits (b) Influence on AE energy

Figure B.3: Influence of fibre surface treatment on acoustic emission in bending.

The increasing number of hits is caused by the increase in data-acquisition time as a result of the strength. Both noise, which is presumed to be more or less constant in time, and debonding, initiated at local defects, generate more hits. The fact that a shift to higher amplitudes takes place can also be explained by the increase in strength of the composites. The local stress relaxations due to micro-failure, like debonding, occur at higher stresses, resulting in higher stress wave amplitudes and higher energy (see figure B.3 (b)). In the amplitude distributions of the composites with on the 50% and 100% treated fibres, where this shift has taken place, these two sources can even be distinguished. Noise: amplitudes in the range 25 to 40 dB, debonding: amplitudes in the range 40 to 55 dB (see figures B.13 (e),(f) and B.14 (e),(f)).

The change in failure mode from the composites with Apollo fibres to the composites with XA-S fibres has also been noticed in the acoustic emission results. Compared to the composites with 100% treated Apollo fibres few hits before failure have been recorded for the tests on composites with XA-S fibres. If there would not have been a change in failure mode, more hits should have been recorded.

B.6

Influence of silicon oil sizing

The influence of the silicon oil sizing of the fibres on the acoustic emission can not be analyzed easily, because here contradictory results of the tensile and bending tests are found, as shown in figures B.4 and B.5.

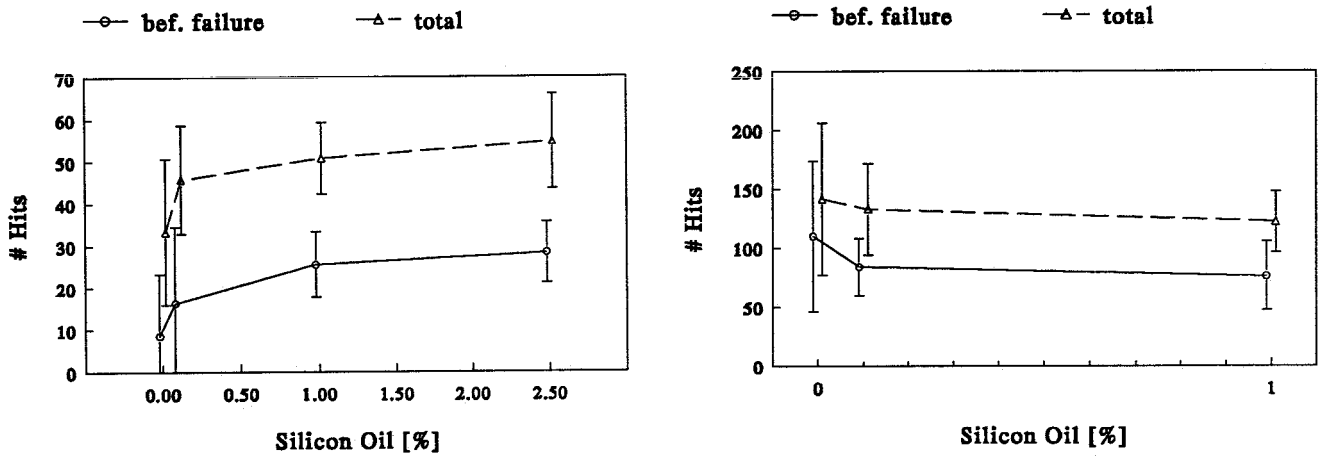

(a) Bending (b) Tension

Figure B.4: Influence silicon oil coating on number of hits, 0% treated fibres.

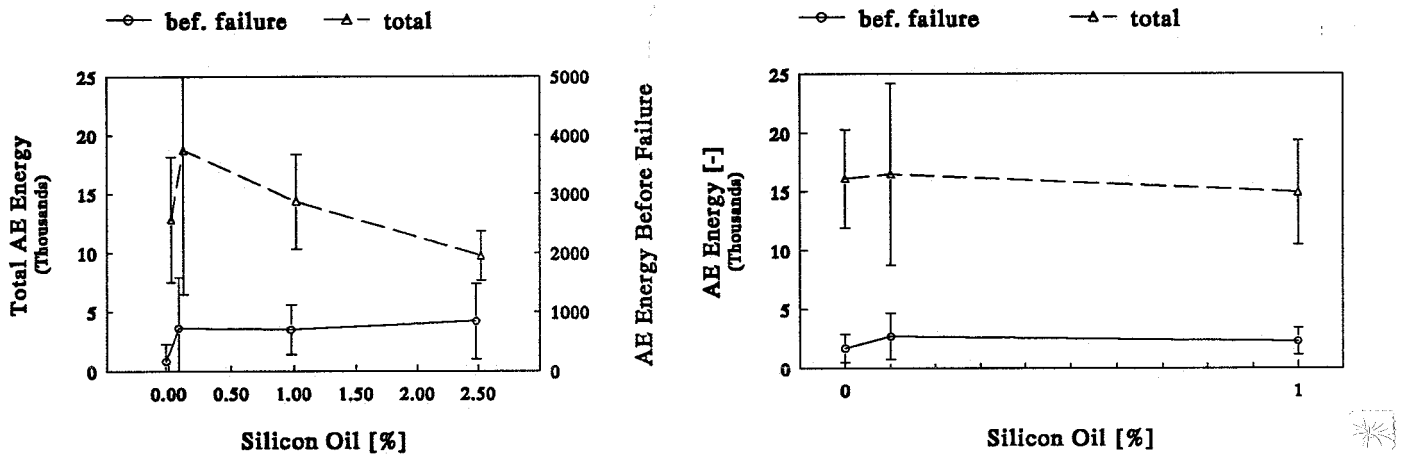

(a) Bending (b) Tension

Figure B.5: Influence silicon oil coating on AE energy, 0% treated fibres.

The explanation of these results must be the rather large deviation in acoustic emission experiments and the difficulty of reporting quantitative results. No specific change in acoustic emission caused by the silicon oil sizing of the fibres is found in the plots of acoustic emission (see § B.6), thus it can be concluded that the failure mode is not changed by the silicon oil sizing. From the fact that no dramatic decrease in number of hits has been found as a function of the silicon oil sizing, the conclusion can be drawn that the bonding in the interface of composites with unsized 0% treated fibres was not strong, because no extra acoustic emission was generated, compared to the 2.5% sized fibres (no bonding at all), during this debonding (see table B.5).

The effect on the 100% treated fibres is clear. The number of hits strongly decreases and the amplitude distribution shows a shift to lower amplitudes, both due to the decrease in strength.

B.5 Explanation of AE settings

Threshold: Only signals exceeding the threshold are recorded. Threshold has to be set just above the noise level.

Gain: The gain only affects the value energy of the recorded signals.

PDT: The 'Peak Definition Time' is used to determine the real maximum of the AE signal and is being reset after every hit.

HDT: The 'HIT Definition Time' defines the end of a hit. Every new exceeding of the threshold resets the HDT.

HLT: The 'Hit Lockout Time' is the time interval the system uses to acquire data, preventing the system to acquire reflections of AE signals.

B.6 Acoustic emission plots

Representative acoustic emission measurements on the epoxy and carbon/epoxy composites are shown in this section. These measurements are presented in the following figures:

- Uni-axial tension:	- epoxy:	epoxy 2 (fig. B.6)
	- CFRE:	- 0% treated Apollo: cc1003 (fig. B.7)
		- 0% treated Apollo, 0.1% sil. oil sizing: cc1103 (fig. B.8)
		- 0% treated Apollo, 1% sil. oil sizing: cc1205 (fig. B.9)
		- 100% treated Apollo, 1% sil. oil sizing: cc1304 (fig. B.10)
- Three-point bending:	CFRE:	- 0% treated Apollo: cc1007 (fig. B.11)
		- 10% treated Apollo: cc302 (fig. B.12)
		- 50% treated Apollo: cc510 (fig. B.13)
		- 100% treated Apollo: cc608 (fig. B.14)
		- 0% treated Apollo, 0.1% sil. oil sizing: cc1107 (fig. B.15)
		- 0% treated Apollo, 1% sil. oil sizing: cc1207 (fig. B.16)
		- 0% treated Apollo, 2.5% sil. oil sizing: cc801 (fig. B.17)
		- 100% treated Apollo, 1% sil. oil sizing: cc1308 (fig B.18)
		- XA-S: carb620 (fig. B.19)

Figure B.6: Acoustic emission data of epoxy, in tension.

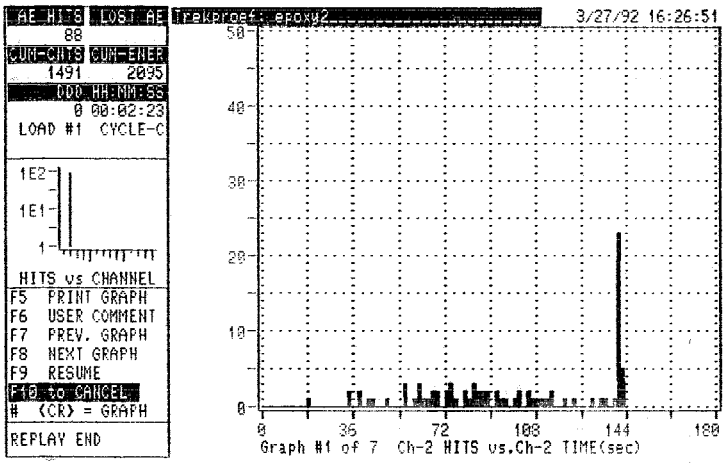

(a)

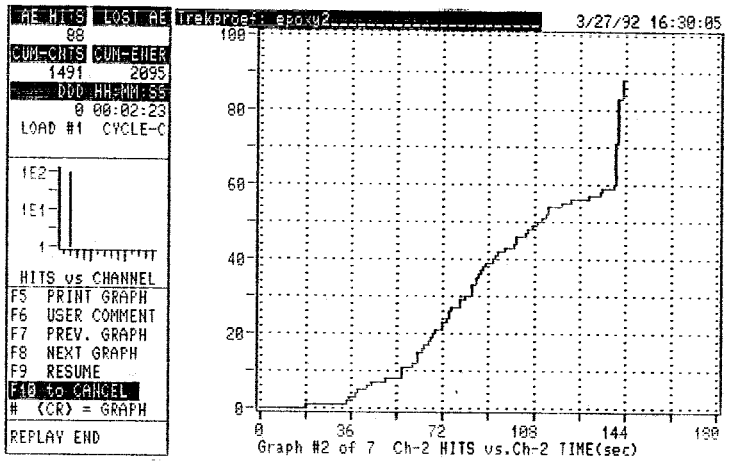

(b)

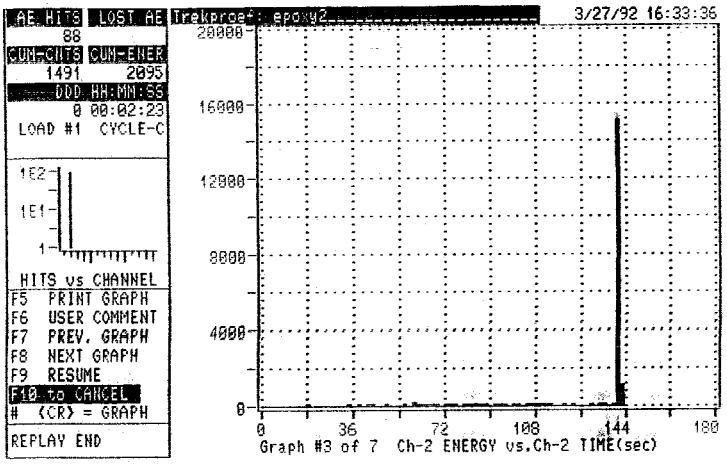

(c)

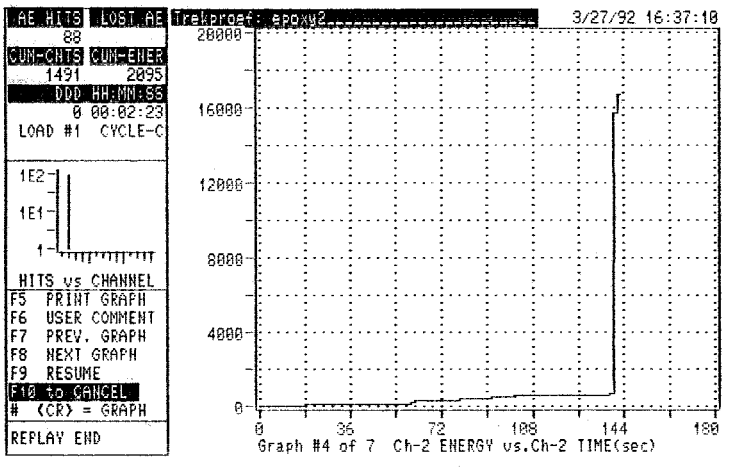

(d)

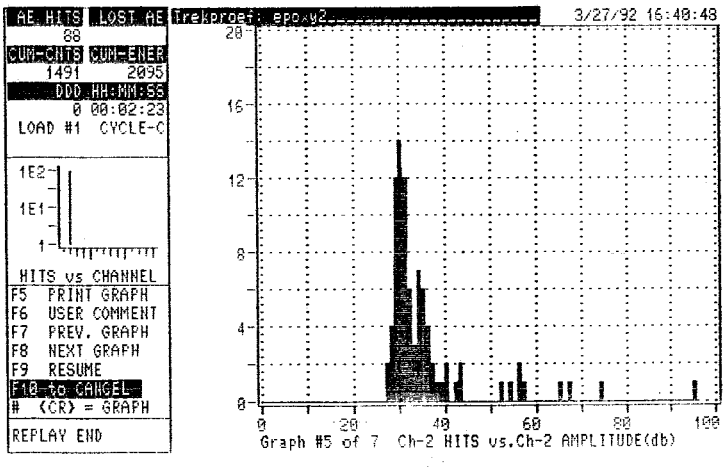

(e)

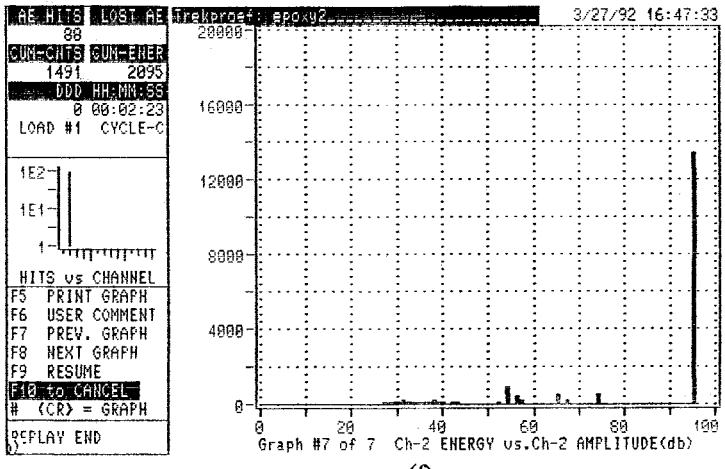

(f)

Figure B.7: *Acoustic emission data of composite with 0% treated Apollo fibres, in tension.*

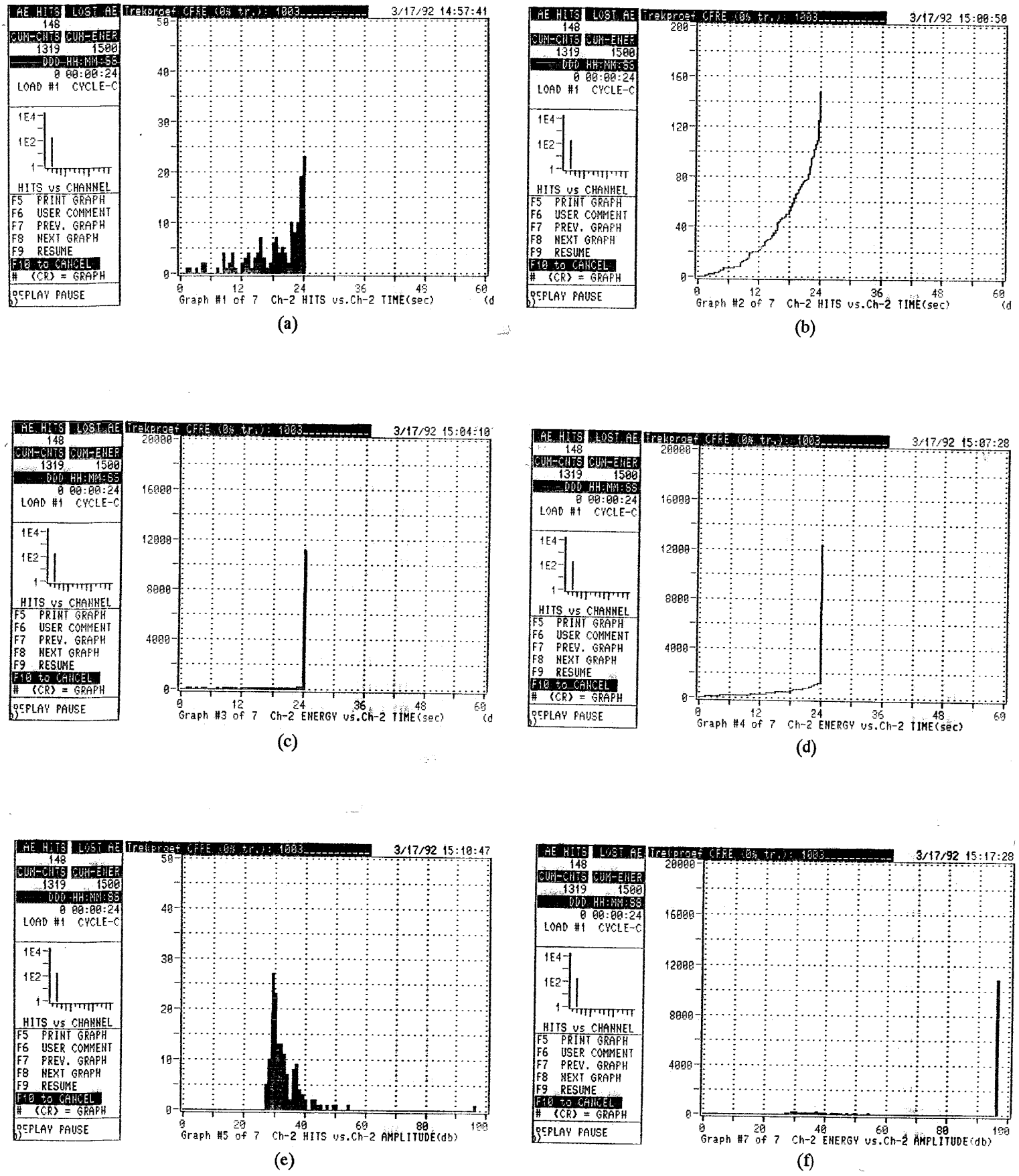

Figure B.8: *Acoustic emission data of composite with 0% treated Apollo fibres with 0.1% silicon oil sizing, in tension.*

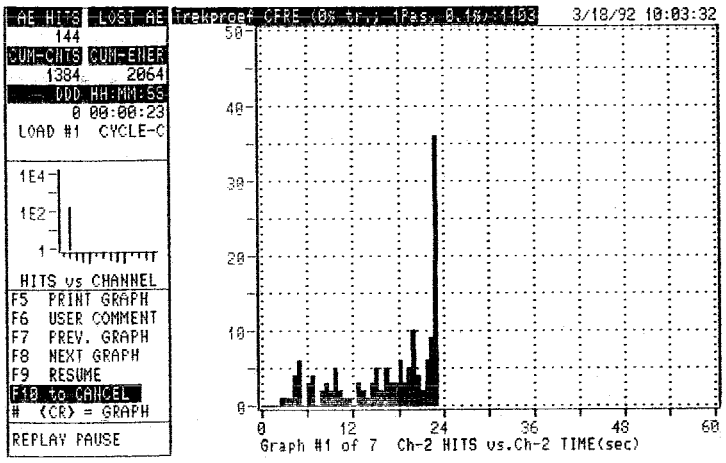

(a)

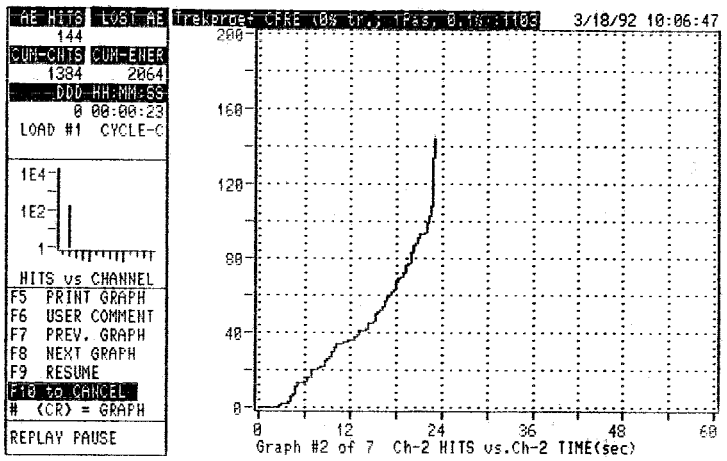

(b)

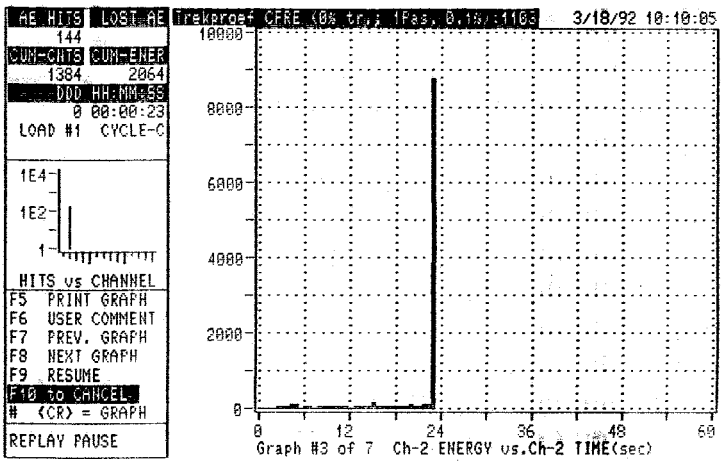

(c)

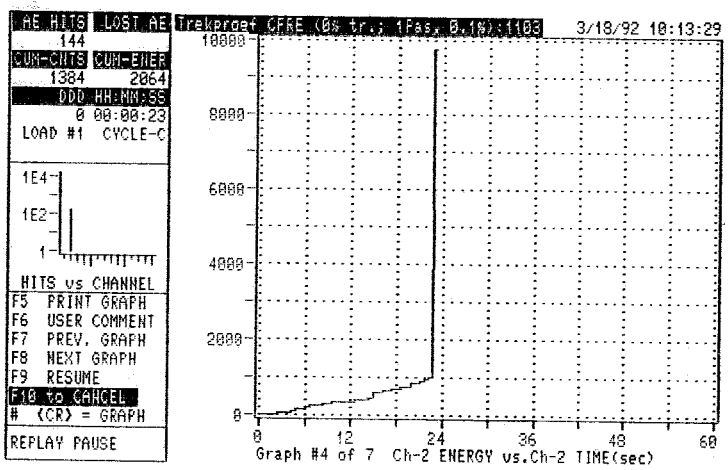

(d)

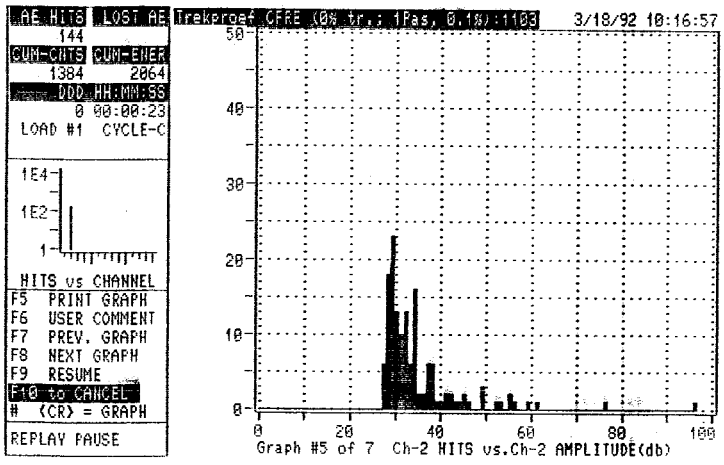

(e)

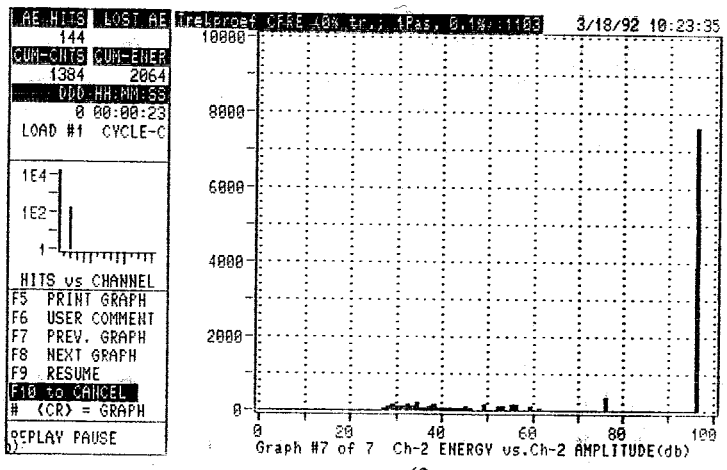

(f)

Figure B.9: *Acoustic emission data of composite with 0% treated Apollo fibres with 1% silicon oil sizing, in tension.*

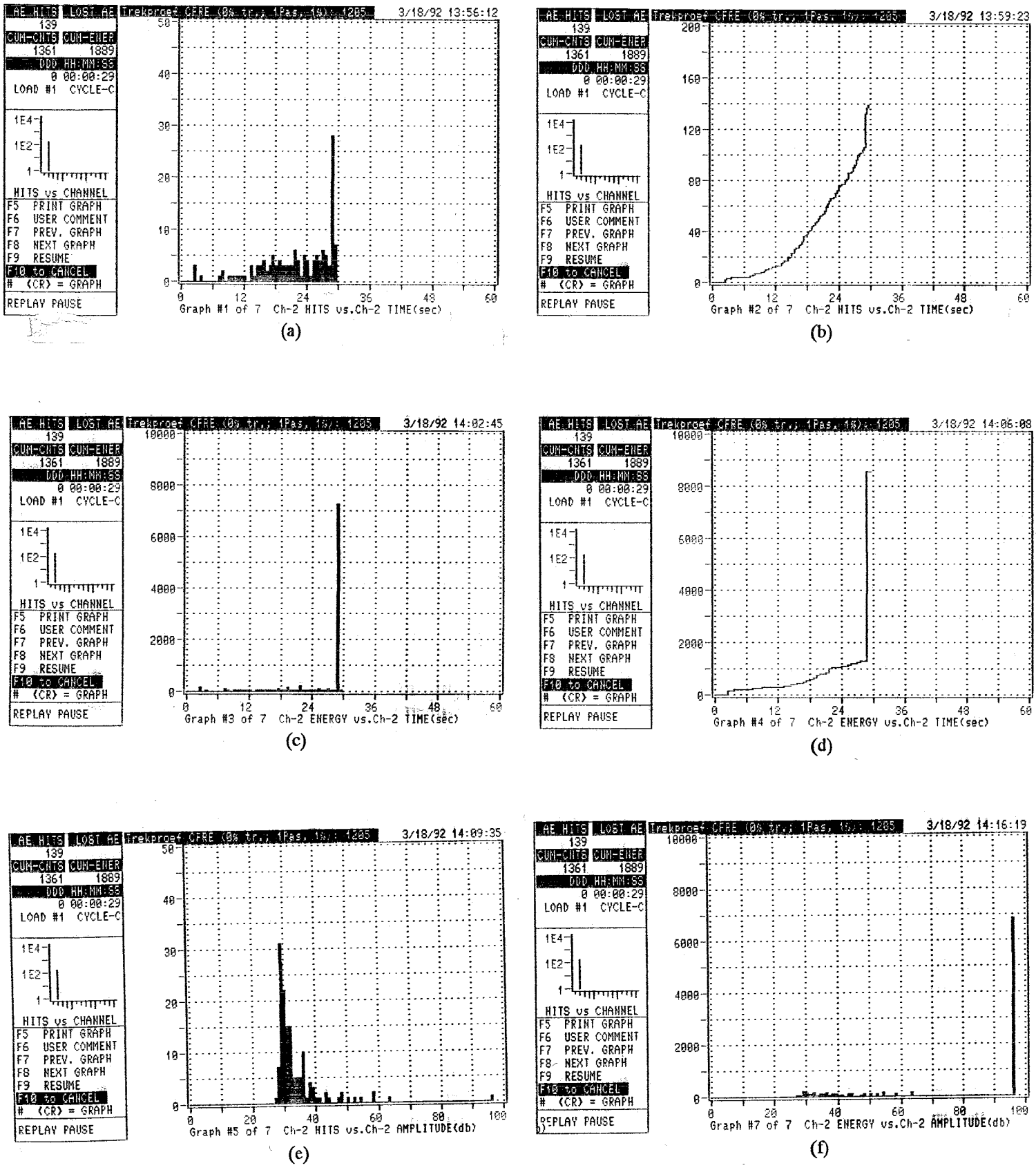

Figure B.10: *Acoustic emission data of composite with 100% treated Apollo fibres with 1% silicon oil sizing, in tension.*

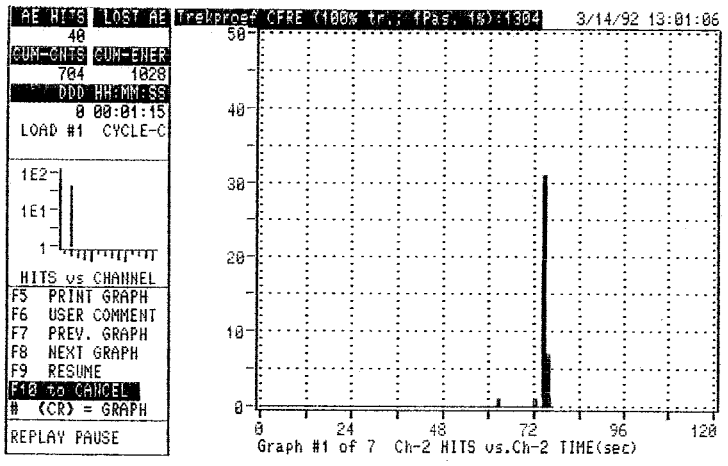

(a)

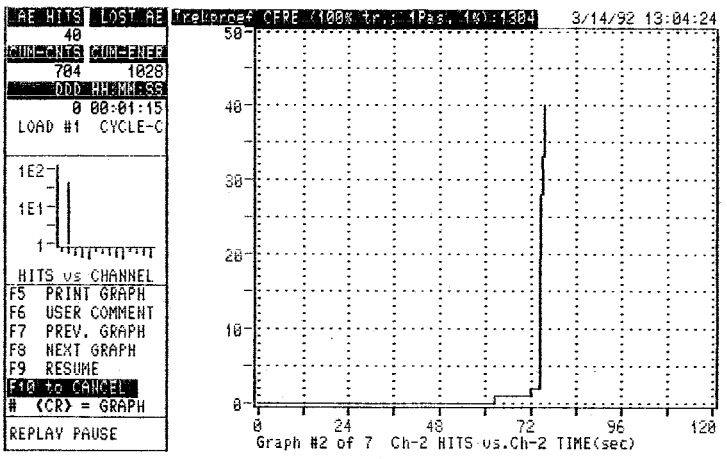

(b)

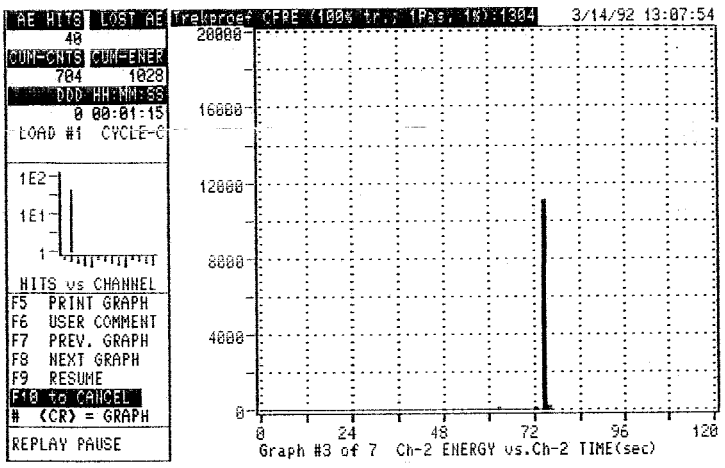

(c)

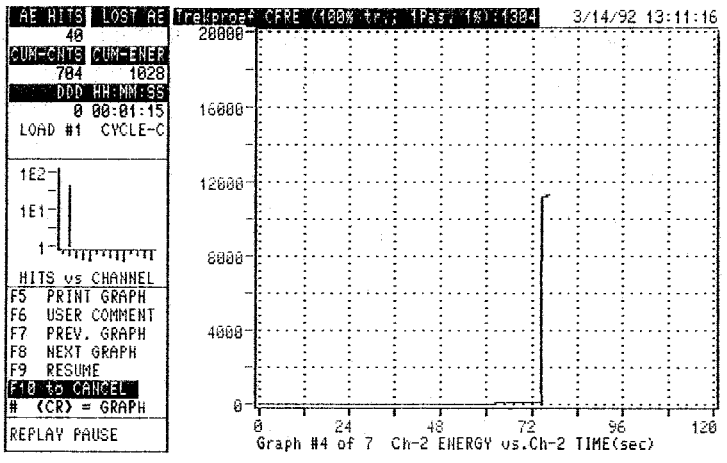

(d)

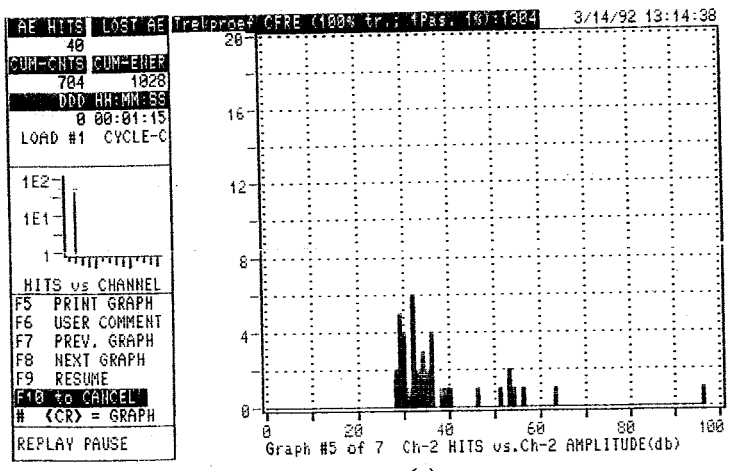

(e)

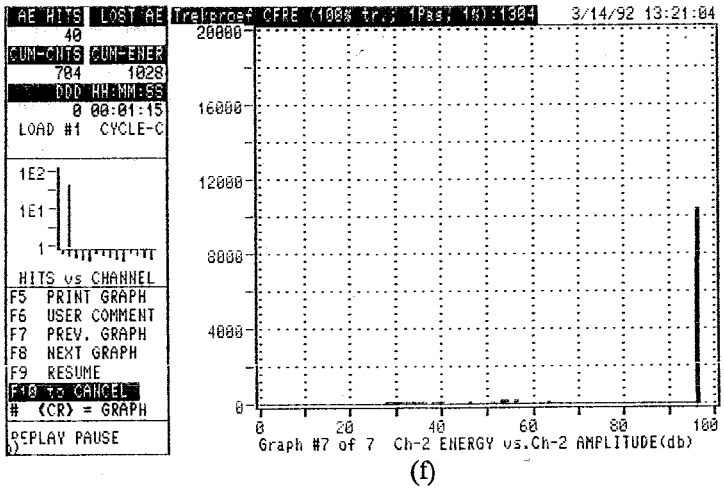

(f)

Figure B.11: *Acoustic emission data of composite with 0% treated Apollo fibres, in bending.*

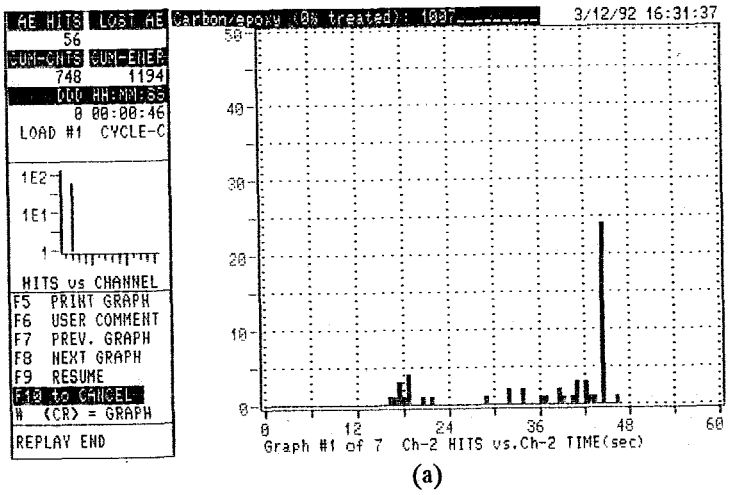

(a)

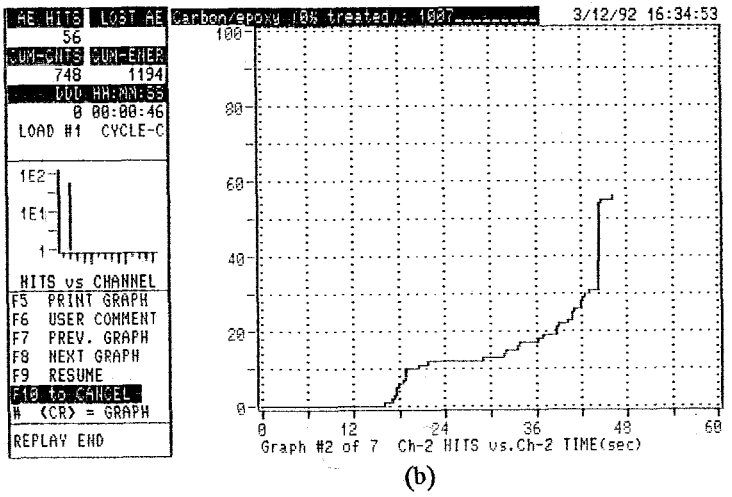

(b)

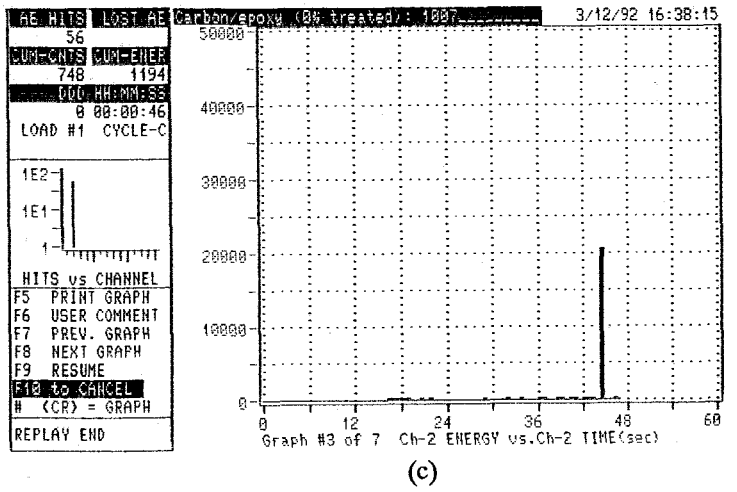

(c)

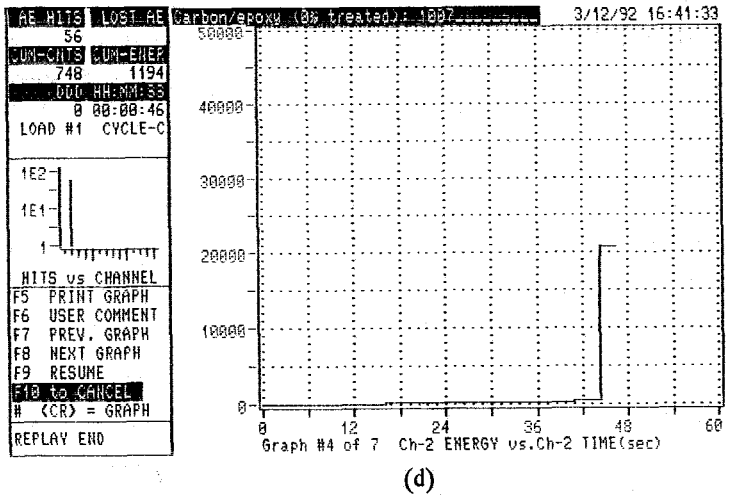

(d)

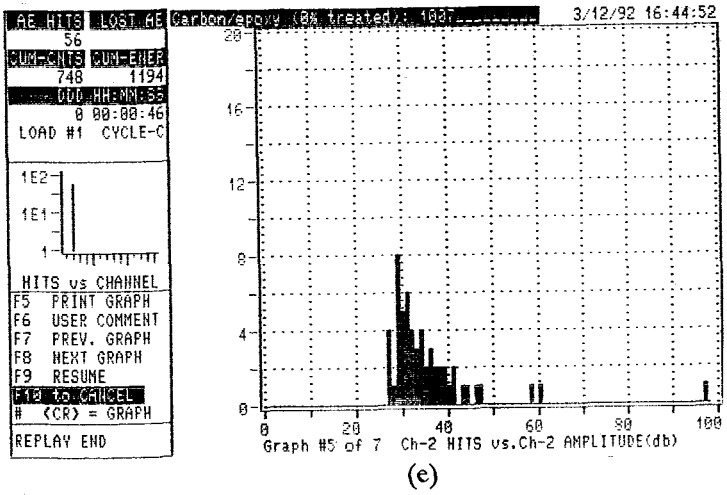

(e)

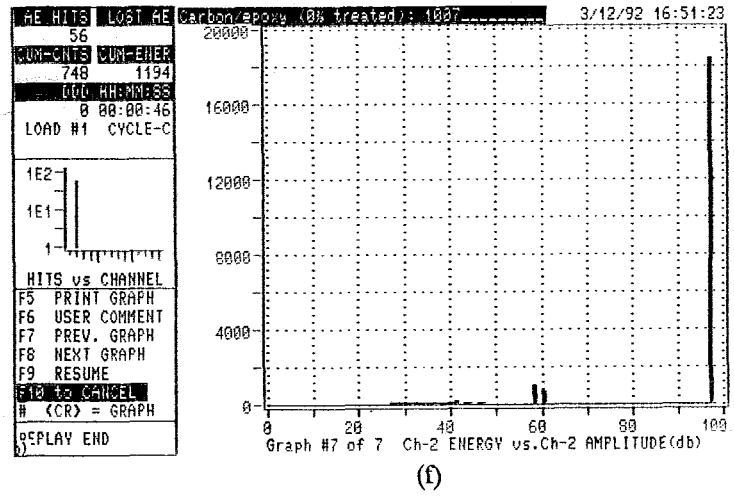

(f)

Figure B.12: *Acoustic emission data of composite with 10% treated Apollo fibres, in bending.*

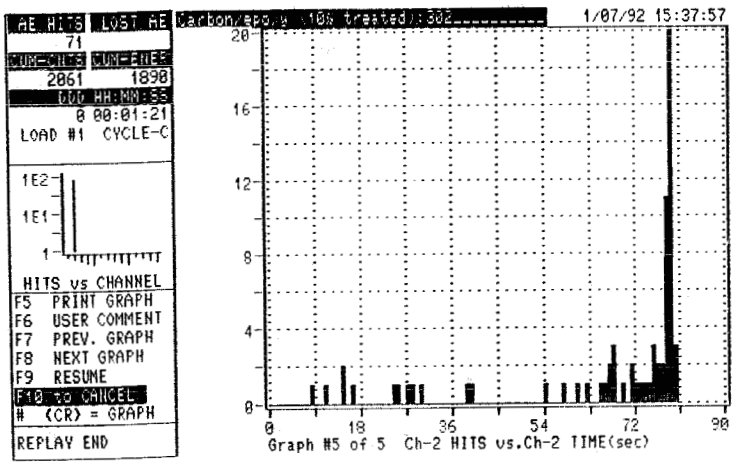

(a)

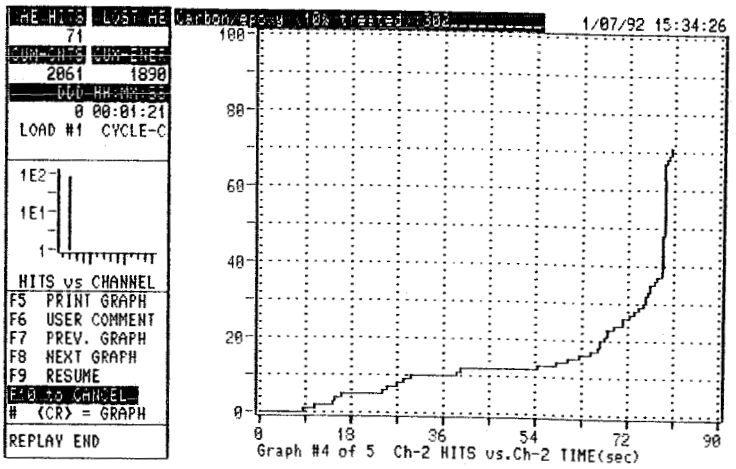

(b)

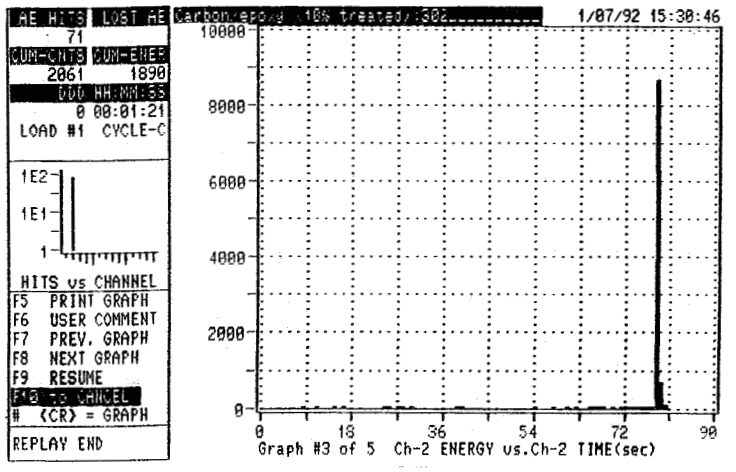

(c)

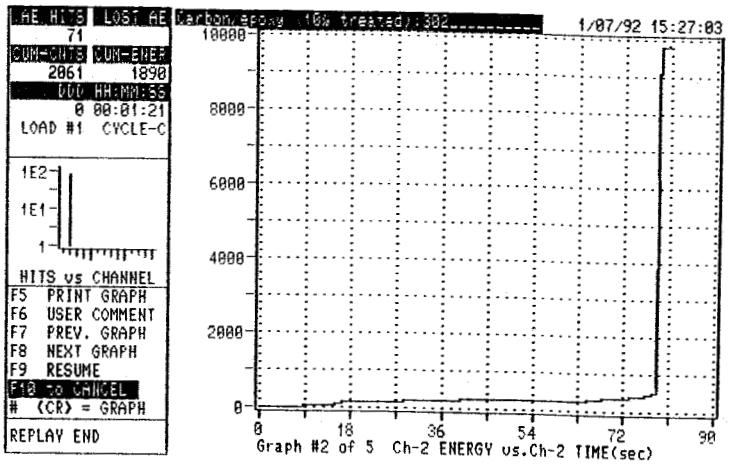

(d)

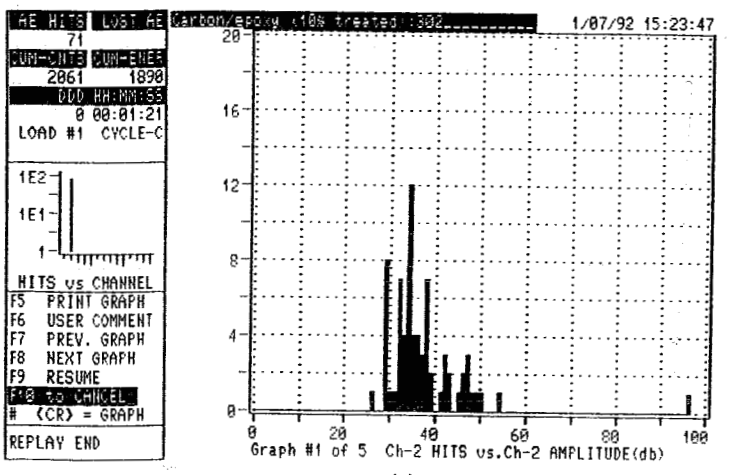

(e)

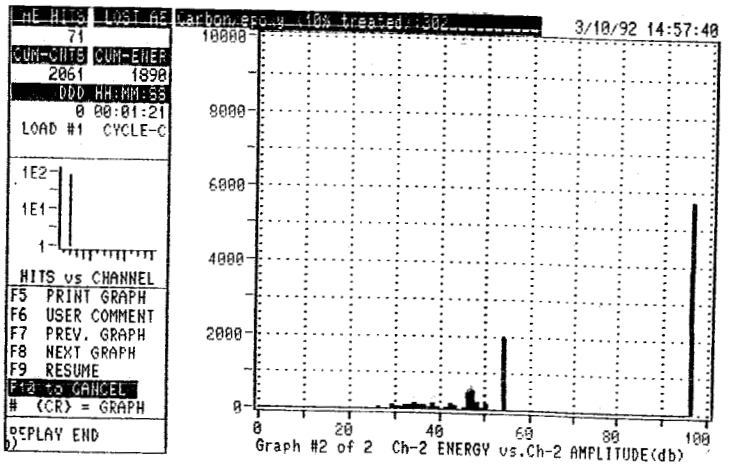

(f)

Figure B.13: *Acoustic emission data of composite with 50% treated Apollo fibres, in bending.*

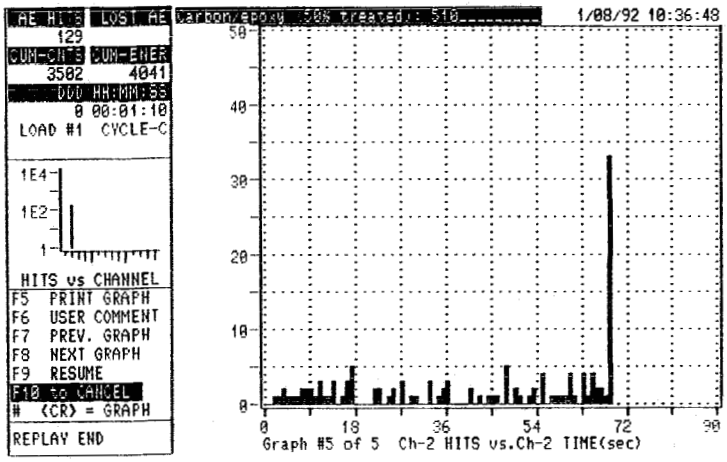

(a)

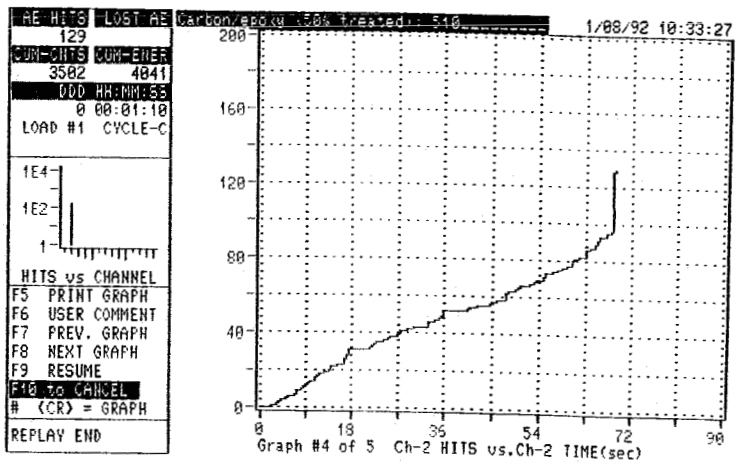

(b)

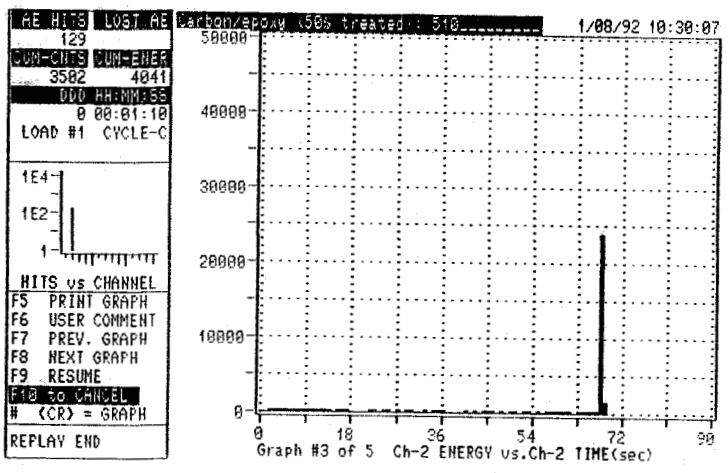

(c)

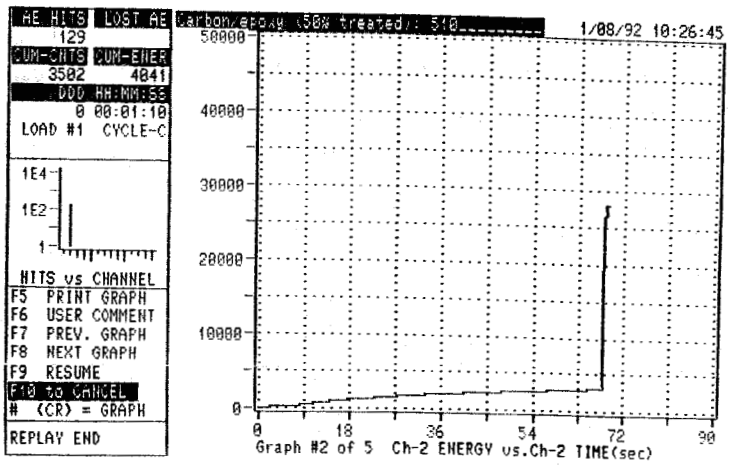

(d)

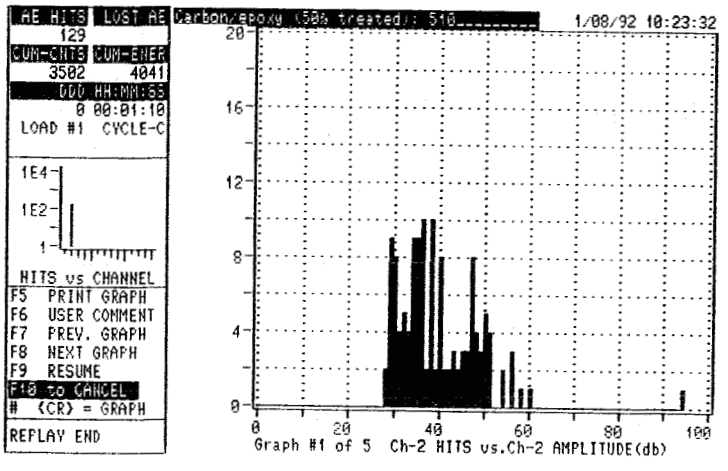

(e)

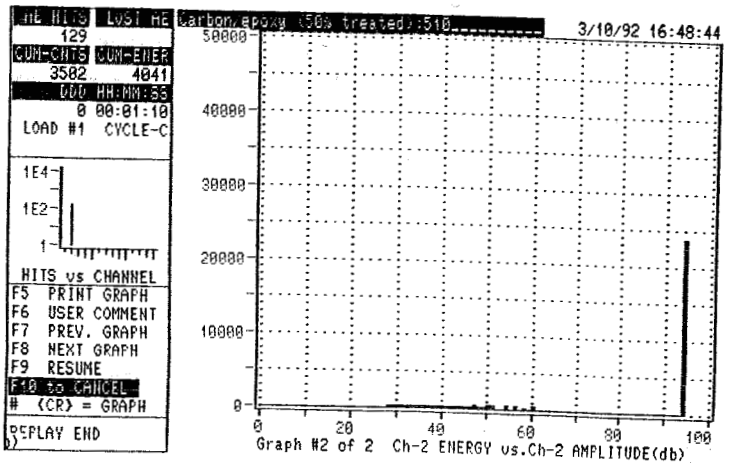

(f)

Figure B.14: *Acoustic emission data of composite with 100% treated Apollo fibres, in bending.*

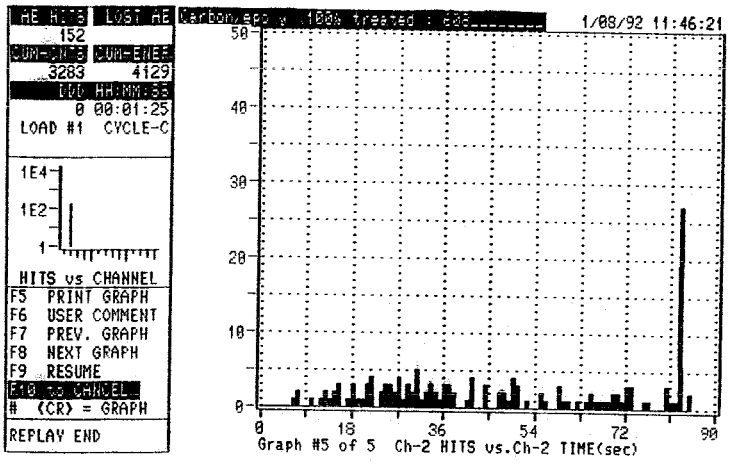

(a)

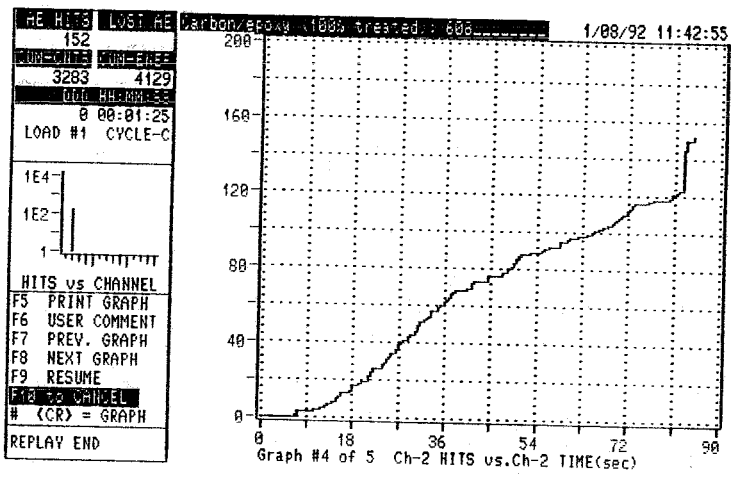

(b)

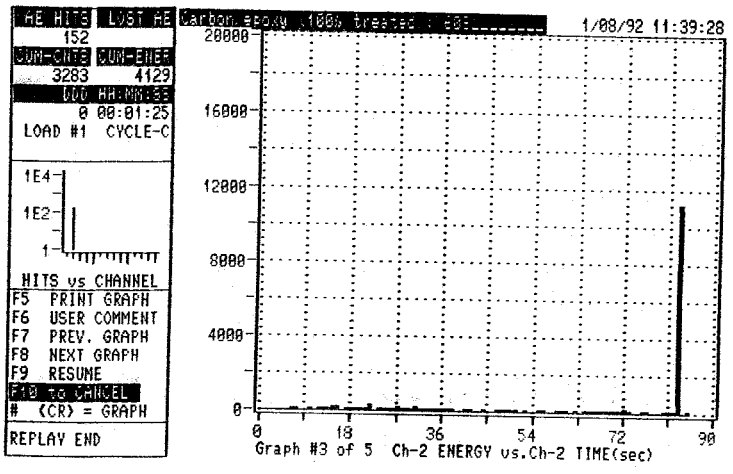

(c)

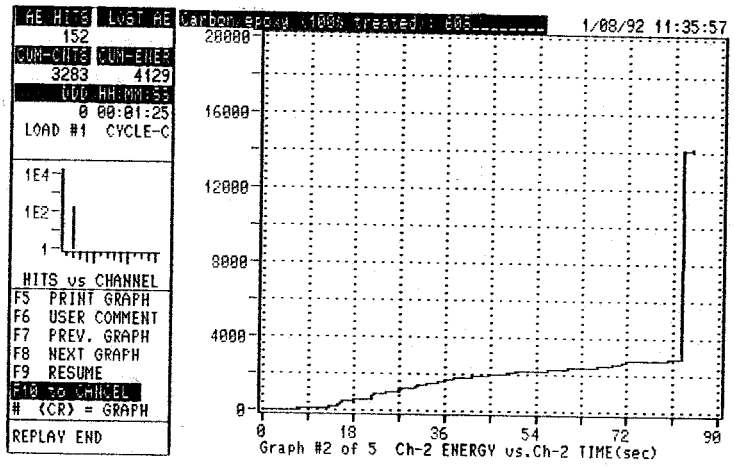

(d)

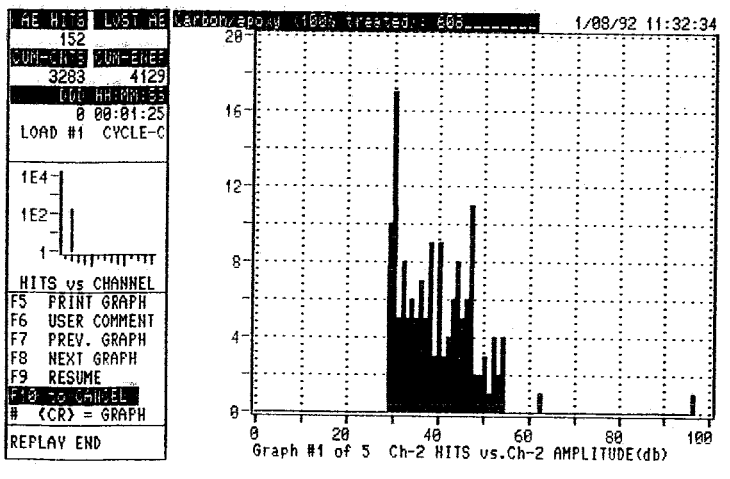

(e)

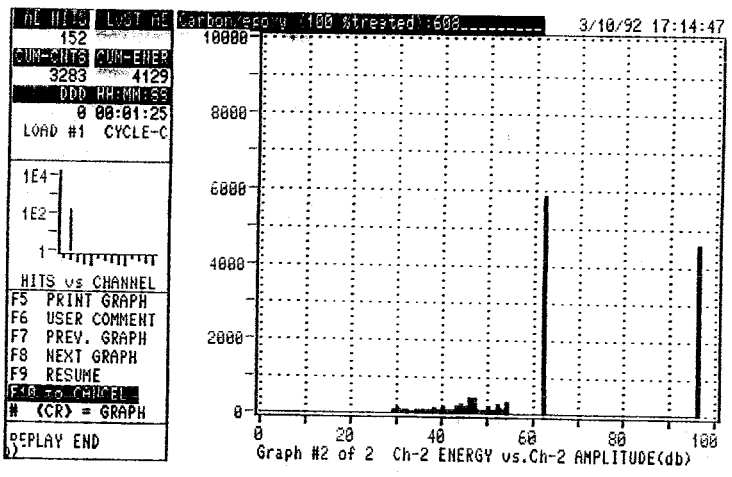

(f)

Figure B.15: Acoustic emission data of composite with 0% treated Apollo fibres with 0.1% silicon oil sizing, in bending.

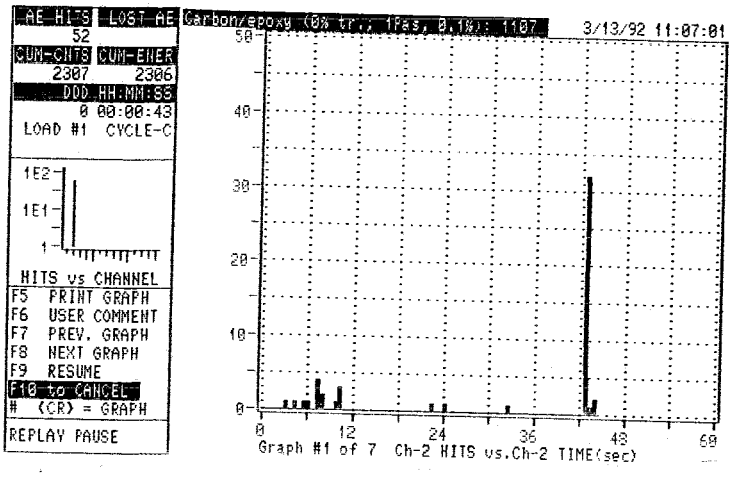

(a)

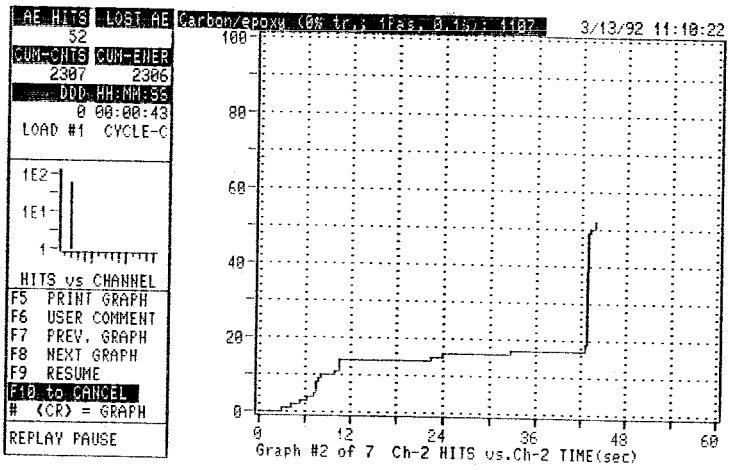

(b)

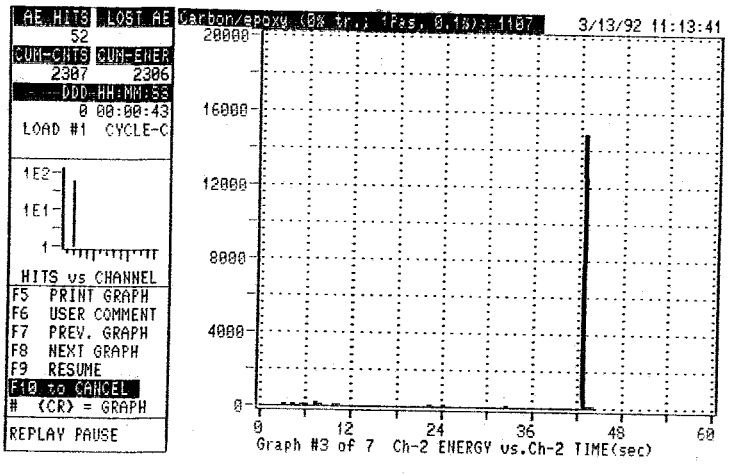

(c)

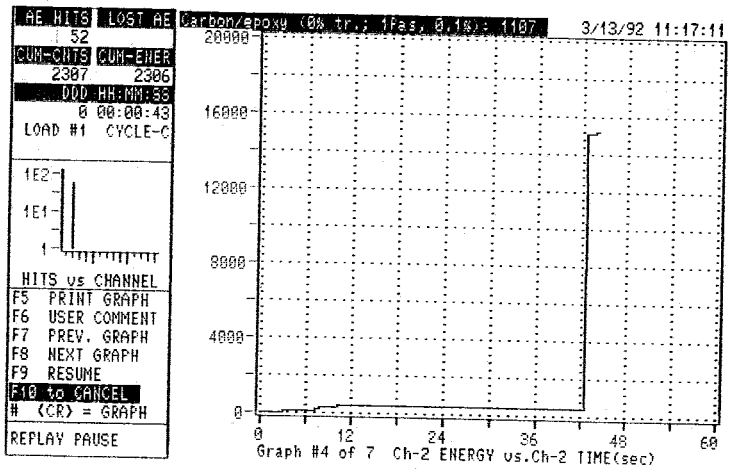

(d)

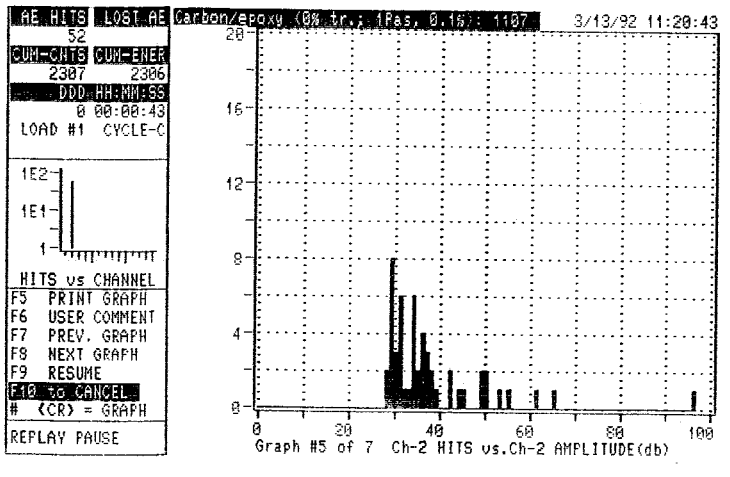

(e)

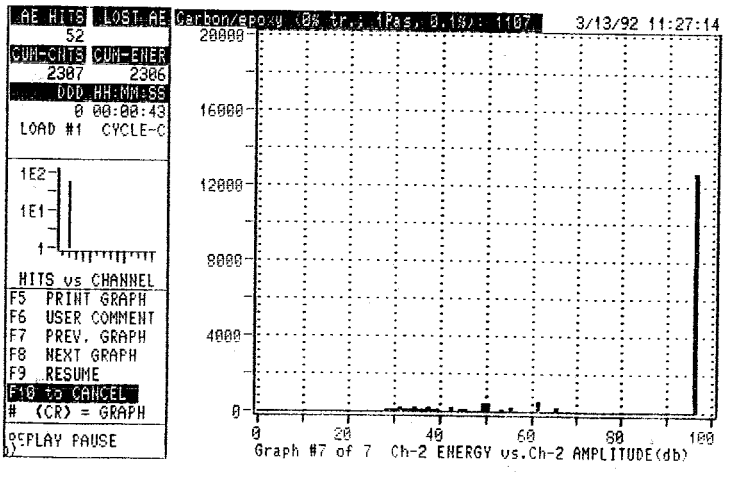

(f)

Figure B.16: *Acoustic emission data of composite with 0% treated Apollo fibres with 1% silicon oil sizing, in bending.*

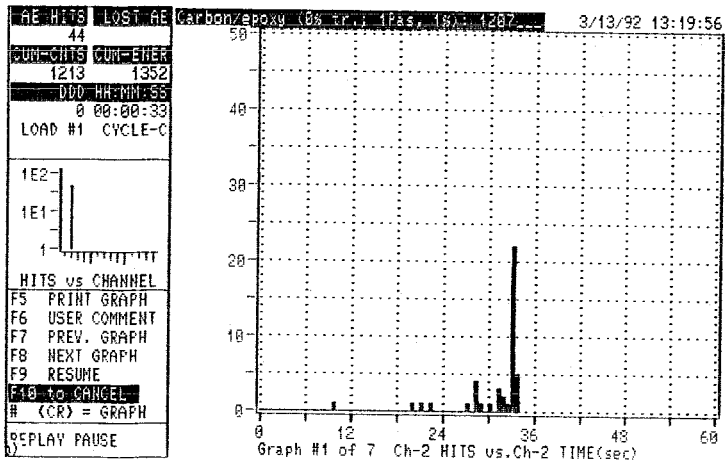

(a)

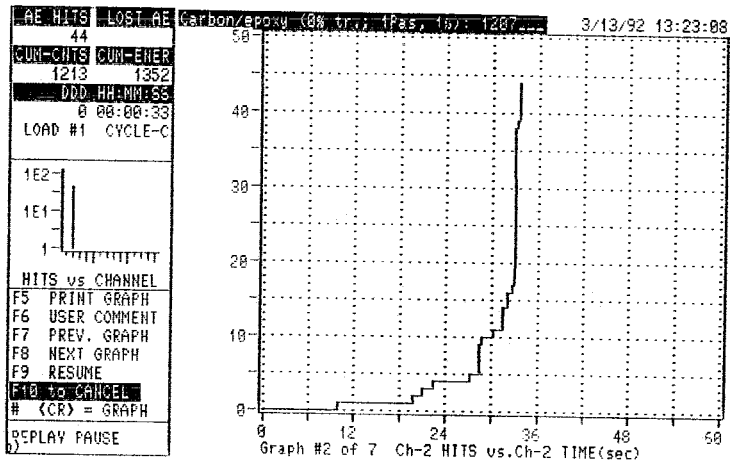

(b)

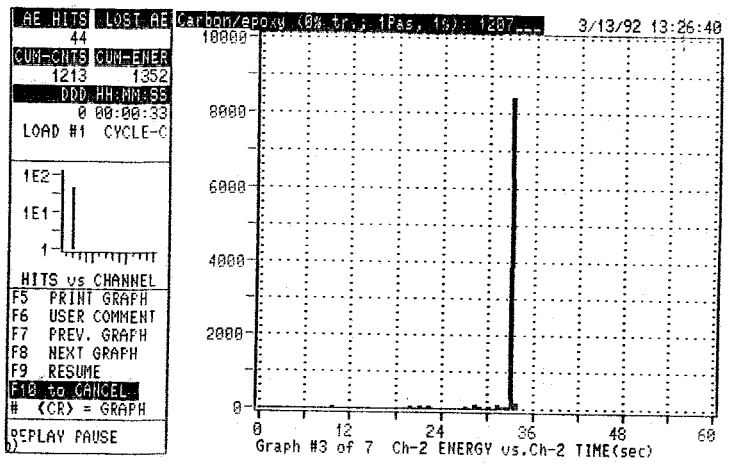

(c)

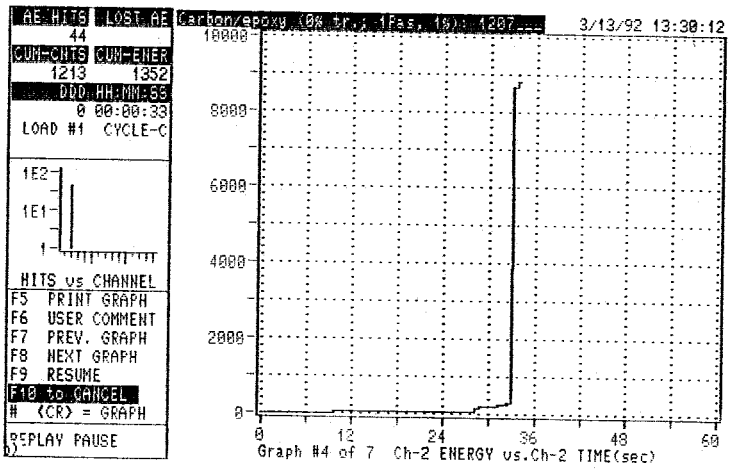

(d)

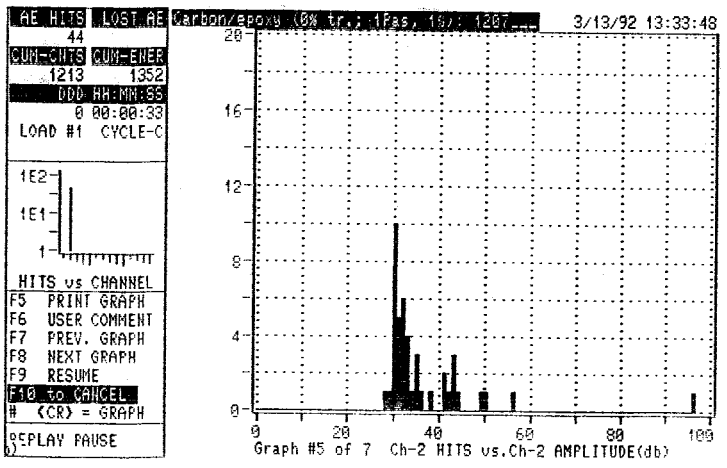

(e)

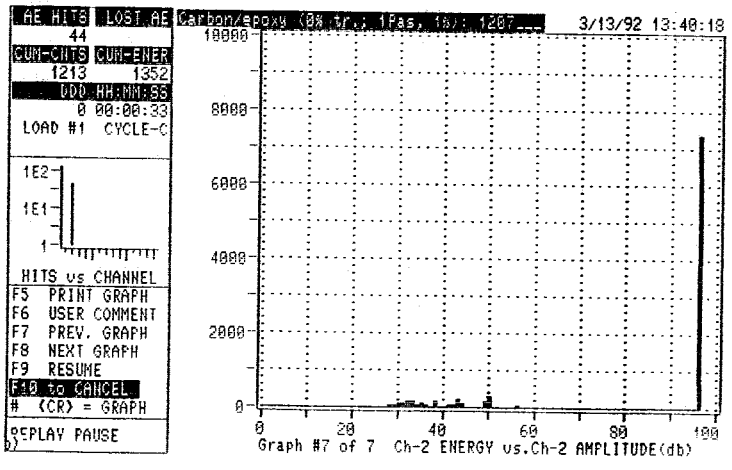

(f)

Figure B.17: *Acoustic emission data of composite with 0% treated Apollo fibres with 2.5% silicon oil sizing, in bending.*

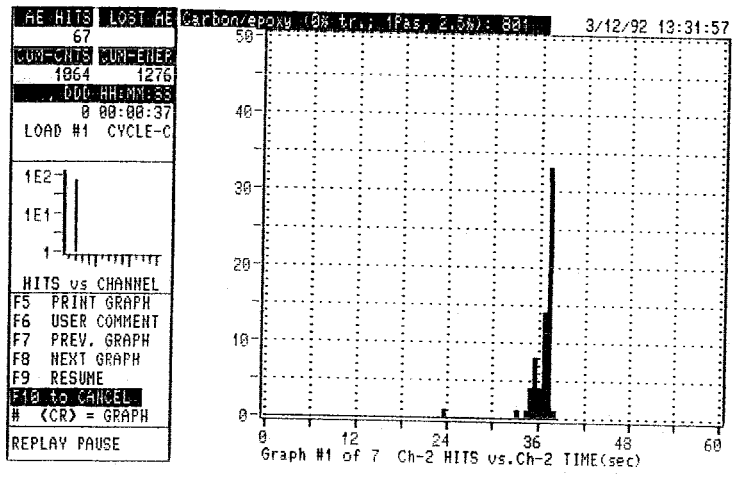

(a)

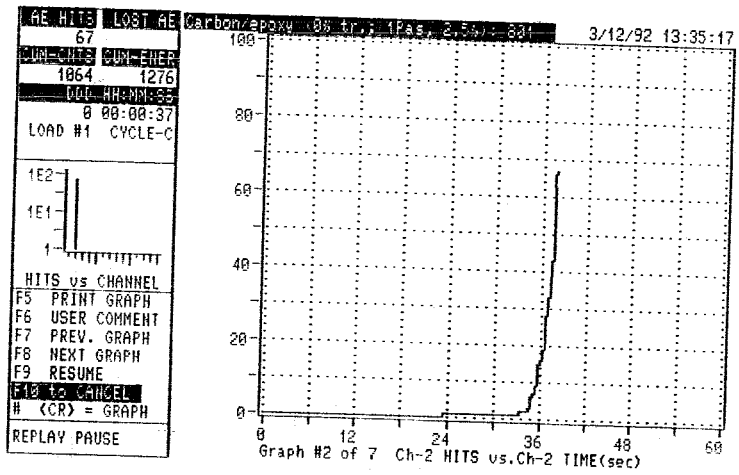

(b)

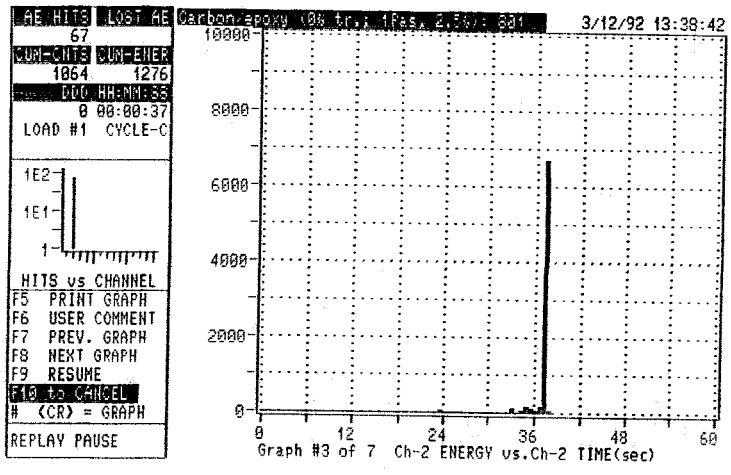

(c)

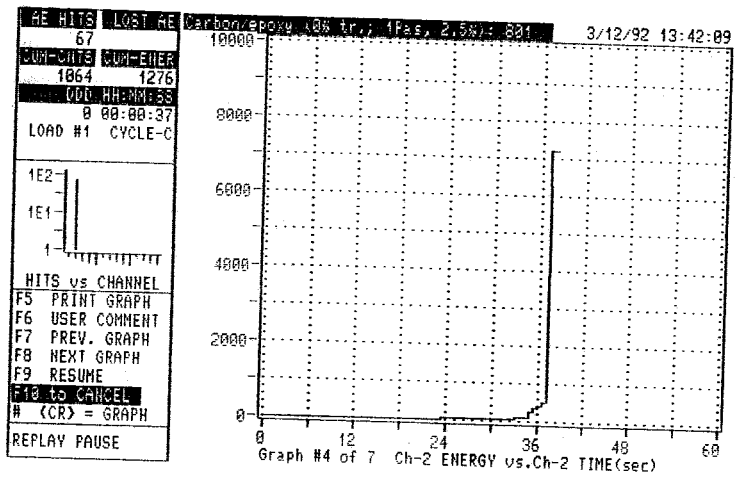

(d)

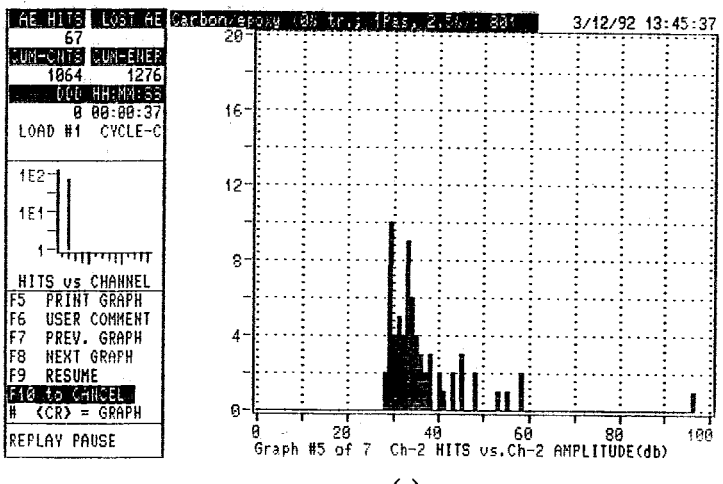

(e)

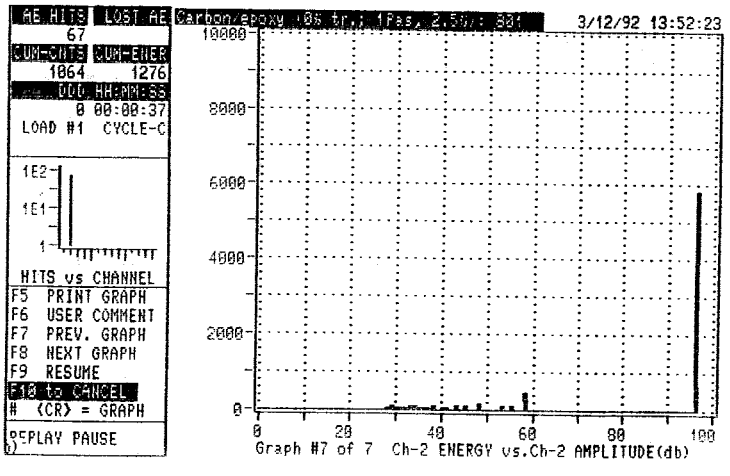

(f)

Figure B.18: *Acoustic emission data of composite with 100% treated Apollo fibres with 1% silicon oil sizing, in bending.*

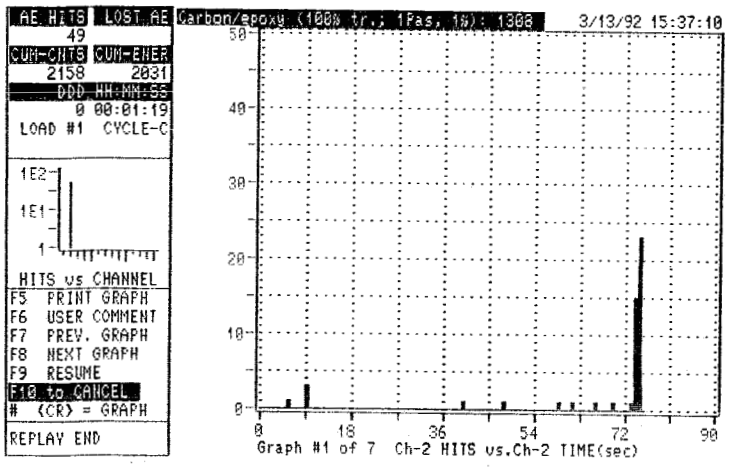

(a)

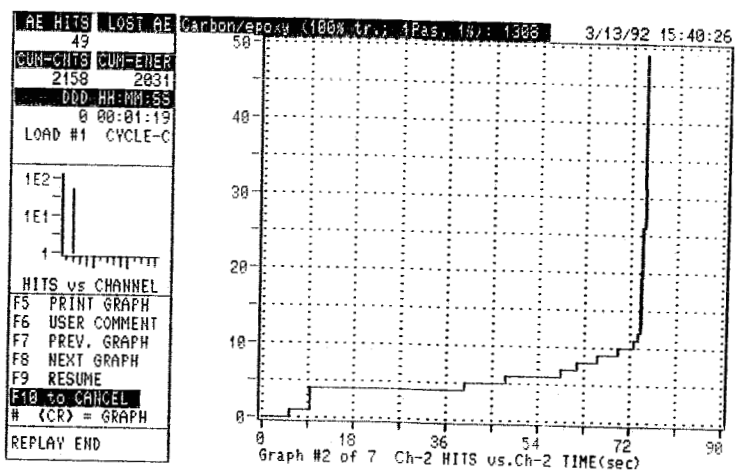

(b)

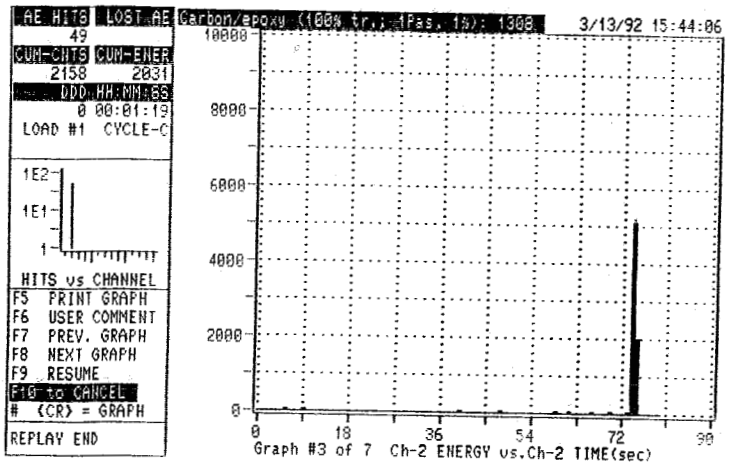

(c)

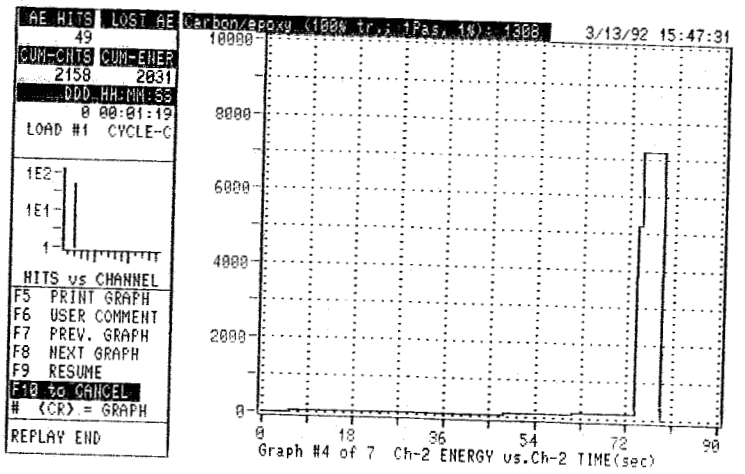

(d)

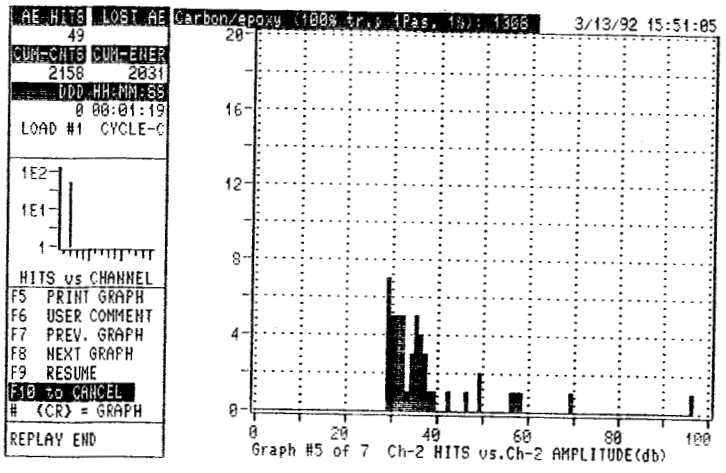

(e)

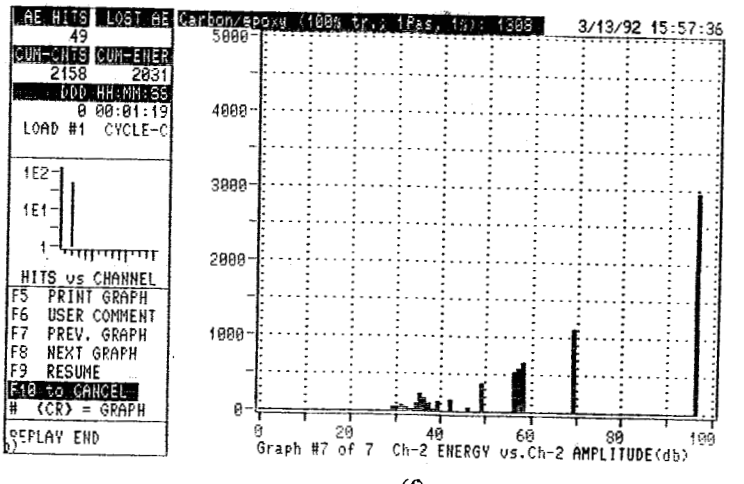

(f)

Figure B.19: Acoustic emission data of composite with XA-S fibres, in bending.

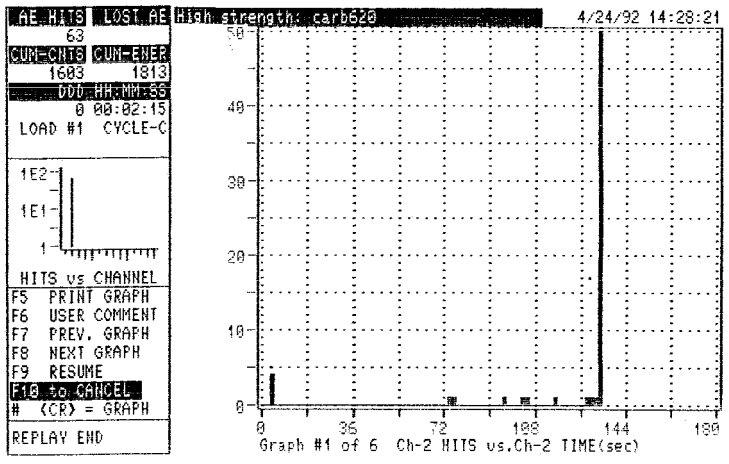

(a)

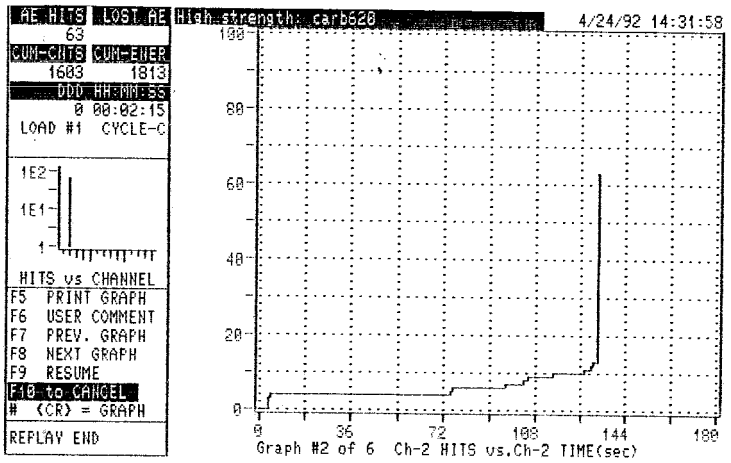

(b)

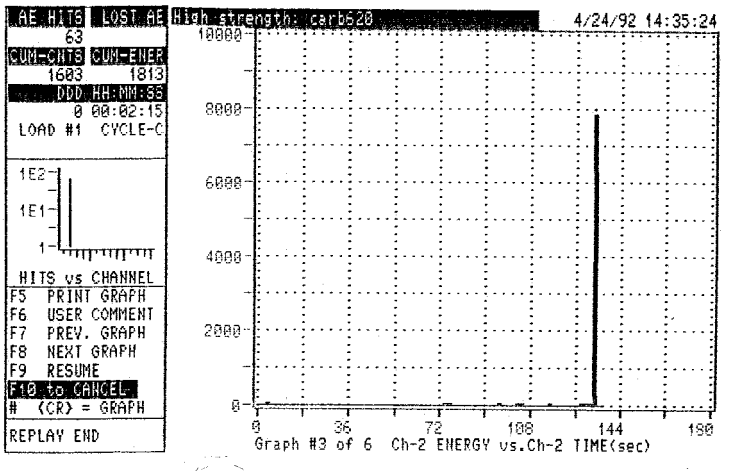

(c)

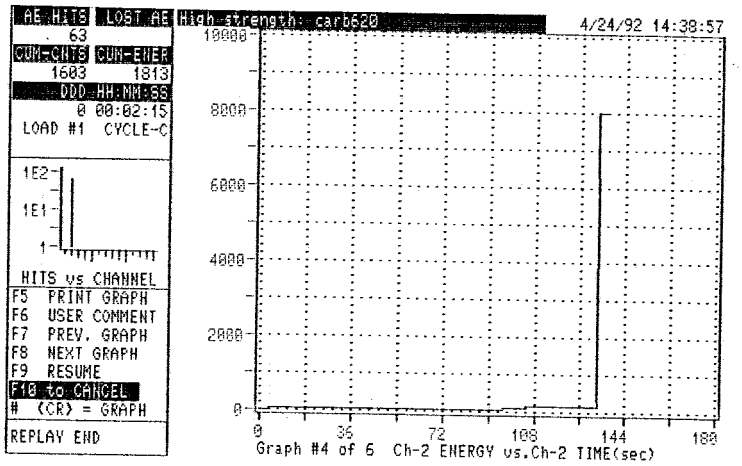

(d)

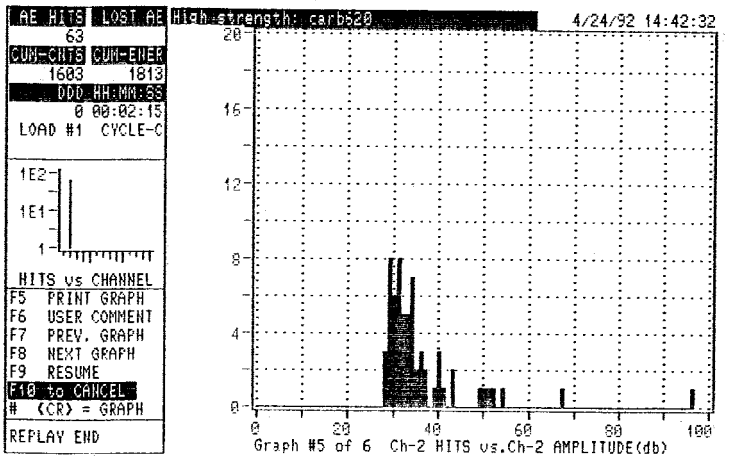

(e)

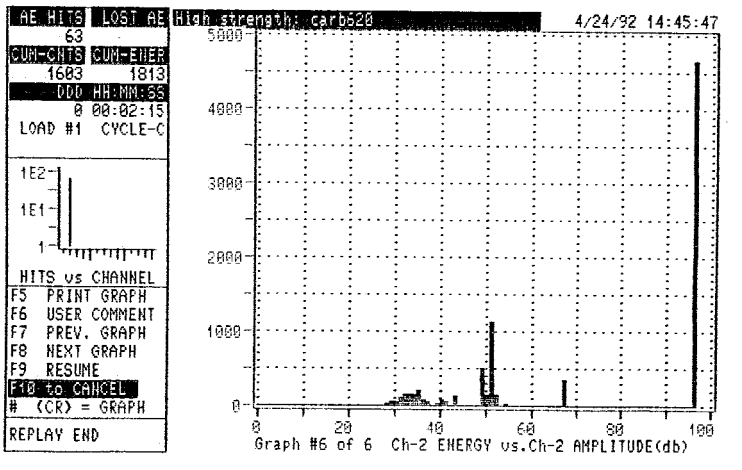

(f)

Appendix C: Scanning Electron Microscopy results

Scanning Electron Microscopy (SEM) analyses on fracture surfaces of the tested materials is performed. Both suvey and detail pictures are taken. The pictures show the failure mode of the different tested materials.

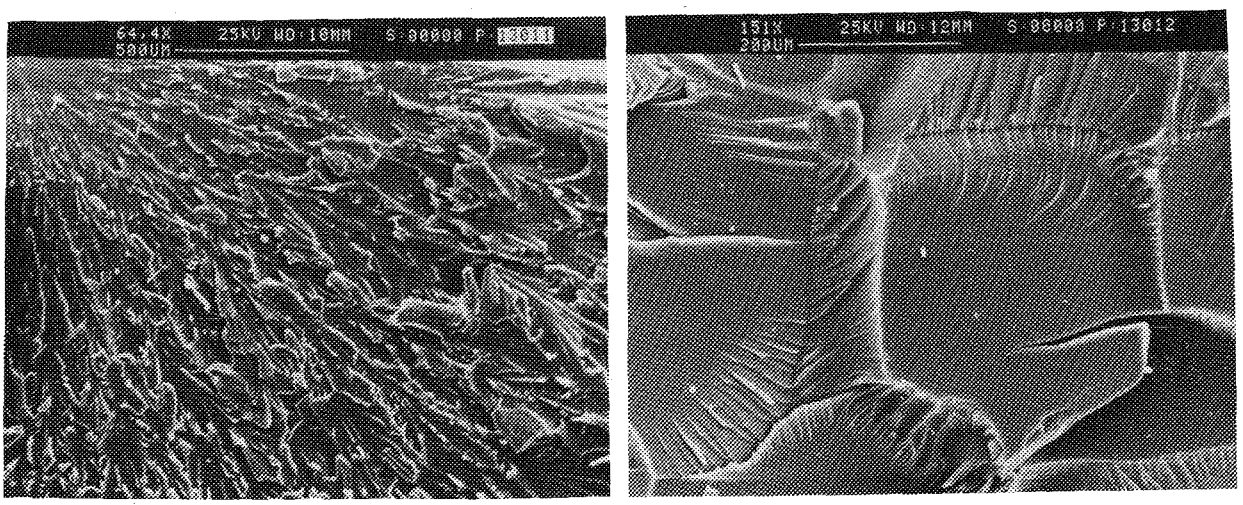

Figure C.1: Fracture surface of pure epoxy, survey and detail.

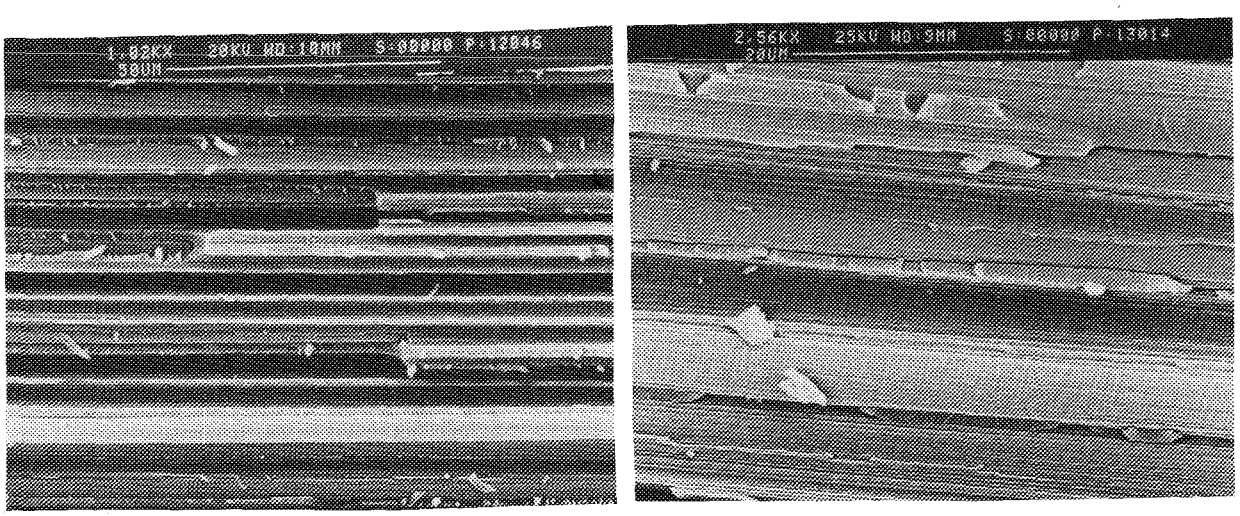

Figure C.2: Fracture surface of a composite with 0% treated Apollo fibres, survey and detail.

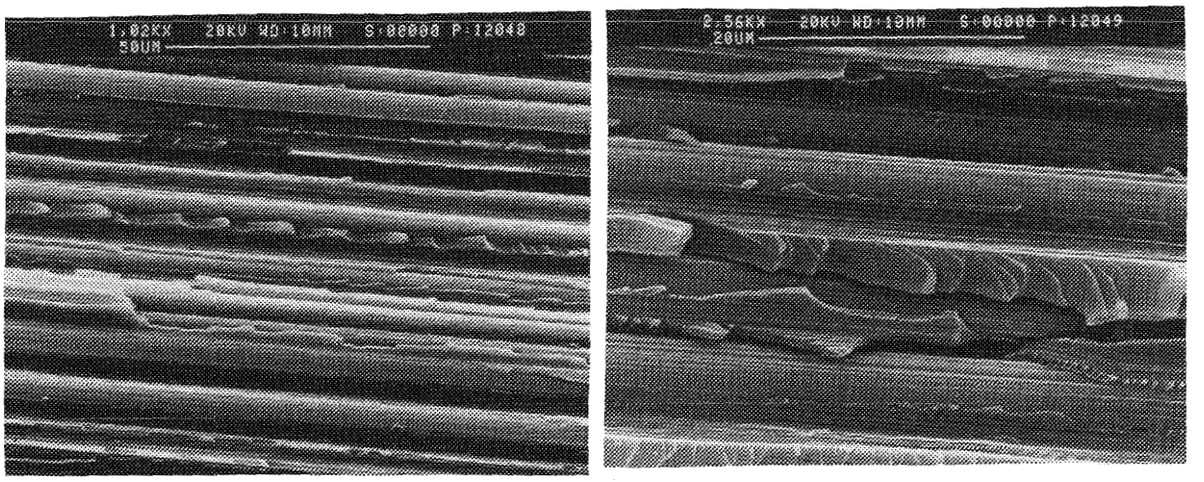

Figure C.3: *Fracture surface of a composite with 10% treated Apollo fibres, survey and detail.*

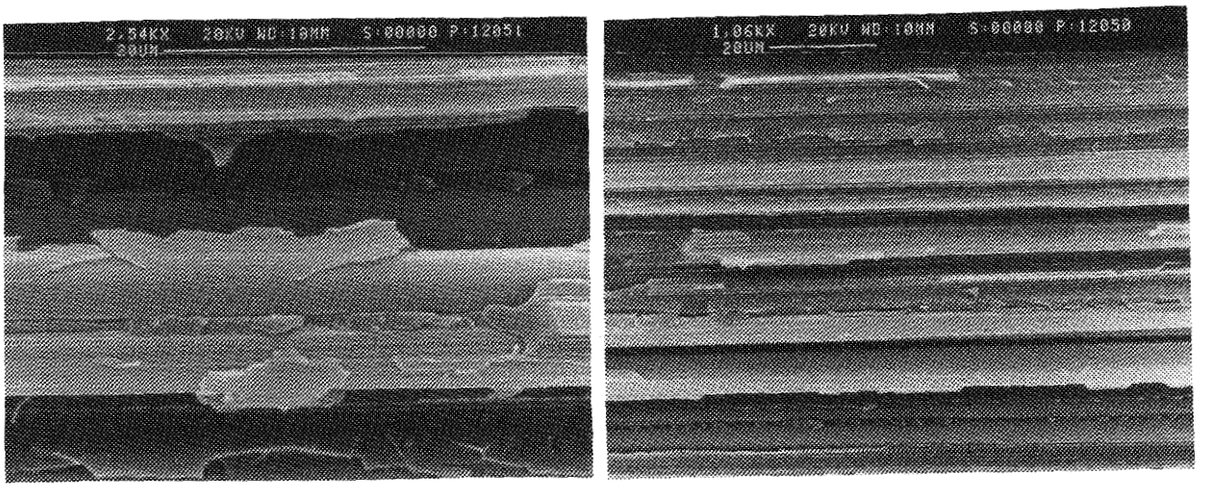

Figure C.4: *Fracture surface of a composite with 50% treated Apollo fibres, survey and detail.*

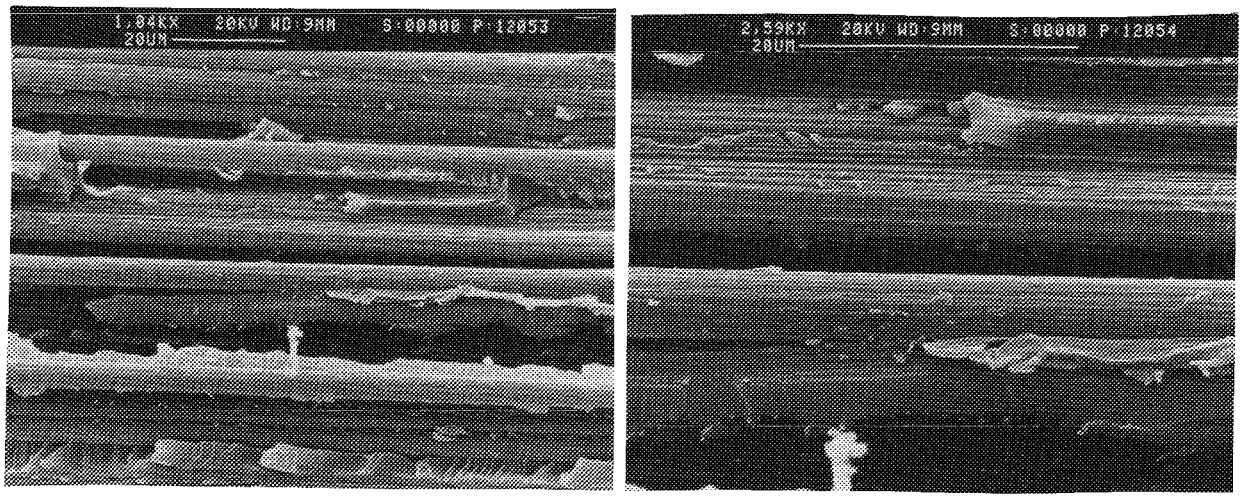

Figure C.5: *Fracture surface of a composite with 100% treated Apollo fibres, survey and detail.*

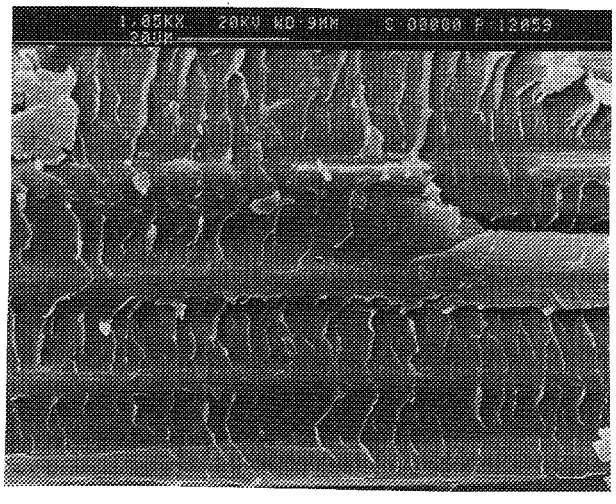

Figure C.6: *Fracture surface of a composite with XA-S fibres, survey.*

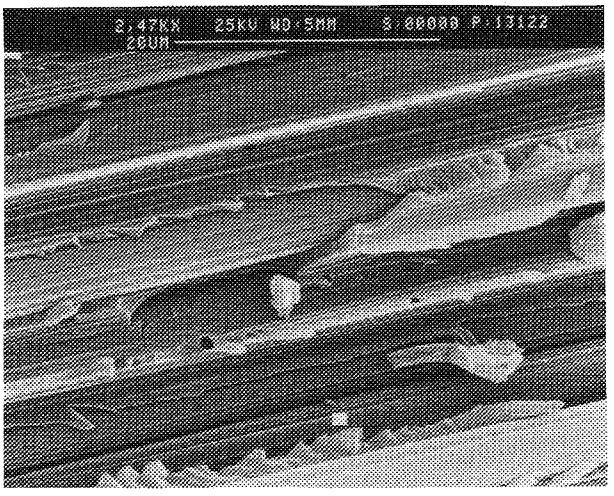

Figure C.7: *Fracture surface of a composite with 0% treated and 2.5% silicon oil sized Apollo fibres, detail.*